Suomi National Polar-orbiting Partnership
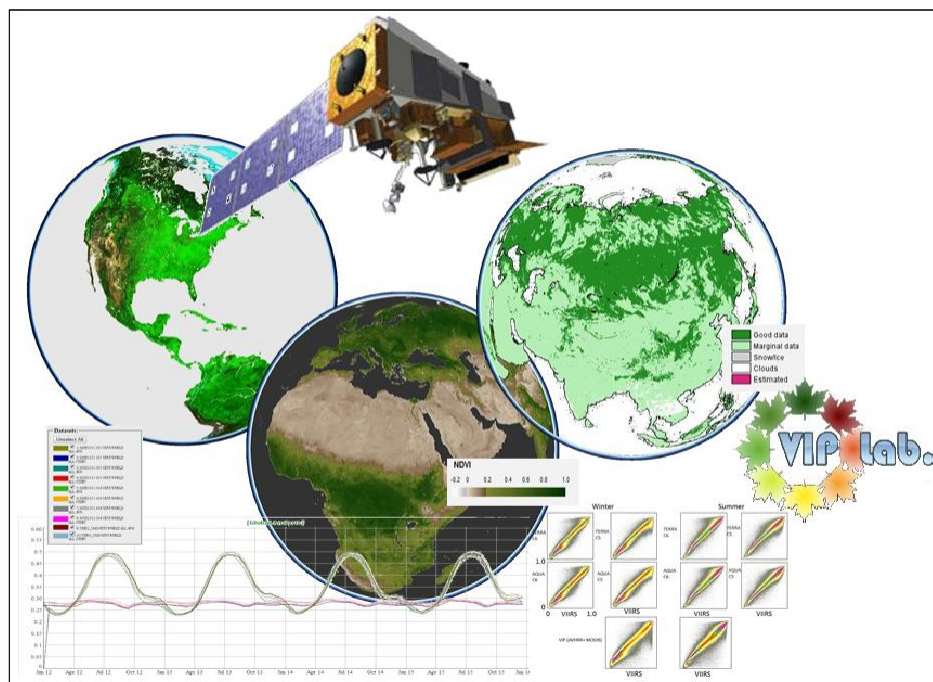
Visible Infrared Imaging Radiometer Suite

Vegetation Index Product Suite
User Guide
&
Abridged Algorithm Theoretical Basis Document

Version 2.1.2

Kamel Didan, Armando Barreto Munoz, Tucker J. Comptom, Jorge E. Pinzon

Science Team

The Suomi National Polar-orbiting Partnership (S-NPP) Visible Infrared Imaging Radiometer Suite (VIIRS) Vegetation Index Algorithm and Product suite is a multi-institutions effort lead by the University of Arizona and funded by NASA. This effort aims at designing, testing, evaluating, and implementing a set of science and production algorithms for the generation of a consistent suite of Vegetation Index data products that build on the NOAA-AVHRR and NASA-EOS MODIS time series and science traditions.

The University of Arizona

- Kamel Didan (PI) [didan@email.arizona.edu]
- Armando Barreto Munoz

NASA Goddard Space Flight Center

- Tucker J. Compton
- Jorge E. Pinzon

Change Log

Many passages in this document are from our previous EOS MODIS documentation (MODIS ATBD and User Guide) with revisions and improvements when necessary to capture VIIRS specifics. This is a result of the high degree of similarity between the two sensors, algorithms, and product suites, and to keep a level of consistency across the time series.

- The abridged ATBD with a summary of the science algorithm starts at page 3
- The User Guide starts at page 26
- The Error and Characterization starts at page 62
- The Continuity section starts at page 67

Note: This live document will change to capture and reflect the status of the science algorithms, product suite, and any necessary amendments to this effort. Updates to this document will be posted on the PI Science Computing Facility website [vip.arizona.edu], the VIIRS Land science team, and related NASA websites.

This is a list of changes and updates made to this document.

Date	Status	Comments
07/01/2016	First internal draft	Never made public
01/01/2017	Second draft	For internal review (never made public)
09/01/2017	First pubic draft	This is the first draft to be released to the public
09/01/2017	Document URL created	Draft will be made public with focus on User Guide
9/12/2017	Changes to the 1km product to start using the I1 (red)/I2 (NIR) bands when computing VIs.	Products suite is still in test mode and products will be public soon.
01/10/2018 (**V2.1**)	Corrected the Data ranges and Fill value for some of the VI products.	Public release ready.
01/22/2018 (**V2.1.1**)	Corrected few typos in the Data Tables	Public release ready.
02/14/2018 (**V2.1.2**)	Corrected table referencing in text	Public release ready.

Table of Contents

List of Tables

List of Figures

Foreword

Several recent events have highlighted the need for long-term satellite observations of the Earth system. Climate change and anthropogenic activities are expected to significantly influence the functioning of terrestrial ecosystems and thereby alter the fluxes of energy, mass and momentum between the land surface and the atmosphere. There has been partial success in closing this feedback loop of climate–vegetation– interactions. However, the accurate characterization of the land surface vegetation and its seasonal manifestation remains crucial to this effort. The accurate quantification in space and time of the land surface vegetation describes the boundary conditions necessary to land surface-atmosphere interactions in models, subsequently better climate modeling, and change monitoring.

Land surface vegetation and related parameters are a central component of Earth Observing and an integrator of climate and anthropogenic drivers. While land surface vegetation is measured by various direct and indirect observational methods, the vegetation index time series, from various Earth Observing and Imaging Systems, is by far the most successful and globally explicit data record. The international Committee on Earth Observing Satellites (CEOS) convened a Vegetation Index/Phenology workshop, in Summer 2006 and Fall 2016, to bring together producers and users of global VI time-series data and discuss the current state of the global VI time series records, their accuracy, validation status, derivation methods, and how to quantify their uncertainty. The community recognizes the value of the long term AVHRR-NDVI, the expanding MODIS NDVI/EVI record, and the emerging S-NPP VIIRS data record and their importance to science and global change research. Any new data record should consider steps to integrate important and significant improvements brought by EOS-MODIS science to insure not only backward but also forward compatibility with newer sensors and products. VIIRS is building on this ongoing 35+ year old NDVI time series and will expand the 17+ year MODIS Enhanced Vegetation Index time series. The VIIRS Vegetation Index effort is also addressing issues in the records, methodologies, community requirements, and will for the first time quantitatively and explicitly address the uncertainty in these records in the proper spatial context.

Vegetation indices are now a standard tool of Earth system science. They continue to play a central role in global change research, in terrestrial ecology, land cover and land use change, carbon cycle, and a host of other themes. Vegetation indices also support ecosystem and climate models by providing a proxy and an easy tool for the spatial scaling of a list of parameters about the land surface, primary production, and vegetation phenology in particular. Their pervasive use is due to the simple, robust, and intrinsic characteristics. Their formulation makes no assumptions about the observations or the data used to derive them, which minimizes the biases and leads to consistent time series data that can be assimilated easily into all sorts of applications, models, and research topics. VIIRS Vegetation Index time series is expected to build upon and continue this tradition and expand the time series for another 30+ years considering the upcoming operational Joint Polar Satellite System (JPSS) VIIRS series.

The S-NPP VIIRS vegetation index (VI) algorithm and product suite is building on the EOS MODIS land surface product suite and will provide a reliable spatial and temporal measures of coarse resolution global vegetation metrics useful for monitoring the Earth's land surface vegetation activity, distribution, and composition while supporting phenological studies, change detection, and model parameterization. Gridded vegetation index maps are regularly generated at a quasi-8 day, 16-day, and monthly intervals.

Three vegetation index algorithms are produced globally, the historical Normalized Difference Vegetation Index (NDVI), one of the longest remote sensing based time series data records. S-NPP VIIRS NDVI will provide a direct link to the heritage NOAA-AVHRR NDVI time series. The 'Enhanced' vegetation index (EVI), introduced with EOS-MODIS as an improved and highly sensitive index in high biomass regions. EVI improves vegetation monitoring by the de-coupling and mitigation of the canopy background signal and an empirical correction of atmosphere influences. The third is the 2-band EVI2, a reformulation of the standard 3-band EVI, that aims at sensor continuity and elimination of the blue band from the equation. EVI2 provides a transition index that will eventually replace EVI and eliminate the need for the blue band, while providing a robust and direct mechanism for backward compatibility and forward continuity with any sensor that lacks the blue band, like AVHRR.

S-NPP VIIRS VI algorithms improve the standard EOS MODIS VI compositing methodologies by minimizing the impact of residual clouds and atmosphere contaminants. The VIIRS VI suite uses surface reflectance corrected for molecular scattering, ozone absorption, aerosols, and employ a constrained view angle maximum value composite (CV-MVC) methods aimed at reducing the sun-target-sensor angular variations. In addition, all VI data provide a detailed per-pixel quality assurance (QA) flags to aid post processing. The suite consists of 8-day, 16-day, and monthly tiled products at 500m and 1km, and global coarse resolution cloud free and gap filled Climate Modeling Grid (CMG) products.

This document describes the product suite, some of the theoretical basis for the development and implementation of these S-NPP VIIRS VI algorithms (with more detail in the ABTD document), their characterization, error, uncertainty and overall performance.

1. Introduction

One of the primary interests of observing the Earth surface with global imagers is to characterize and measure the role of vegetation in large-scale global processes with the key goal of understanding how the Earth functions as a system. This requires an understanding of the global distribution of vegetation types as well as their biophysical, functional, structural properties, and spatial/temporal variations. While many direct spectral images interpretation methods exist the simpler method of spectral bands ratioing, or Vegetation Indices (VI), remains one of the most robust empirical methods for characterizing land surface vegetation health and activity (Tucker 1979, Huete et al. 2002, Tucker et al. 2005). Vegetation indices are designed to enhance the vegetation reflected signal from measured spectral responses by making use of the distinctive soil-vegetation characteristic in the red-edge area of the spectrum. Vegetation indices combine two (or more) spectral bands in the **red (0.6 - 0.7 *µm*), NIR wavelengths (0.7-1.1 *µm*),** and **Blue (0.44-0.5 *µm*)** regions (Tucker 1979, Huete et al. 2002). Vegetation indices time series inform us about the status of vegetation health during the growing season and as it changes in response to environmental, climate, and anthropogenic drivers. Time series measures of vegetation index have been shown highly correlated with flux tower photosynthesis measurement and integrate the response of vegetation to change in environmental factors providing valuable information about land cover, land use, primary production, and carbon cycle to global change research.

A recent development of the study of land surface vegetation with remote sensing time series data is the characterization of vegetation growing season or phenology. While phenology is the study of change of all living things over time, in this context phenology is the study of vegetation change over time using remote sensing data and tools (Beaubien, et al. 2003, Zhang et al. 2003, White et al. 2009). Because vegetation phenology affects terrestrial carbon cycle across a wide range of ecosystem and climate regimes (Baldocchi et al. 2001; Churkina et al. 2005; Richardson et al. 2009) accurate information related to phenology is important to studies of regional-to-global carbon budgets. The presence of leaves also influences land surface albedo (Moore et al. 1996; Ollinger et al. 2008) and exerts strong control on surface radiation budgets and the partitioning of net radiation between latent and sensible heat fluxes (Chen and Dudhia, 2001; Yang et al. 2006). Thus, the phenological dynamics of vegetated ecosystems influence a host of eco-physiological processes that affect hydrologic processes (Hogg et al. 2000), nutrient-cycling, (Cooke and Weih, 2005), and land-atmosphere interactions (Heimann et al. 1998). Many data sets related to plant growing season have been collected at specific sites or in networks focused on individual plants or plant species, still remote sensing provides the only way to observe and monitor land cover, vegetation, and phenology at global scale and at consistent and regular intervals. Satellite phenology encompasses the analysis of the timing and rates of vegetation growth, senescence, and dormancy at seasonal and interannual time scales. To that end, vegetation indices, which capture the aggregate functioning of a canopy (Asrar et al. 1984, Huete et al. 2002 and 2008), are the most robust and widely used proxies for extracting phenology information (White et al. 2009).

1.1. The S-NPP VIIRS Platform

The Suomi National Polar-orbiting Partnership (Suomi NPP, formerly the NPOESS Preparatory Project) satellite was launched on October 28, 2011 to provide continuity for more than 30 operational and science-quality data records initiated by the earlier MODerate Imaging Spectroradiometer (MODIS) aboard Terra and Aqua NASA Earth Observing System (EOS) satellites. The VIIRS Vegetation Index algorithm and product suite will continue this data record that dates back to 1981, when NOAA's Advanced Very High Resolution Radiometer (AVHRR) started this continuum (Tucker 1979, Tucker et al. 2005, Huete et al. 2002, Brown et al. 2006, Didan 2010) and

will extend these data records to the next decades and beyond. This vital Earth science time series has played a key role in supporting the monitoring, detection, and quantification of global land vegetation properties and change over time and space.

The Suomi NPP mission is also the bridge between NASA's EOS satellites and the Joint Polar Satellite System (JPSS) of the National Oceanic and Atmospheric Administration (NOAA) and provides a demonstration and validation of JPSS program, sensors, and data products (Goldberg et al. 2011, Murphy et al. 2001, Cao et al. 2013, Justice et al. 2013). With more than 4 years of largely NOAA operational use, NASA has initiated an EOS-MODIS like effort to support the generation of research quality climate data records (CDR) from the Suomi NPP (and eventually JPSS-VIIRS) platforms to support the science community interested in continuity, accuracy, and consistency of this long term data record and to provide for a transition to JPSS-VIIRS.

The Visible Infrared Imaging Radiometer Suite (VIIRS) is similar to the EOS MODIS instruments that have been collecting critical Earth science data since early 2000 and have continued to build a long-term climate observations record dating back to 1981 by AVHRR. VIIRS, one of five sensors aboard the Suomi NPP platform, collects visible and infrared measurements of the land, atmosphere, cryosphere, and oceans. Key land products from VIIRS are the vegetation indices, both NDVI and EVI (referred to as EVI3 sometimes in this document). While these are currently generated by NOAA for operational purposes, NASA Earth system objectives is the application of the more rigorous EOS methods to Suomi NPP data in order to generate a higher quality data and serve the science community while supporting Earth system science research (Justice et al. 2013).

NOAA's goal for VIIRS were and will continue to be mostly focused on near real time operational and application oriented data needs. However, NASA's role in the initial years between pre- and post-launch was the evaluation of sensor data records (SDRs) and environmental data records (EDRs) and assess their suitability for Earth system science. Although the SDR/EDR VIIRS products vary greatly in their quality and suitability for Earth system science, the initial assessment indicates they are suitable for Earth system science and applications (Vargas et al. 2013, Justice et al. 2013). The NASA test Vegetation index data from VIIRS, generated by an older version of the EOS-MODIS VI Algorithm has shown that VIIRS VI time series is comparable to data from MODIS. Most importantly, the initial evaluation denotes that MODIS Algorithms are applicable to VIIRS provided sensor considerations are observed.

1.2.   Motivation and Background

Driven by a steady increase in atmosphere CO_2 concentration (Fig. 1a), climate change is expected to significantly impact the two key climate drivers of land surface vegetation, precipitation and temperature (Fig. 1, Figure 2 & 3). This will in turn alter the functioning of terrestrial ecosystems and thereby alter fluxes of energy, mass and momentum between the land surface and the atmosphere (Melillo *et al.* 1996; Watson *et al.* 1996; Mintz, 1984; Dickinson & Henderson-Sellers, 1988; Rowntree, 1988; Bonan et al. 1992, Saleska et al. 2016, Wu et al. 2016). There has been limited success in closing this feedback loop of climate–vegetation– interactions, however, the accurate characterization of land surface phenology, i.e., the seasonal timing and annual sequence of events in plant life (Fig. 1b), is crucial to this effort, and to link land surface – atmosphere interactions in models (Claussen, 1994). Vegetation is a key component of ecosystem functioning and processes. Numerous studies have demonstrated that climate processes operating at seasonal

and interannual time scales (e.g., ENSO) are identifiable in the vegetation dynamic (Braswell et al. 1996; Asner et al. 2000, Myneni et al. 1997).
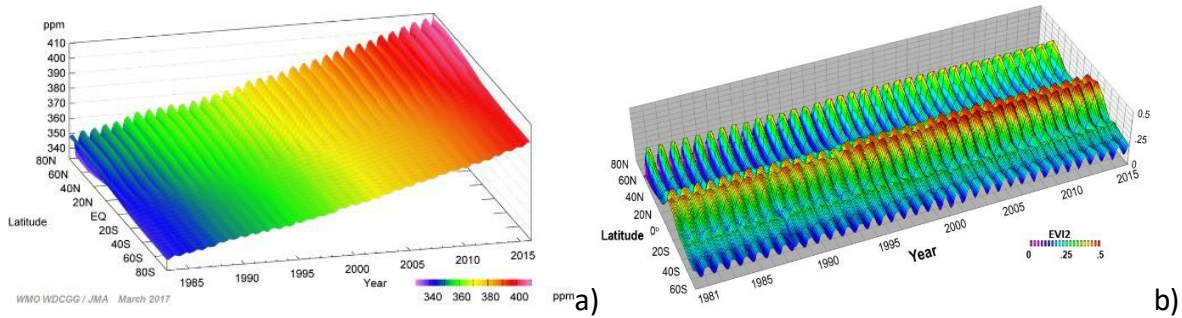
Figure 1. Time-series representation of zonally (20° latitudinal bands) averaged CO_2 and EVI2. CO2 data from WMO WDCGG/Japan Meteorological Agency [http://ds.data.jma.go.jp/ghg/kanshi/ghgp/co2_e.html]. VI data from the MEaSURES-2006 VIP ESDRs (https://vip.arizona.edu/viplab_data_explorer.php). Vegetation volume, distribution, and phenology timing drive the noticeable differences between the Northern and Southern hemisphere. EVI2 time series captures the CO_2 seasonality and the spring pulse, illustrating the affinity between VIs and Ecological metrics of the carbon cycle.
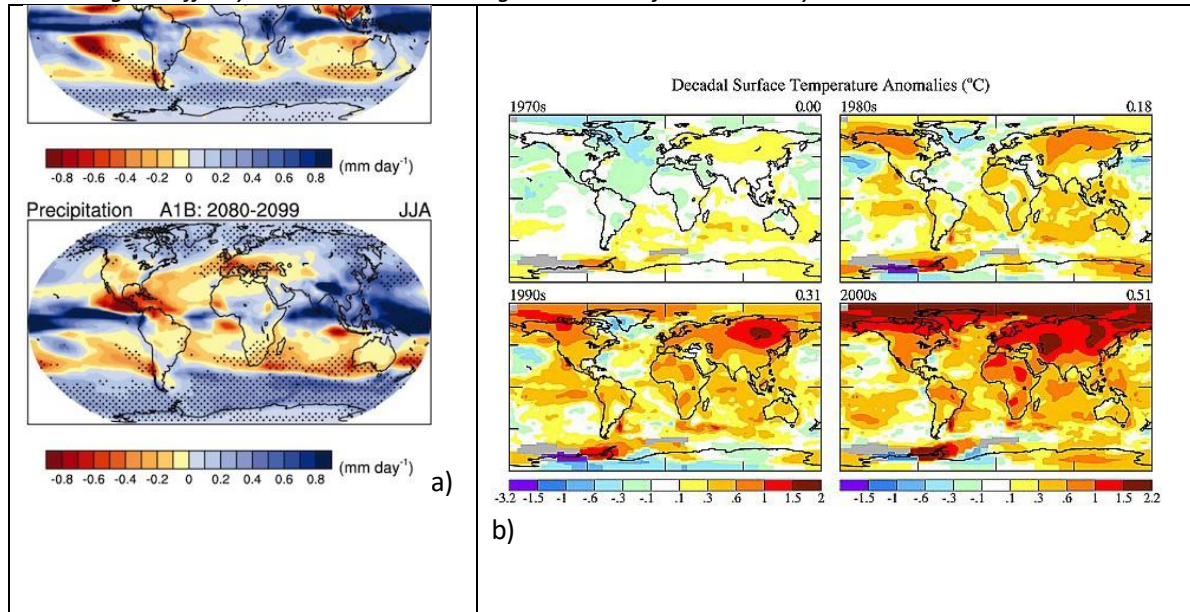
Figure 2: a) Multi-model mean changes in precipitation (mm day^{-1}) for boreal winter (DJF) and summer (JJA). Changes are given for the SRES A1B scenario, for the period 2080 to 2099 relative to 1980 to 1999. Dotting denotes areas where the magnitude of the multi-model ensemble mean exceeds the inter-model standard deviation (Meehl et al. 2007, reproduced from IPCC). b) decadal temperature anomalies (Hansen et al. 2010).

Recent work indicates that the effects of climate change are manifested in landscape vegetation dynamic (Fig. 3) (Randerson et al. 1999, Huete et al. 2006, Saleska et al. 2016). Shifts in phenology depict an integrated vegetation response to environmental change and influence local biogeochemical processes, including nutrient dynamics, photosynthesis, water cycling, soil moisture depletion, transpiration, and canopy physiology (Reich & Borchert 1988; Herwitz 1985). Knowledge of phenologic variability and the environmental conditions controlling their activity are further prerequisite to inter-annual studies and predictive modeling of land surface responses to climate change (Myneni et al. 1997; Shabanov et al. 2002; White et al. 2002; Huete et al. 2006; Saleska et al. 2007; Huete et al. 2008; Keeling 1996a, 1996b, Saleska et al, 2016; Herrmann et al.

2016). With major shifts in global temperature and precipitation patterns anticipated (ICCP, 2006), there is increased concern on how land surface vegetation and phenology will change in response to global warming, land cover change, and shifts in land use activities (Schwartz & Reed, 1999; deBeurs and Henebry, 2005; Cochrane et al. 1999; Gedney & Valdes, 2000; Lambin et al. 2003).
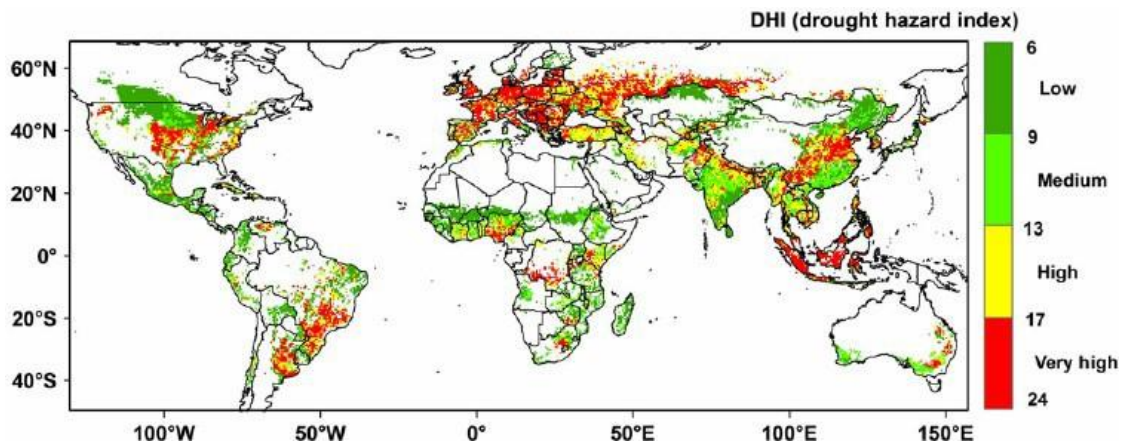
Figure 3: Global Map of Drough Hazard Index (Geng et al. 2016). The spatial nature of these phenomena requires spatially explicit global quantification of the vegetation (ex: VI time series).

Satellite vegetation indices have played a major role in monitoring seasonal vegetation dynamics (Henderson-Sellers 1993 & 1995, Huete et al. 2002, Saleska et al. 2007, Herrman and Didan 2016) and interannual comparisons of vegetation activity. Satellite studies using vegetation index time series seasonal profiles have shown how broad-scale changes in land use and land cover change affect land surface phenology (White et al. 2002, 2009, Huete et al. 2006). The temporal profile of the normalized difference vegetation index (NDVI) has been shown to depict phenologic events such as, length of the growing season, peak greenness, onset of greenness, and leaf turnover or 'dry-down' period and the time integral of the VI over the growing season has been correlated with NPP/GPP (Running and Nemani, 1988; Prince, 1991; Justice et al. 2000; Goward et al. 1991; Tucker and Sellers, 1986; Huete et al. 2008). VIs are integrative, consistent, and robust observations of photosynthetic potential, a key climate parameter (Running et al. 1988). There is evidence from satellite data that the phenology of key biomes is changing in response to shifts in climate (Myneni et al. 1997; Keeling et al. 1996; White et al. 2002; Bogaert et al. 2002; Jia et al. 2003; Huete et. al. 2006 & 2008, Saleska et al. 2007), e.g., Myneni et al. (1997) used a 10 year AVHRR-NDVI time series of northern Boreal forests to show a warming trend, whereby the length of the growing season had increased by nearly 2 weeks. Whether these trends will persist, change direction, or disappear altogether requires accurate observation and the compilation of long term data records.

While the MODIS era is waning down, the continuity of these records is critical to the research and application remote sensing communities. In this document we will present a detailed description of the S-NPP VIIRS VI product suite and production algorithms, drawing from the EOS MODIS experience.

1.3.   A Context for Long Term Vegetation Index Data Records

Whereas single mission or sensor specific measurements of vegetation index exist, the length of these records is usually limited due to the mission life expectancy, usually few years, engineering and technological changes that necessitates new designs and improvements, and changes in data processing methods and science algorithms which denotes need for multiple reprocessing. In practice these limitations impose a restriction on the data usefulness in particular when addressing long term phenomenon and trends because they lack representation, or in statistical context they cannot support the generation of an accurate and representative long term normal. Extending these

records beyond the short life time framework of the sensor has been both a goal and a challenge. The data record(s) discussed in this document were proposed within the framework of NASA's Earth Observing Systems and the measurements this effort requires. In this document we will discuss two global data records that characterize land surface vegetation, the NDVI and EVI (and the alternative EVI2). These two records are complementary, in that they do provide slightly different insights about the vegetation health and productivity (Huete et al. 2002) with NDVI being the more sensitive one to chlorophyll (red band) and EVI being more sensitive to canopy structure (NIR band).

This effort will extend and continue the 35+ years VI data records from the NOAA AVHRR and EOS MODIS into the post-EOS S-NPP (and JPSS) VIIRS era. This record has resulted in significant Earth system science insights related to global and regional agricultural primary production, inter-annual fluctuations and impacts of ENSO on primary production, phenology variations over time, and trends in land cover and changes driven by climate (Huete et al. 2006 & 2008, Saleska et al. 2016, Herrmann and Didan et al. 2016). Whereas integrated AVHRR NDVI time series have been shown to correlate with annual net primary production across biome types, more recent applications of highly calibrated MODIS and SPOT-VGT VIs have demonstrated their utility for estimates of gross primary productivity (GPP) at local scales (Sims et al. 2008, Rahman et al. 2005). Vegetation indices are now being used to better characterize the structure, metabolism, and overall photosynthesis and transpiration which drive changes in gross primary productivity.

With EOS-MODIS, a new index, the Enhanced Vegetation Index (EVI) became a new standard tool (Huete et al. 2002). EVI data has been incorporated into the Vegetation Photosynthesis Model to produce tower-calibrated predictions of GPP carbon fluxes across a series of biomes (Xiao. 2005, Huete et al. 2008, Zhang et al. 2017). VIs are a tool of choice for characterizing vegetation phenology (Zhang et al. 2003, White et al. 2009), which are critical to understanding ecosystem functioning and associated seasonal patterns of carbon, water, and energy fluxes. VIs from the MODIS sensor provided for the first time an accurate depiction of seasonality in dense Amazon rainforests with strong correlation with tower-calibrated GPP measurements of carbon fluxes in both intact rainforest and forest conversion sites (Huete et al. 2006 & 2008, Saleska et al. 2007 & 2016, Wu et al. 2016, Seddon et al. 2016).

While these findings continue to stimulate scientific debates, some of the recent work points to the key role of data processing methods and production algorithms (Huete et al. 2002, Samanta et al. 2010, Morton et al, 2014, Wu et al. 2016, Saleska et al, 2016, Herrmann et al. 2016) as the most critical if we are to make progress in making sense of what these data records are narrating. The community expects the VI record to continue with the same level of rigor, accuracy, continuity, and spatial and temporal scales.

2. VIIRS product #13, Gridded Vegetation Indices (VNP13 Level 3 suite)

The level 3 gridded vegetation indices are standard products designed to extend the significant VI time series derived from AVHRR and MODIS (Huete et al. 2002). The level 3 spatial and temporal gridded vegetation index products are composites of daily surface reflectances. They are generated at 500m, 1km, and 0.05° (~5.6km) every 8 days (quasi), 16 days, and calendar month. Three vegetation index (VI) algorithms are produced globally for land:
- The standard Normalized Difference Vegetation Index (NDVI), referred to as the "continuity index" to the existing NOAA-AVHRR and MODIS derived NDVI. At the time of S-NPP launch

(2011) there was nearly a 30-year NDVI record from AVHRR and MODIS (1981- and 2000-). VIIRS NDVI will extend this long term data record for use in operational monitoring studies.
- The second is the "Enhanced" vegetation index (EVI) with improved sensitivity over dense vegetation conditions (Huete et al. 1997, Saleska et al. 2007).
- The third index is a backward compatible 2-band EVI2 index based on the red and NIR only (Jiang et al. 2008) and is a modified EVI that eliminates dependency on the blue band and addresses some of the operational EVI issues.

These VIs complement each other in the context of global vegetation studies and provide for better extraction of canopy biophysical parameters. These products are generated by a suite of improved EOS-MODIS compositing science algorithms, based on the Constrained View Angle Maximum Value Composite. The representative pixel-day output is selected as close to nadir as possible to minimize the impact of variable viewing geometry (Bidirectional Reflectances) and standardize the data as practically as possible while retaining full traceability to the sensor observations. Each pixel generated at the respective resolution will have a NDVI, EVI, EVI2, Red, NIR, Blue, Green, three SWIR surface reflectances, the sensor and solar zenith, relative azimuth, pixel quality assurance parameters, and a pixel reliability metric that indicates the suitability of the data for research and applications. The product suite is designed to support consistent, precise, seasonal and inter-annual, monitoring of the Earth's vegetation and is capable of detecting change and support the derivation of many structural and biophysical vegetation parameters.

2.1. Key Science Applications of the Vegetation Index

Vegetation indices have a long history of use in a wide range of disciplines, owing to their simplicity and long list of applications:
- Inter- and intra-annual global to local vegetation monitoring;
- Gross and Net primary production and carbon cycle and balance via empirical correlation;
- Global biogeochemical, climate, and hydrologic modeling by providing simple methods to approximate key parameters in support of these efforts;
- Natural, anthropogenic and climate change detection;
- Agricultural activities (crop yield, plant stress, ET, precision agriculture);
- Drought studies;
- Landscape disturbances (Infestations, Fires, deforestation, weather related land cover disturbances, etc.);
- Land cover and land cover change products;
- Biophysical estimates of vegetation parameters (%Green Cover, fAPAR, LAI);
- Public health issues (vector borne diseases, valley fever, etc.);
- New innovative topics that uses VI as a proxy to answer questions (bird migration, biome shifts, even ant colonies dynamics, etc.)

3. Vegetation Indices

Two key Climate Data Records (CDR), or Earth Science Data Records (ESDR) (naming convention differences reflect NOAA and international community and NASA nomenclatures) identified in a NASA white paper on Vegetation Indices (Huete et al. 2006, Friedl et al. 2006) are the NDVI and EVI (or EVI2). Both of these data records are now standard measurements generated from multiple sensors, including MODIS since 2000 (Huete et al. 2002), from AVHRR since 1982, and now VIIRS since 2012 (Vargas et al. 2013) aboard S-NPP and eventually aboard the Joint Polar Satellite System (JPSS) mission (Welsch et al. 2001).

A key parameter of the Earth system is Net Primary Productivity (NPP) as it describes the seasonal carbon cycle (Dungan et al. 1994, Guan et al. 2015). Terrestrial NPP measures the rate of

CO_2 uptake by green active vegetation through the process of photosynthesis minus the respiration. NPP exerts a significant influence on the climate system and its seasonal and interannual changes are fundamental inputs to models of global climate and global change (Saleska et al. 2007, Huete et al. 2008, Nemani et al. 2003). Whereas accurate in situ measurements of NPP are usually the norm for plot size studies, the extrapolation of this parameter to its broader spatial scale cannot be considered without approximation and/or modelling. For over 35 years remote sensing provided the only appropriate tool to estimating and modeling this entity (Running et al. 2002, Prince et al. 1991, Nemani et al. 2003, Huete et al. 2008). The estimation is either through complex biogeochemical modeling (Nemani et al. 2003) or by using vegetation indices as proxies (Prince et al. 1994, Mynnei et al. 1997, Huete et al. 2008, Saleska et al. 2016, Guan et al. 2015). The vegetation index time series is intended for monitoring the annual change in vegetation health, productivity, and phenology, while providing a solid foundation for exploring long-term trends and disturbances in vegetation resulting from global climate alterations and anthropogenic pressure (Eidenshink, 1992, Myneni et al. 1997, Saleska et al. 2007). There are many vegetation index formulations, but most are based on the ratio of near-infrared and red surface reflectances. While, NDVI values, or from any other index, are not intrinsic physical quantity (Tucker 1979, Huete et al. 2002) research has shown that VIs can be used for the accurate characterization of vegetation due to its strong relationship to particular biochemical and physical properties of plants, such as Leaf Area Index (LAI), Absorbed photosynthetically active radiation (APAR), fractional vegetation cover (FVC), and gross primary production (GPP) and biomass/yield.

The theoretical basis for empirical-based vegetation indices is derived from examination of typical spectral reflectance signatures of leaves (Fig. 4). The reflected energy in the visible is very low as a result of high absorption by photosynthetically active pigments (chlorophyll), with maximum absorption values in the blue (470 nm) and red (670 nm) wavelengths. Whereas, most of the near-infrared radiation (NIR) is scattered (reflected and transmitted) with very little absorption, in a manner dependent upon the structural properties of a canopy (LAI, leaf angle distribution, leaf morphology) (Tucker 1979, Rouse et al. 1973). As a result, the contrast between red and near-infrared responses is a sensitive measure of vegetation amount, with maximum red−NIR differences occurring over a full canopy and minimal contrast over targets with little or no vegetation. For low and medium amounts of vegetation, the contrast is a result of both red and NIR changes, while at higher amounts of vegetation, only the NIR contributes to increasing contrasts as the red band becomes saturated due to chlorophyll absorption.
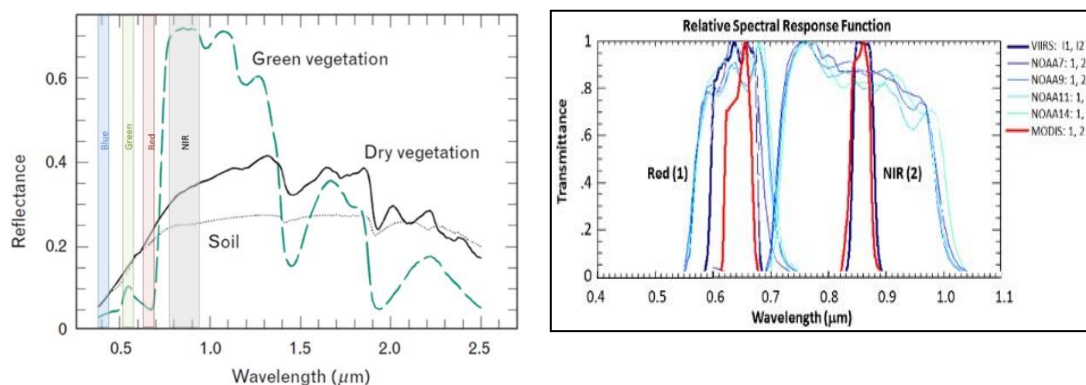
Figure 4. Plants absorb and reflect light differently depending on the wavelength and plant health status. The photosynthetic process absorbs most of the visible light (blue-red region) and vegetation reflect much of the near-infrared (NIR). These differences permit the separation of healthy from stressed plants and/or other objects. The inset shows the position of the various spectral bands for the three main sensors AVHRR,

MODIS, and VIIRS.

Spectral vegetation indices are among the most widely used satellite data products providing key measurements for climate, phenology, hydrologic, and biogeochemical studies, and land cover/land cover change detection. There is currently a consistent NDVI record extending for more than 3 decades from the NOAA AVHRR series (Gutman et al. 1995, Brown et al. 2006), which have contributed significantly to the advancement of Earth System Science, in particular to global biome, agricultural primary production; interannual fluctuations and impacts of ENSO and other climatic disturbances, especially droughts, on primary production; phenology; and climate change and variability. Compared with other land products, and due to their simplicity, VI's are more readily fused across sensor systems facilitating an underlying need to ensure continuity of critical data sets to study climate-related processes.

3.1.   Theory of Vegetation Indices

The red-NIR contrast can be quantified through the use of ratios (NIR/red), differences (NIR−red), weighted differences (NIR−k•red), linear band combinations (x_1•red+x_2•NIR), or a hybrid combination. Vegetation indices are measures of this contrast and thus are integrative functions of canopy structural (%cover, LAI, LAD) and physiological (pigments, photosynthesis) parameters.

Many studies have explored how red and near-infrared (NIR) reflected energy interacts with the canopy, particularly the photosynthetically active leaves and how that relates to the amount of green material within the canopy (Colwell, 1974, Tucker, 1979). Because photosynthesis is mostly driven by the visible part of light (blue to red, 0.4-0.7um) most of that energy is then absorbed with little reflected back depending on biomass, and this is due to chlorophyll absorption (Myneni, 1994; Gamon et al. 1995; Running and Nemani, 1988). On the other hand, the NIR energy part of the spectrum is mostly scattered by the healthy turgid leaves, either through reflection or transmission through the canopy. This process of interaction, that starts with incident solar irradiance travelling through the atmosphere to the canopies, will depend on the atmospheric composition, conditions, background, canopy structure and composition, and angular considerations (Bidirectional Reflectance, change of the magnitude of reflected light based on the angle of incidence and view) (Morton et al. 2014, Schaff et al. 2002). With the same amount of active green biomass on the ground the amount of reflected energy change with these factors making it challenging to use it directly as a simple measure of plant biophysical characteristics. Single band values are then of little practical and operational use for vegetation monitoring on a global basis. A work around this challenge is to combine two or more reflectance from different spectral regions into an equation or 'vegetation index' (VI).

The simple ratio (SR) proposed by Jordan (1969) divides the NIR (radiance, digital count, or corrected/uncorrected reflectance) by the 'red' reflectance. SR follows this formulation:

$$SR = \frac{\rho_{nir}}{\rho_{red}} \qquad (1)$$

Because red light is mostly absorbed by photosynthesis, the reflected portion measured by the sensor over dense canopies becomes very small and the ratio, which is unbounded, becomes too high to make much sense.

3.1.1. Normalized Difference and Enhanced Vegetation Indices

Deering (1978) proposed a simple normalization procedure that limits the index. This resulting index, called Normalized Difference Vegetation Index (NDVI) standardizes the VI values to between [−1 and +1], and is expressed as:

$$NDVI = \frac{\rho_{NIR} - \rho_{red}}{\rho_{NIR} + \rho_{red}} \qquad (2)$$

where ρ can be digital counts, radiances, top of atmosphere (TOA) apparent reflectances, Top of canopy surface radiances, surface reflectances, or even hemispherical spectral albedos. For most terrestrial land cover, except snow and water, the lower boundary of this NDVI index appraoches zero. However, depending on the atmosphere status, soil or canopy background color, NDVI yields slightly different values for the same canopy and surface conditions (Jackson and Huete, 1991).

As a ratio, the NDVI has the advantage of minimizing certain types of band-correlated noise (positively-correlated) and influences attributed to variations in direct/diffuse irradiance, clouds and cloud shadows, sun and view angles, topography, and atmospheric attenuation. Ratioing can also reduce, to a lesser degree, calibration issues (Rao et al. 1994; Vermote et al. 1995, Huete et al. 2002) bidirectional reflectance distribution dependencies, and instrument-related noise and errors. The extent to which ratioing can reduce noise is dependent upon the correlation of noise between red and NIR responses and the degree to which the surface exhibits Lambertian behavior. While the NDVI Range is theoretically between -1 and 1, for most land vegetation the [0-1] range is the practical dynamic range, with [-1 -0] being a residual range resulting from the formulation with very limited meaningful application in wetlands studies, inland water, water color, snow/ice discrimination. For all practical purpose VIs are mostly considered in the [0-1] range, in particular in the areas not prone to persistent snow cover.

The main disadvantage of ratio-based indices tends to be their non-linearities exhibiting asymptotic behaviors, which leads to insensitivities to vegetation variations over certain land cover conditions (Huete 1988). Ratios also fail to account for the spectral dependencies of additive atmospheric (path radiance) effects, canopy-background interactions, and canopy bidirectional reflectance anisotropies, particularly those associated with canopy shadowing.

Studies have shown NDVI to be strongly related to Leaf Area Index (LAI), green biomass, and fAPAR (Tucker et al. 1981; Asrar et al. 1984; Sellers 1985; Running and Nemani, 1988; Goward and Huemmrich, 1992, Myneni and Williams 1994). Relationships between fAPAR and NDVI have been shown to be near linear (Pinter, 1993; Begue, 1993; Wiegand et al. 1991; Daughtry et al. 1992; Myneni and Williams 1994). This is in contrast to the non-linear correlation with LAI, especially when LAI >= 2.

NDVI is usually derived from atmospherically corrected (for ozone absorption, water vapor, molecular scattering, and aerosols) Top of Canopy (TOC) (Huete et al. 2002), and more recently viewing geometry normalized reflectance (Zhang et al. 2003). The 'ratioing' capabilities of NDVI cancel out large proportion of signal variations that result from calibration, noise, atmosphere, and changing sun - target-satellite angles, and topography. Seasonal profiles of the NDVI time series depict vegetation activity and enables interannual and intra-annual comparisons of these profiles.

The NDVI profiles depict the growing season phenologic activity, including the start, end, and length of the growing season (White et al. 2009). A 10-year time series record of consistent AVHRR-NDVI showed for the first time how the northern Boreal forests growing season has increased by nearly 2 weeks (Myneni et al. 1997). Similar NDVI seasonal profiles over Africa showed how desert expands and contracts in the Sahel (Tucker et al. 1986) in response to rainfall variability. Integrated over the seasonal cycle, NDVI has been correlated with Net Primary Productivity (NPP) (Running and Nemani, 1988; Prince, 1991; Justice et al. 1985; Goward et al. 1991; Tucker and Sellers, 1986). A multitude of other studies have shown the NDVI to proxy the carbon fixation by plants, land cover change, land use, evapotranspiration (Raich and Schlesinger, 1992; Fung et al. 1987; Sellers, 1985; Asrar et al. 1984; Running et al. 1988; Running, 1990; IGBP, 1992). More recently NDVI has been used to proxy bird migration (Nietos et al. 2015; Kelly et al. 2016), vector borne

disease (Epstein et al. 1993; Hay et al. 1999), even ant colonies dynamic (Lassau et al. 2005, Liu, et al. 2012) and host of other topics.

3.1.2. Enhanced Vegetation Index and the 2-band EVI (EVI2)

The biophysical performance of satellite VI measures of greenness has been consistently tested and proved useful and well correlated with continuous flux tower measurements of photosynthesis (Huete et al. 2006; Xiao et al. 2005, Rahman et al. 2005, Wu et al. 2016), which provide valuable information about the carbon cycle, phenology, and the seasonal and inter-annual changes in ecosystems. An accurate depiction of seasonal vegetation dynamics is a desired prerequisite for accurate ecosystem modelling, and improves confidence in VI products and model capabilities to predict longer term, inter-annual vegetation responses to climate variability. While the utility of the NDVI has been well established in climate science, one major weakness is its nonlinear behavior and saturation (Fig. 5) in high biomass vegetated areas (Huete et al. 2002; Ünsalan & Boyer, 2004; Gitelson, 2004; Vaiopoulos et al. 2004). Reduction of saturation effects and improved linearity adds to the observed accuracy in estimating biophysical parameters from the VI values and provides a mechanism for multi-sensor (resolution) scaling of VI values.

The enhanced vegetation index (EVI) was developed to optimize the vegetation signal with improved sensitivity in high biomass regions and improved vegetation monitoring through a de-coupling of the canopy background signal and a reduction in atmosphere influences (Huete et al. 1997; Huete et al. 2002).
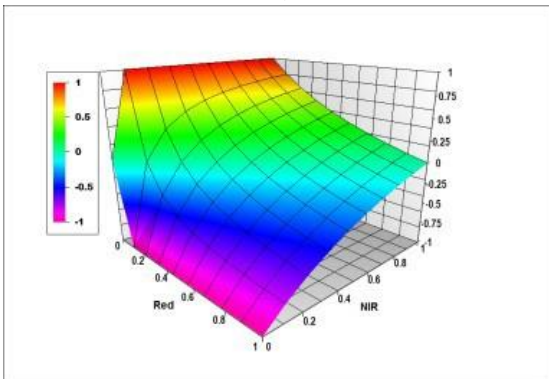
Figure 5: NDVI saturation, illustrated by the region of the curve where NDVI values remain unchanged or change little while NIR & Red change in response to canopy structure and biochemistry changes.

To also minimize the impact of turbid atmosphere on the VI one can use the difference in blue and red reflectances as an estimator of the atmosphere influence level (Huete et al 1997). This concept is based on the wavelength dependency of aerosol scattering cross atmosphere sections. In general, the scattering cross section in the blue band is larger than that in the red band. When the aerosol concentration is higher, the difference in the two bands becomes larger. This information is used to stabilize the index value against variations in aerosol concentration levels. EVI incorporates this atmospheric resistance concept as in the Atmospheric Resistant Index (ARVI, Kaufman et al. 1992), along with the removal of soil-brightness induced variations in VI as in the Soil Adjusted Vegetation Index (SAVI, Huete, 1988). The EVI additionally decouples the soil and atmospheric influences from the vegetation signal by including a feedback term for simultaneous correction (Huete et al. 1994). The 3-band EVI is expressed as:

$$EVI = G \frac{\rho_{NIR} - \rho_{red}}{\rho_{NIR} + C1 * \rho_{red} - C2 * \rho_{Blue} + L} \tag{3}$$

Where ρ_x are the full or partially atmospherically corrected (for Rayleigh scattering and ozone absorption) surface reflectances; L is the canopy background adjustment that addresses nonlinear, differential NIR and red radiant transfer through a canopy (based on Beer's law), and C_1, C_2 are the coefficients of the aerosol resistance term, which uses the blue band to correct for aerosol influences in the red band. The coefficients adopted for MODIS and S-NPP VIIRS were L=1, C_1=6, C_2=7.5, and G (gain factor) =2.5.

EVI has been used recently in a wide variety of studies, including those on land cover/land cover change (Wardlow et al. 2007), estimation of vegetation biophysical parameters (Chen et al. 2004; Houborg et al. 2007), phenology (Zhang et al. 2003, 2006; Xiao et al. 2006; Ahl et al. 2006, Huete et al. 2008), Evapotranspiration (Nagler et al. 2005), biodiversity (Waring et al. 2006), the estimation of gross primary production (GPP) (Rahman, et al. 2005; Sims et al. 2006), and for detecting the seasonality in the tics (Saleska et al. 2007; Saleska et al. 2016, Wu et al. 2016).

Comparisons of temporally aggregated flux tower measures of photosynthesis with satellite VI measures of greenness (Fig. 6) have shown a strong seasonal correspondence with the Enhanced Vegetation Index (EVI) from MODIS and SPOT-VGT sensors (Xiao et al. 2004, 2005; Rahman et al. 2005; Sims et. al. 2006, Huete et al. 2008). An example of this tight coupling at the Harvard Forest site is shown in Fig. 6. In the case of NDVI, there is some saturation and an overestimation of GPP. MODIS and SPOT-VGT EVI were also shown to depict phenology cycles in dense Amazon rainforests for the first time, confirmed by a strong linear and consistent relationship between seasonal EVI and tower-calibrated GPP measurements of carbon fluxes in both intact rainforest and forest conversion to pasture/agriculture sites in the Amazon (Huete et al. 2006; Xiao et al. 2005).
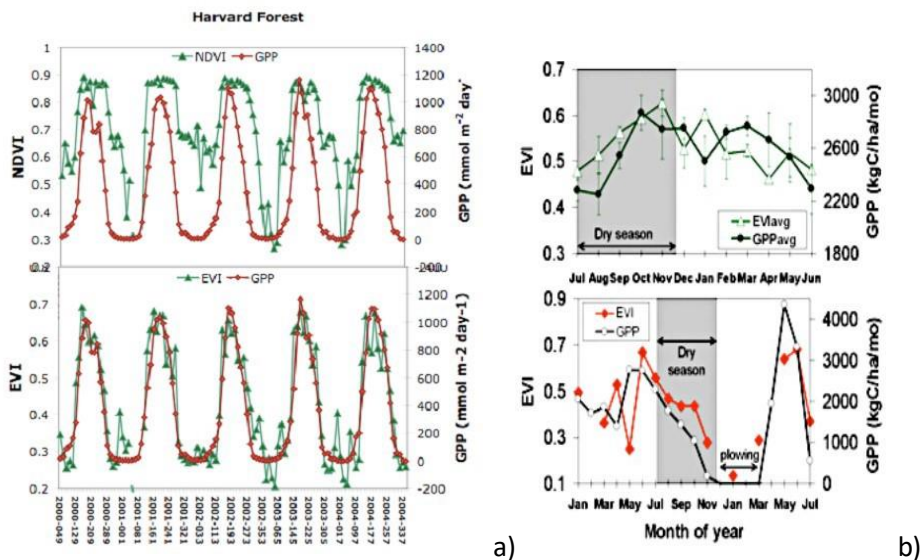
Figure 6. MODIS and SPOT VGT EVI are consistent in their phenological depiction of temperate and tropical ecosystems, providing in-situ based methods for assessment of VI performance and capabilities. a) 16-day MODIS VI's plotted with in-situ 16-day GPP flux measures at Harvard forests. b) Seasonal correspondence of MODIS EVI with tower flux measures of GPP in both intact rainforest (top) and forest conversion to pasture/agriculture (bottom) (Huete et al. 2006).

However, not all sensors (ex: AVHRR) have a blue band and the VIIRS blue band (band M3 at 478 - 498 nm) is spectrally different from EOS-MODIS counterpart (459 – 479 nm), which introduces potential differences. Addressing these issues may require adjusting the EVI coefficients (C2) for each new sensor to mitigate this continuity issue. Adjusting the EVI algorithm to work with other sensors' blue band will create problems in the long run. Additionally, 1) changing the C2 coefficient will add further confusion to what is supposed to be simple VI science algorithms creating further problems with backward compatibility with AVHRR and VIIRS, and future sensors that may yet again change the blue band, 2) some of the known issues in the EVI make adjusting the blue band C2 coefficient inadequate as it leaves other EVI problems

unresolved (Ex: poor performance over snow/ice and residual clouds). This suggested a need for a new formulation of EVI that addresses the Blue bands issues and preserves the advantages of EVI. A new EVI formulation, based on only two bands (red and NIR), was proposed by Jiang et al. 2008) evaluated, and successfully adopted to S-NPP VIIRS and to a MEASURES multi-sensors VI record (Didan et al. 2016).

3.1.3. The Compatibility 2-band EVI2 Algorithm

Recent cross-sensor studies have shown the feasibility of NDVI and EVI translation across several sensors systems (Gallo et al. 2005; Miura et al. 2006; Brown et al. 2006). EVI extension, however, is limited to only sensors that carry a blue channel, which includes SPOT-VGT, SeaWiFS, VIIRS, and other instruments. In contrast to the red and NIR bands, sensor-dependent blue channels are generally not as compatible and often do not overlap, e.g., the MODIS (459-479 nm), MERIS-blue (440-450 nm), and VIIRS-blue (478-498 nm) channels do not overlap, a spectral issue that restricts the compatibility of cross-sensor EVI values. Thus, it is recommended that cross-sensor algorithms should be based on VIs without a blue band (Fensholt et al. 2006, Jiang et al. 2008).

Since the blue band in the EVI does not provide additional biophysical information about vegetation properties, rather is aimed at reducing noise and uncertainties associated with highly variable atmospheric aerosols, a 2-band adaptation of EVI was developed to be compatible with EVI (Huete et al. 2006, Jiang et al. 2008). An earlier version of the 2-band EVI (EVI2) was used as the "backup algorithm" for MODIS EVI product for cases when the blue band yields problematic VI values, mainly over dense snow, or pixel with extensive subpixel clouds. The EVI2 remains functionally equivalent to the EVI, although slightly more prone to aerosol noise, which is becoming less significant with continuing advancements in atmosphere correction (Vermote et al. 2002, Lyapustin et al. 2012).

EVI2 is a 2-band adaptation of the EVI that eliminates the need for blue band, considering the blue provides no additional biophysical information and removing it does not compromise the index biophysical significance (Jiang et al. 2008). The 2-band adaptation of EVI is fully compatible with the 3-band standard EOS-MODIS EVI. The advantages of EVI2 is that it remains functionally equivalent to the 3-band EVI. and is based on a linearization method (Jiang et al. 2008) and geometrical analysis of spectral angles in the red-near infrared reflectance space.

The EVI2 is based on a linearization method and geometrical analysis of spectral angles in the red-Near infrared reflectance space (Fig. 7).
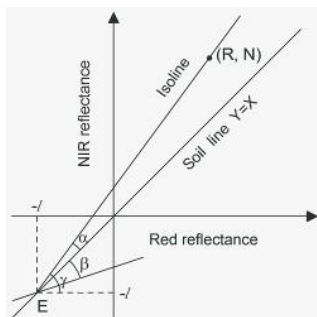
Figure 7. The isolines of the EVI/SAVI and their angles in red-NIR reflectance space

A linearized vegetation index (LVI) comparable to the EVI is obtained by adjusting the constant angle $\pi/4$ to a variable angle β, or soil background adjustment factor,

$$LVI(\beta) = \tan\left[arctan\left(\frac{SAVI}{1+L}\right) + \beta\right] \qquad (4)$$

Where: β describes a line across E deviating from the soil line in clockwise direction in Fig. 7. The LVI value of the soil line, Y=X, (LVI$_0$) is, LVI$_0$ = tan(β), which is described as,

$$LVI = G'\left[\tan\left(\alpha + \beta\right) - \tan\beta\right] = G\frac{\left(N - R\right)}{N + R\tan\left(\pi/4 + \beta\right) + L/\left(1 - \tan\beta\right)} \qquad (5)$$

Where a gain factor, G′, is multiplied in order to maintain the amplitude of the LVI as that of the EVI,

$$G = \frac{G'\sec^2 \beta}{(1 - \tan \beta)}$$ (6)

With optimal β and G, the differences between the LVI values and the EVI values could be minimized and become very small when atmospheric effects are insignificant and this optimal LVI is used as the 2-band EVI, i.e. EVI2 (Jiang et al. 2008). For a given combination of L and β, there is a single, optimal G that minimizes mean absolute difference (MAD) between EVI and EVI2, which results in G = 2.5 similar to the standard 3-band EVI, and the optimal parameter values for the EVI2 equation becomes:

$$EVI2 = 2.5 \frac{\rho_{NIR} - \rho_{red}}{\rho_{NIR} + 2.4 * \rho_{red} + 1}$$ (7)

The resulting relationship between EVI and EVI2 show their strong correspondence for the entire range of values (Fig. 8). The coefficient of determination between EVI and EVI2 is high (R^2=0.9986) with the Mean Absolute Difference (MAD) of 0.00346 reflectance units. It is important to note that because the 2-band EVI lacks the blue band it becomes prone to atmosphere contamination, although with modern atmosphere correction this issue is minimal, while maintaining the other advantages of EVI, being the minimization of background variation and the additional canopy sensitivity.
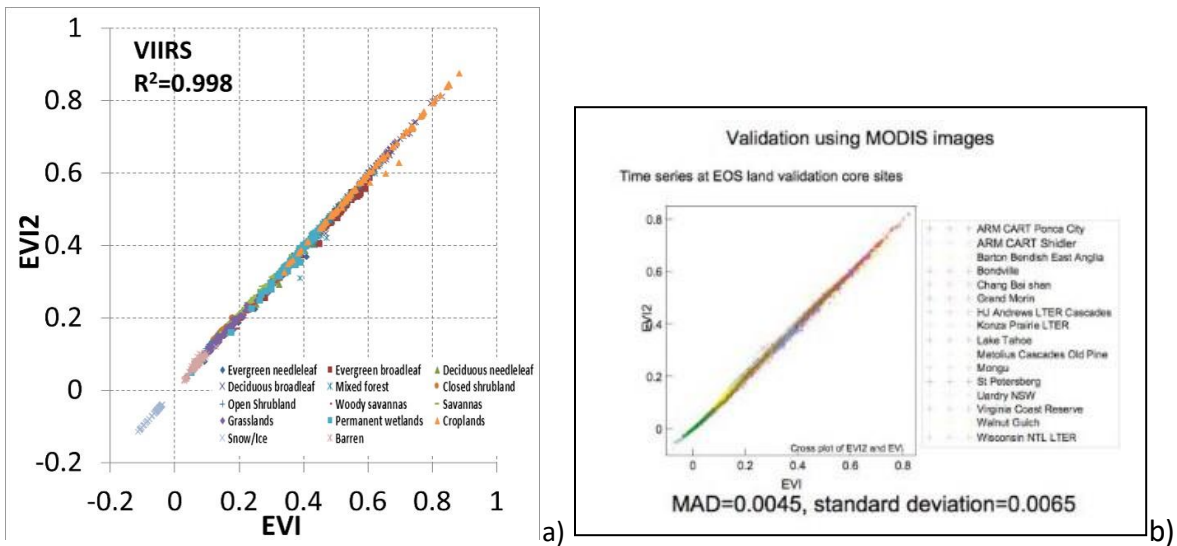
Figure 8. a) Relationship between EVI and EVI2 with 15-year MODIS and 5-year VIIRS data from 40 test validation sites). The correlation is almost 1:1, except for few EVI outliers. Data was strictly filtered.
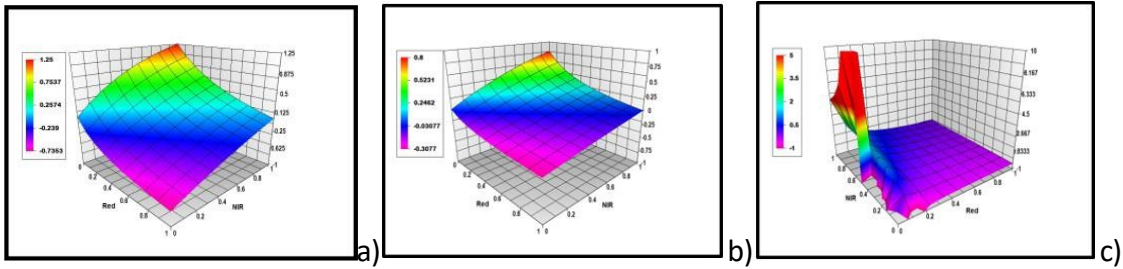
Figure 9. EVI2 Performance a) throughout the full red/NIR dynamic range in contrast with the EVI (3-band) performance. b) EVI under normal land surface conditions (Blue <0.1) and c) in the presence of snow/ice (Blue>0.1), where EVI becomes erratic.

EVI3 and EVI2 show a strong correspondence throughout the entire range of values and the global coefficient of determination between EVI3 and EVI2 is **r^2=0.998** with a mean absolute difference of **0.004**. This suggests and validates the decision of adopting EVI2 (requiring only red and NIR) as an effective backward (older sensors) and forward (newer sensors) compatible index for EVI (EVI3) and supports using it as a better long term alternative for VIIRS. This simplifies the continuity question, especially for EVI across sensors (Didan et al. 2010 & 2016, Marshall et al. 2016).

4. Compositing

VIs are usually generated from multi-day data through a process of composting (Holben 1986) to help remove clouds and minimize atmosphere contaminants (Huete et al. 2002). The process of selecting a representative day from a period of days is called 'compositing'. Compositing is typically performed over a pre-set period of days (7 [week], 8 [half the revisit period of a typical satellite], 10, 15 [bi monthly], 16 [synchronized with the satellite revisit, case of Terra/Aqua or S-NPP], etc… days) related to atmosphere (to minimize clouds). Daily data are analyzed to select a single cloud and gap free mosaic of pixels with minimal atmospheric and a sun-target-sensor close to nadir as possible (Holben, 1986, Huete et al. 2002). Moderate and coarse resolution sensors, such as MODIS, AVHRR (Agbu et al. 1994), *Systeme Pour l'Observation de la Terre 4-VEGETATION (*SPOT4-VEGETATION, Archard et al. 1994), SeaWiFS (Sea-Viewing Wide Field-of-View Sensor; Hooker et al. 1992), GLI (*Global Imager;* Nakajima et al. 1998), VIIRS (Justice et al. 2013) acquire global bi-directional radiance data of the Earth's surface under different solar illumination angles (Schaff et al. 2002) which introduce additional variability that need to be addressed (Morton et al. 2014) or mitigated.

Whereas, AVHRR-NDVI time series was never a standard product, rather was produced differently by different groups using the Maximum Value Compositing (MVC) technique (Holben 1986). This algorithm selects the daily observations with the highest NDVI value, as maximizing NDVI effectively eliminates all data issues (NDVI tend to decrease with clouds and other atmosphere issues). This procedure has minimal data quality checks (Goward et al. 1994; Eidenshink and Faundeer, 1994) as none was present in AVHRR data at the time. Residual cloud and atmospheric contamination tend to lower NDVI values, and hence a maximum NDVI would theoretically select the least cloudy and contaminated pixel. Moreover, the influence of atmospheric contamination and residual cloud cover increases with optical path length, hence the MVC tends to select the observation with the smallest view zenith angle (least optical path length), and smallest solar zenith angle although this angle does not change a lot during the composite period and is location and season dependent. This process standardizes the selected values (Holben 1986; Cihlar et al. 1994a) and minimizes most issues.

MVC works nicely over near-Lambertian surfaces where the primary source of pixel variations within a composite cycle is associated with atmosphere contamination and path length, however, its major shortcoming is that the anisotropic, bi-directional influences of the surface is not adequately considered or corrected. The bidirectional spectral behavior of numerous, 'global' land cover types and terrestrial surface conditions are highly anisotropic due to canopy structure, mutual shadowing, and background and soil contributions (Kimes et al. 1985; Leeuwen et al. 1994; Vierling et al. 1997). And while, ratioing of the NIR and red spectral bands to compute vegetation indices minimizes the surface anisotropy it does not remove surface anisotropy (Walter-Shea et al. 1997, Morton et al. 2014, Schaff et al. 2002) due to the spectral dependence of the BRDF response (Gutman, 1991; Roujean et al. 1992). The atmosphere counteracts and dampens the surface BRDF signal, mainly through the increasing path lengths associated with off-nadir view angles and/or sun angles. The maximum NDVI value selected is thus, related to both the bidirectional properties of the surface and the atmosphere, which renders the MVC-based selection unpredictable. The MVC favors cloud free pixels, but does not necessarily pick the pixel closest to nadir or with the least atmospheric contamination. Although the NDVI tends to increase for atmospherically corrected reflectance, it does not mean that the highest NDVI is an indication of the best atmospheric correction. Many studies show the MVC approach to select off-nadir pixels with large, forward-scatter (more shaded) view angles and large solar zenith angles, which are not always cloud-free or atmosphere clear (Goward et al. 1991; Cihlar et al. 1994b, 1997). This degrades the potential use of the VI for consistent and accurate comparisons of global vegetation types.

The MVC method tends to work better with atmospherically uncorrected data (Cihlar et al. 1994a), although numerous inconsistencies result (Gutman, 1991; Goward et al. 1991, 1994; Cihlar et al. 1994b, 1997). The MVC approach becomes even less appropriate with atmospherically-corrected data sets, since the anisotropic behavior of surface reflectances and vegetation indices is stronger (Cihlar et al. 1994b). The influence of surface anisotropy and bidirectional reflectances on the VI composited products becomes more pronounced with atmospherically corrected surface reflectances (Cihlar et al.1994a). Under many atmosphere conditions, the nadir view direction may produce the lowest VI value.

Alternatives to simply choosing the highest NDVI value over a compositing period, include integrating or averaging all cloud-free pixels in the period. Meyer et al. (1995) argued the importance and impact of surface anisotropy and sun/sensor geometry on the NDVI (from AVHRR), and suggested that averaging all high quality NDVI values was superior to the MVC approach. The Best Index Slope Extraction (BISE; Viovy et al. 1992) method reduces noise in NDVI time series by selecting against spurious high values and through a sliding compositing cycle.

Huete et al. (2002) proposed a modified Maximum Value Compositing (MVC) technique that relies on still maximizing the NDVI value, but preceded by a process of data filtering based on ancillary quality assurance (QA) information, the method is enhanced further by minimizing the viewing geometry. The pixel observations are analyzed to retain only the highest quality days based on the per pixel QA. The observation corresponding to the smallest view angle is then selected from the top 2/3 NDVI Values if possible. The method performance depends on the prevalence of clouds in particular. Over the tropics and the Taiga regions the lack of cloud free data reduces the method to the classical MVC, over other regions where clouds are not as problematic the method tends to select lower view angle whenever possible (Huete et al. 2002).

At the heart of producing science quality remote sensing data from frequently cloudy, noisy, atmosphere contaminated daily observations with spatial gaps is a production algorithm for multi-day compositing. Compositing evolved from a simple cloud screening approach based on the maximum value composite of NDVI images (Holben, 1986) to a robust quality assurance (QA) driven algorithm that also reduces aerosol influences and minimizes BRDF impacts by constraining the

view angle. The compositing algorithm used for EOS-MODIS VI is the Quality Assurance (QA) driven Constrained View Angle (CV) Maximum Value Composite (QA CV-MVC, Huete et al. 2002) and will select the best observation from a preset number of days. The method first eliminates cloudy and poor data based on the per-pixel QA and then selects the top 2/3 NDVI observations (MVC), to finally selects the observation with the smallest view angle (Figure 10).
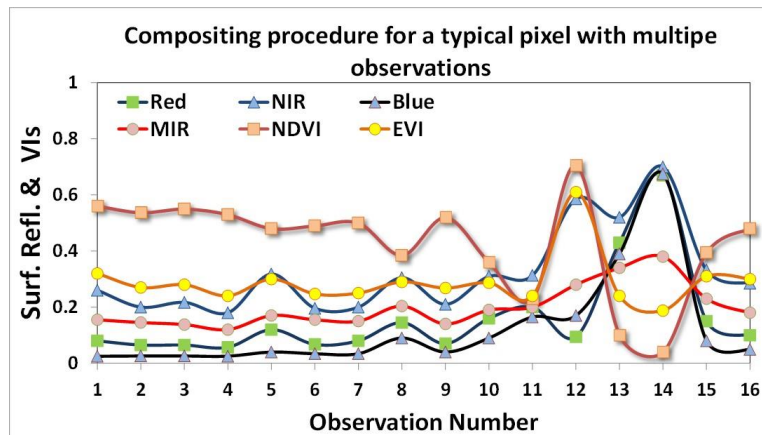
Figure 10: QA CV-MVC compositing algorithm. Daily data are QA analyzed and arranged into classes from best (left, stable with minimum noise) to worst (right, noisy data). The observation with the smallest zenith angle from the n-highest NDVI is selected. 'n' is usually set to 2 or 3 (Huete et al. 2002).

This implementation minimizes sensor view variations associated with the anisotropic surface reflectance properties (i.e., BRDF) and helps reduce spatial and temporal discontinuities in the composited product. This same method implemented in EOS-Terra/Aqua MODIS VI composting algorithm is used to generate the VIIRS VI time series with some minor enhancements.

One of the issues associated with compositing data using the CV-MVC method is the assumption that picking the observation with the lowest view zenith angle from the top 'n' NDVI observations guarantees the best observation. While that may be true in terms of BRDF, and makes sense if the top NDVI values are only slightly different due to BRDF, in many instances using the view angle to pick the best observation leads to selecting the lower NDVI and sometimes even poor quality data (when there is limited number of good observations only to choose from). With VIIRS, we introduced a work around based on the use of View Angle bins. By grouping the data into view angle bins of [0-30°] and [> 30°] and then using the MVC we guarantee selecting the best possible observation based on maximizing the NDVI with a reasonable view angle, assuming view angle < 30 degrees insurances minimum BRDF and bowtie effect (which is already less problematic in VIIRS – Fig. 16).

The VIIRS VI algorithm performance, as was the case with MODIS, depends heavily on the provision of QA flags, with VIIRS using an identical per-pixel QA approach to the EOS-MODIS QA flags we expect the algorithms performance to be generally similar. There remains some QA performance issues in VIIRS, such as cloud and snow/ice (Vargas et al. 2013), but are expected to be addressed with new iterations of VIIRS reprocessing (Justice et al. 2013).

4.1.   Composite Algorithm Spatial Considerations

The EOS-MODIS and Suomi-NPP-VIIRS sensor-viewing configuration, while slightly different, results in considerable spatial overlap between orbits when away from the Equator. VIIRS controls

the pixel growth rate at the edge of the scan, which in turn minimizes the bow-tie effects. The sensors field of view or swath does not line up with the projection (Sinusoidal) grid pixels (Fig. 11 & 12), which has spatial implications that needs to be addressed during compositing to capture the grid pixel proper biophysical content. VIIRS compositing algorithm uses the EOS-MODIS VI '*weighted average pixels*' scheme to reconstruct the grid/pixel from all the finer L2/L2G overlapping observations. The VI algorithm suite makes use of all available observations rather than retaining only the observation with the maximum overlap (some Land algorithms use this strategy).
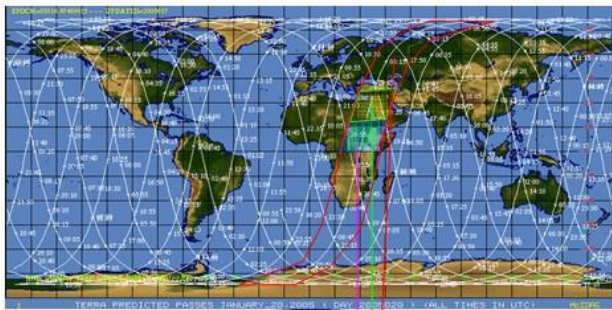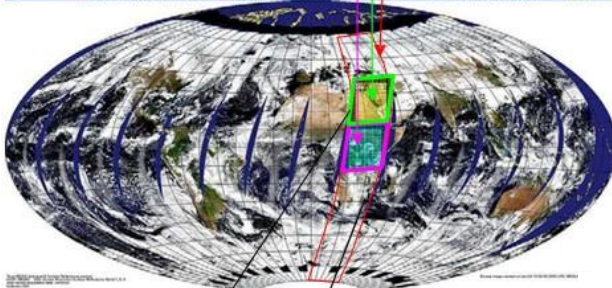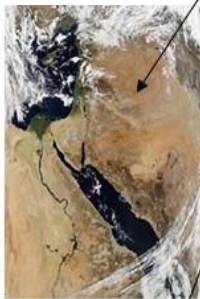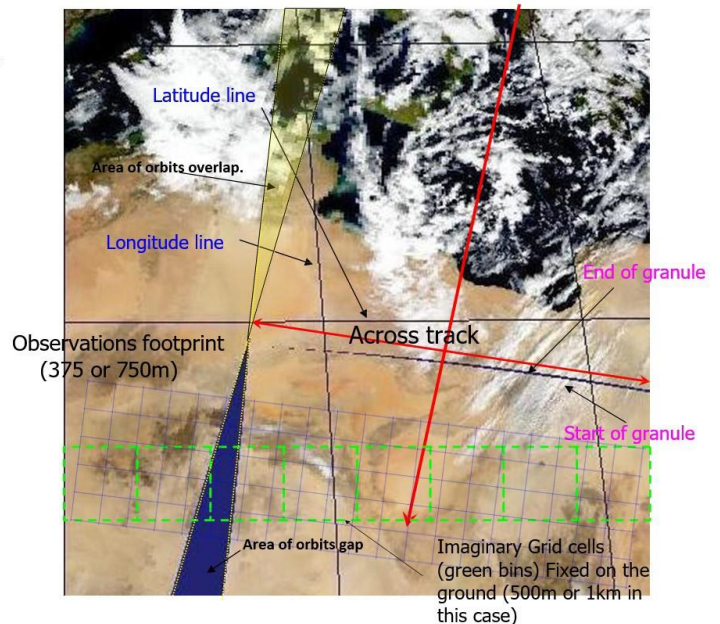
Figure 11: VIIRS viewing geometry and observations layout. Not to scale and orientation and layout are only informative. The lower right figure shows the relation between orbits, observations, grids, and overlap.
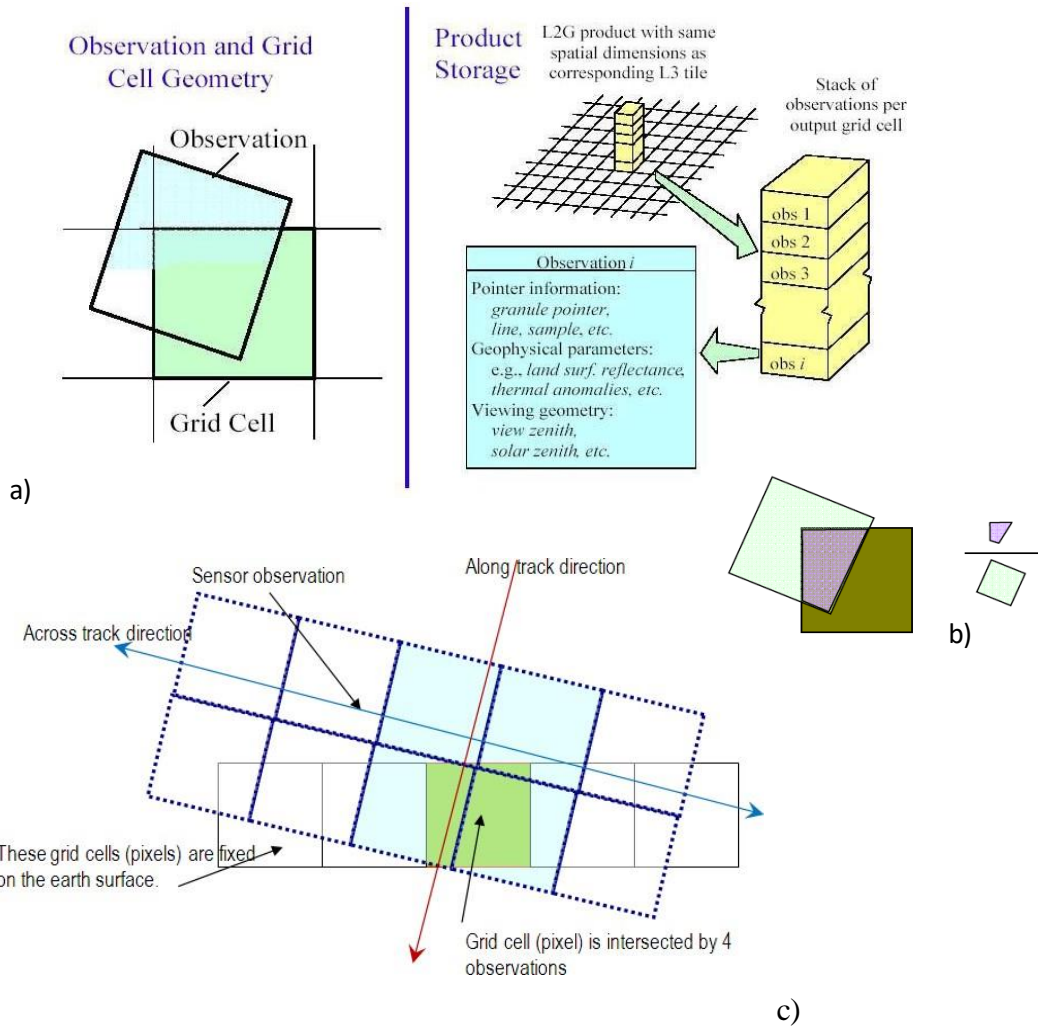
Figure 12: a) Level 2G processing. Each observation is assigned to a fixed grid cell along with an observation coverage that indicates the degree of overlap (b). Depending on the latitudinal location the number of observation assigned to a particular grid cell will vary and can be very high, resulting from the number of orbits (highest overlap at the poles) and the size of observation which tends to grow away from the center of the scan (Wolfe t al. 1998). The Inset (b) shows how the observation coverage is computed, and it is the area of overlap to the observation size itself. c) Daily L2G grid cell observations are reconstructed from orbital/granule data. Each grid cell will be constructed from all overlapping observations.

The construction of the grid cell follows this equation:

$$SR = \frac{\sum_{i=1}^{n} \omega_i SR_i}{\sum_{i=1}^{n} \omega_i}$$
(8)

where SR is the surface reflectance of the grid pixel. SR_i and ω_l are the surface reflectance of the underlying L2 observations adjusted by their degrees of overlap.

4.2.   BRDF Considerations

Although VIs can be generated with any level data, the standard now is fully atmospherically corrected and standardized surface reflectances based VIs. VIs are usually derived from calibrated radiances and are usually computed from surface directional reflectances that have been atmospherically-corrected to remove absorbing gases, molecular scattering, aerosols, and water

vapor (Justice et al. 2013). Additionally, the VI products will normally be produced under local solar zenith angle conditions that may result in second-order seasonal and latitudinal biases (Huete et al, 2006, Morton et al, 2014). Bidirectional reflectance distribution function (BRDF) considerations are traditionally not addressed during standard VI production. Similar to EOS-MODIS, the VIIRS Land product suite implemented a standardized viewing geometry correction algorithm to generate a nadir equivalent land surface reflectance (VIIRS nBAR [VNP43 suite], Schaaf et al. 2002). While this product standardized the view angle to nadir, the sun angle was only standardized to the local solar noon since no fixed global sun angle could be adopted. This product is available to users who wish to generate a BRDF adjusted VI product suite (Zhang et al. 2003), however our SCF team will only generate VIs from the directional data not adjusted for viewing geometry to retain consistency with EOS-MODIS and to minimize the biases that may result from the choice of a BRDF correction method and loss of traceability to sensor data, since a BRDF adjusted data is modeled and not a true sensor collected observations.

Other potential venue to dealing with the BRDF is the adoption of surface reflectance inputs corrected by the MAIAC approach (Lyapustin et al. 2012) and/or a hybrid method like the one proposed by Morton et al. (2014). No standardized single method or model for BRDF correction exists, although all are based on the same principles. For these reasons, our suite of algorithms will not attempt to explicitly and directly correct for BRDF effects except by constraining the view angle during compositing. This leaves the users the option of exercising their preferred and research/project specific BRDF correction model (Morton, et al, 2014). Furthermore, if and when the VIIRS Land team, in particular the surface reflectance science team(s), start to generate a consistent operational BRDF corrected surface reflectance suite our algorithm will ingest these data and produce a BRDF- standardized VIIRS VI product suite.

4.3.   VIIRS Output observations QA and Pixel Reliability

All S-NPP VIIRS Land products use a per-pixel QA system of flags to characterize the atmosphere and inform about processing which is very similar to EOS-MODIS approach. A pixel is assigned a list of QA attributes (cloud, cloud shadow, aerosol load, snow/ice, land water mask, etc.) stored in binary bit fields. These QA attributes assist with post processing and provide users with a systematic approach to analyze the data and decide what to retain and discard. As robust and comprehensive as this information is, average users found it quite challenging to work with because:

- Complexity of QA data structure, especially the use of binary bit fields that require special tools to work with; and
- No unique method on how to work with or combine these QA flags into operational data post-processing scheme. In most cases, users used only few of these flags or even used them improperly.

This made the per-pixel QA information a challenge to work with for a large segment of the user community. A solution was proposed for the EOS-MODIS VI (Didan & Huete, 2006) to help synthesize this QA information into a simple ordinal rank. This is particularly important as the VIIRS mission takes shape and draws from the EOS-MODIS experience. Reanalysis of the MODIS VI product record showed that apart from cloud and snow/ice, aerosol, shadow and

viewing geometry were the most problematic, yet users assume they are properly corrected in the atmosphere correction algorithm. We enhanced the original method (Fig. 13) and implemented additional classes in VIIRS VI data record. In addition to the standard QA, each pixel will have this simple rank or **reliability index** number to help decide if it is of any use to post-processing.
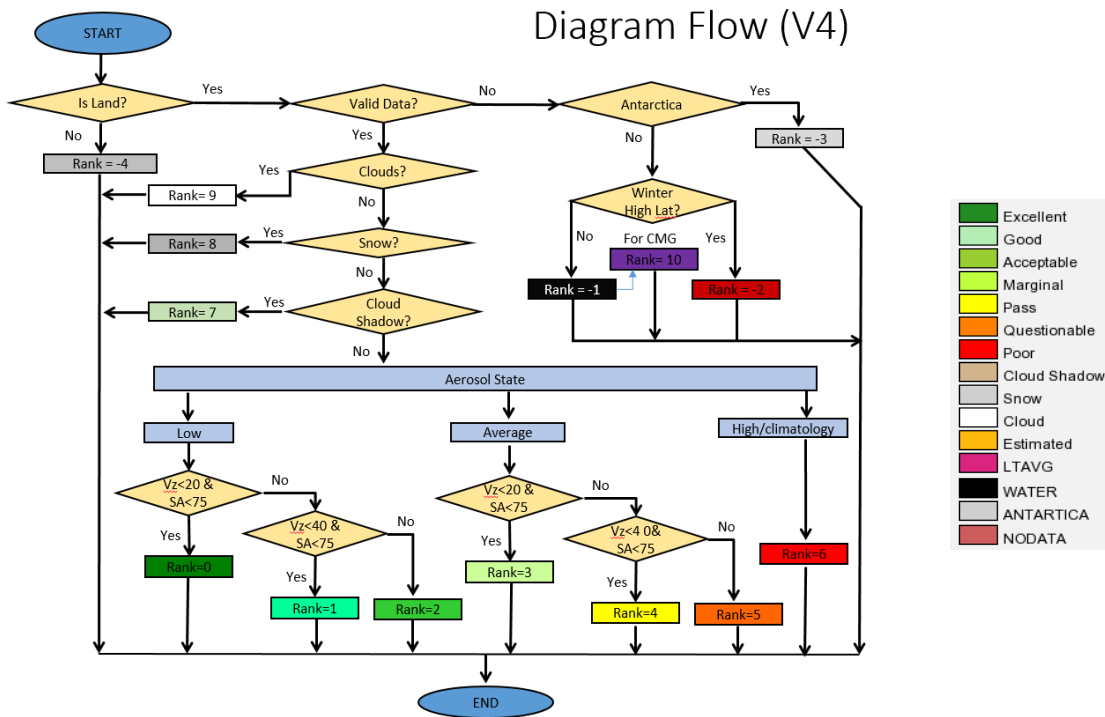
Figure 13: VIIRS Per Pixel Reliability assignment scheme. Some rank classes are specific to the CMG product suite (gap filing).

This data reliability index considers the significance of each QA field and combines this information into a single rank value. The metric indicates the usefulness of the data while eliminating a great deal of inconsistency related to using QA flags. An evaluation of this metric for EOS-MODIS (Didan & Huete, 2006) indicates that this per-pixel reliability index was effective and easy to use. The standard QA flags will continue to be part of the products and users can still apply their own QA post-analysis approach.

4.4. Spatial gaps filling

A large percentage of composited data will be of no science value to applications or research due to the presence of clouds and/or other atmosphere contaminants, particularly over the tropics and in high latitude regions where these problems are persistent for long periods of time. For the modelling community that require strictly high quality data, even if estimated, we only retain high fidelity data (based on QA) in the CMG product suite (Andree et al. 2004, Justice et al. 2003). This results in extensive spatial gaps that need filling. We are currently using a simple interpolation scheme based on long-term data. Using the VIIRS time series data we can generate a mean value for each date from strictly filtered data that is cloud and mostly contaminants free. In case no observations could be found (persistent clouds) we simply leave the observation empty.

As the time series grows, we expected all pixels to have a value in the long term data record that could be used to fill missing days.

5. VIIRS Overview and Instrument Characteristics

The VIIRS sensor aboard S-NPP was conceived based following the long heritage of operational and research instruments, dating back to the seventies, including:

- Advanced Very-high Resolution Radiometer (AVHRR) on NOAA's Polar- orbiting Environmental Satellites (POES).
- Moderate-resolution Imaging Spectroradiometer (MODIS) on NASA's Earth Observing System (EOS) Terra and Aqua satellites.
- Sea-viewing Wide Field-of-view Sensor (SeaWiFS) on GeoEye's SeaStar satellite.

The VIIRS design largely followed the success of MODIS, especially the large number of dedicated and discipline oriented bands, use onboard calibration, and other improvements including a novel pixel size control in the scan direction. And like with Terra/Aqua VIIRS orbits control eliminates the drift that plagued AVHRR.
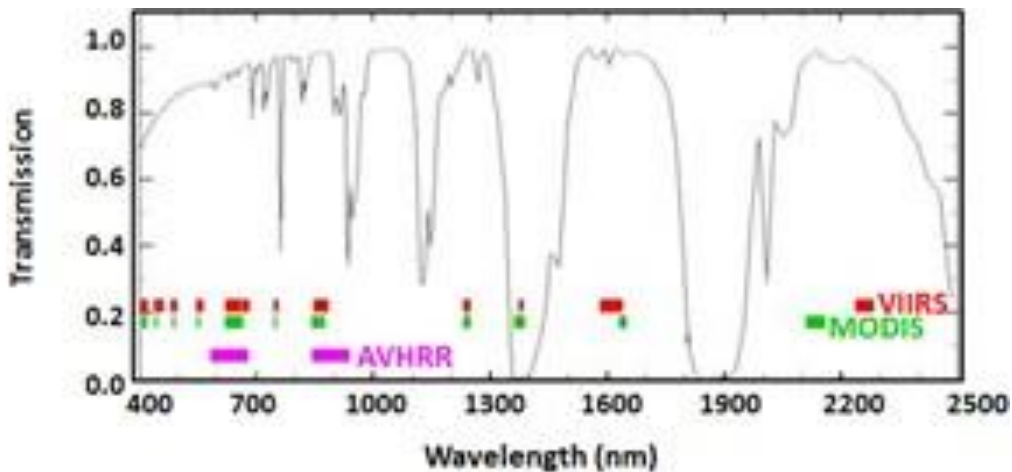
Figure 14: AVHRR, MODIS, and VIIRS Spectral bands

5.1. VIIRS Design and characteristics

The VIIRS is a whiskbroom scanning radiometer with a 112.56° field of view in the cross-track direction. At a nominal altitude of 829 km, the swath width is 3060 km, providing full daily coverage both in the day and night side of the Earth. VIIRS has 22 spectral bands covering the region 0.412 μm to 12.01 μm (Table 1), including 16 moderate resolution bands (M-bands) with a spatial resolution of 750 m at nadir, 5 imaging resolution bands (I-bands) – 375 m at nadir, and one panchromatic DNB with a 750 m spatial resolution throughout the scan. The M-bands include 11 Reflective Solar Bands (RSB) and 5 Thermal Emissive Bands (TEBs). The I-bands include 3 RSBs and 2 TEBs (Cao et al. 2013b).

VIIRS uses six dual-gain RSBs with a wide dynamic range needed for ocean color applications, at the same time without saturating the sensor when observing high reflectance surfaces such as land and clouds. The dynamic range of the dual gain bands in high gain mode is comparable to that of the MODIS ocean color bands, while the dynamic range in the low-gain state is comparable to those of the similar MODIS land bands. The dynamic ranges across all other bands are similar to their MODIS counterparts (Cao et al. 2013b).

VIIRS uses a unique approach to control the pixel growth towards the edges of the scan line – an issues in MODIS, AVHRR, and other instruments. This results in comparable footprints from VIIRS observations from nadir to edge-of-scan.

5.2.   VIIRS Geometric Characteristics

The following text is mostly from Cao et al. (2013b). Each VIIRS I (Imagery) bands has 32 detectors and each M-band has 16 detectors in the along-track direction. These are rectangular detectors with the smaller dimension in the along scan direction. This design accounts for the variable pixel growth rates in the scan and track directions. The sensors sweeps the Earth surface from about -56.28° to +56.28° view angle. Because VIIRS detector spacing is constant, the angular sampling interval is also constant. However, the corresponding horizontal sampling interval, or ground sample distance, in the along-track direction grows as the scan angle moves away from nadir, mainly due to the increased distance between the sensor and the ground, as shown in the lower panel in Figure 12. The scan width increases from 11.7 km at nadir to 25.8 km at the end of scan due to this panoramic effect, called the "bow-tie" effect. The bow-tie effect leads to scan-to-scan overlap, which start to show visibly at scan angles greater than approximately 19°, as shown in the lower panel in Figure 11. The size of overlap is more than 1 and 2 M-band pixels at scan angle greater than 31.72° and 44.86°, respectively. To save the downlink bandwidth, the radiometric readings from these pixels are not transmitted to the ground and will be assigned fill values by the ground software. This is called "bow-tie deletion". As a result, visual artifact of "missing scan line segments" shows up in raw images if the data is displayed in sample space, as shown in the example (upper panel in Figure 11). This artifact does not appear when the image is displayed when the scan is projected (gridded) onto the Earth's surface.

In the scan (cross-track) direction, the constant sampling time interval also results in the growth of HSI as a function of scan angle. The HSI change in the cross-track direction is even larger than that in the along-track direction because it is affected by the Earth's curvature in addition to the increased range between the sensor and the ground. This is shown by the dotted line for the un-aggregated M-band in the upper panel in Figure 12. To minimize variation of the HSI in the scan direction, there are three pixel aggregation modes in the along-scan direction, as shown in the lower panel in Figure 11 for the case of
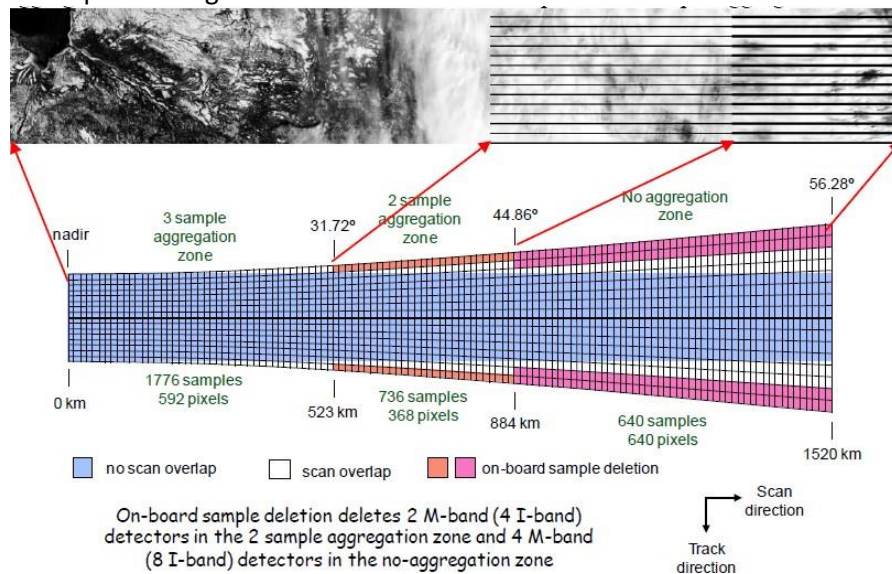
Figure 15: Schematics of bow-tie effect, bow-tie deletion and aggregation scheme for single-gain M-bands (scale is exaggerated in the track direction). Upper: example of bow-tie deletion effect when the raw data is displayed in sample space.
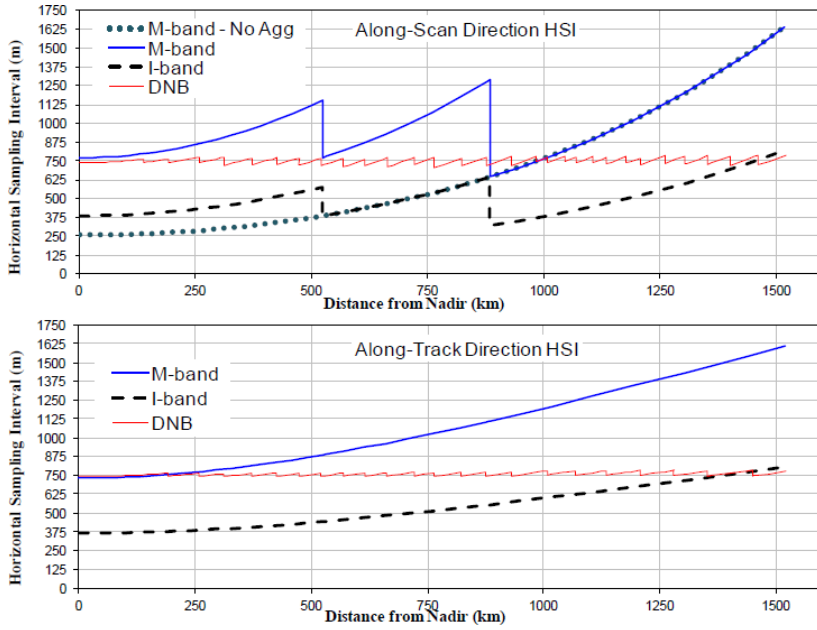
Figure 16: Horizontal Sampling Intervals (HSIs) for single-gain and dual-gain M-bands, I-bands and DNB

This aggregation scheme results in better radiometric and geometric performance for M- and I-bands in the 2-sample and 3-sample aggregation zones. This minimize the bow-tie effect observed in MODIS and eliminates some geometric issues.

5.3.   VIIRS Spectral Bands

The VIIRS 22 spectral bands are optimized for either land or ocean. The nominal VIIRS spectral bands responses are in Figures 13 (a & b), which also shows AVHRR bands for comparisons
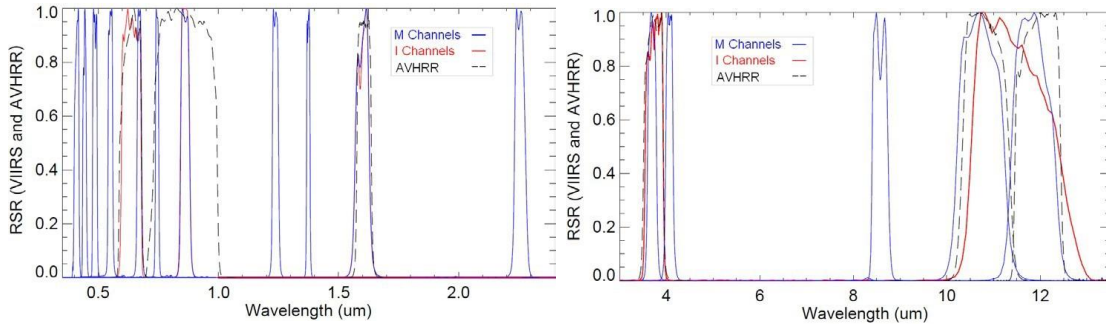
Figure 17: VIIRS spectral bands specifications

Table 1: VIIRS Spectral, Spatial, and Radiometric Characteristics. Green circles indicate the bands used and passed to users in the VI product files. Yellow circles (M5 and M7) indicate the bands used in thee earlier LPEATE versions of the 1km product suite. Most VIIRS spectral bands are comparable to those in MODIS. For the reflective bands most of VIIRS bands have wider bandwidth except for the near-infrared bands that are comparable to those from MODIS.

	Band No.	Driving EDR(s)	Spectral Range (um)	Horiz Sample Interval (km) (track x Scan)		Band Gain	Ltyp or Ttyp (Spec)	Lmax or Tmax	SNR or NEdT (K)	Measured SNR or NEdT (K)	SNR Margin (%)
				Nadir	End of Scan						
Reflective Bands — VisNIR	M1	Ocean Color Aerosol	0.402 - 0.422	0.742 x 0.259	1.60 x 1.58	High	44.9	135	352	723	105%
						Low	155	615	316	1327	320%
	M2	Ocean Color Aerosol	0.436 - 0.454	0.742 x 0.259	1.60 x 1.58	High	40	127	380	576	51.5%
						Low	146	687	409	1076	163%
	M3	Ocean Color Aerosol	0.478 - 0.498	0.742 x 0.259	1.60 x 1.58	High	32	107	416	658	58.2%
						Low	123	702	414	1055	155%
	M4	Ocean Color Aerosol	0.545 - 0.565	0.742 x 0.259	1.60 x 1.58	High	21	78	362	558	54.1%
						Low	90	667	315	882	180%
	I1	Imagery EDR	0.600 - 0.680	0.371 x 0.387	0.80 x 0.789	Single	22	718	119	265	122.7%
	M5	Ocean Color Aerosol	0.662 - 0.682	0.742 x 0.259	1.60 x 1.58	High	10	59	242	360	49%
						Low	68	651	360	847	135%
	M6	Atmosph. Correct.	0.739 - 0.754	0.742 x 0.776	1.60 x 1.58	Single	9.6	41	199	394	98.0%
	I2	NDVI	0.846 - 0.885	0.371 x 0.387	0.80 x 0.789	Single	25	349	150	299	99.3%
	M7	Ocean Color Aerosol	0.846 - 0.885	0.742 x 0.259	1.60 x 1.58	High	6.4	29	215	545	154%
						Low	33.4	349	340	899	164%
Reflective Bands — S/MWIR	M8	Cloud Particle Size	1.230 - 1.250	0.742 x 0.776	1.60 x 1.58	Single	5.4	165	74	349	371.6%
	M9	Cirrius/Cloud Cover	1.371 - 1.386	0.742 x 0.776	1.60 x 1.58	Single	6	77.1	83	247	197.6%
	I3	Binary Snow Map	1.580 - 1.640	0.371 x 0.387	0.80 x 0.789	Single	7.3	72.5	6	165	2650.0%
	M10	Snow Fraction	1.580 - 1.640	0.742 x 0.776	1.60 x 1.58	Single	7.3	71.2	342	695	103.2%
	M11	Clouds	2.225 - 2.275	0.742 x 0.776	1.60 x 1.58	Single	0.12	31.8	10	18	80.0%
Emissive Bands	I4	Imagery Clouds	3.550 - 3.930	0.371 x 0.387	0.80 x 0.789	Single	270	353	2.5	0.4	84.0%
	M12	SST	3.660 - 3.840	0.742 x 0.776	1.60 x 1.58	Single	270	353	0.396	0.12	69.7%
	M13	SST Fires	3.973 - 4.128	0.742 x 0.259	1.60 x 1.58	High	300	343	0.107	0.044	59%
						Low	380	634	0.423	--	--
Emissive Bands — LWIR	M14	Cloud Top Properties	8.400 - 8.700	0.742 x 0.776	1.60 x 1.58	Single	270	336	0.091	0.054	40.7%
	M15	SST	10.263 - 11.263	0.742 x 0.776	1.60 x 1.58	Single	300	343	0.07	0.028	60.0%
	I5	Cloud Imagery	10.500 - 12.400	0.371 x 0.387	0.80 x 0.789	Single	210	340	1.5	0.41	72.7%
	M16	SST	11.538 - 12.488	0.742 x 0.776	1.60 x 1.58	Single	300	340	0.072	0.036	50.0%

6. What is new in this initial S-NPP VIIRS VI Data Record release

This initial S-NPP VIIRS VI data record has gone through a series of refinements and reprocessing prior to this first public release. These changes aimed at implementing learned lessons from the EOS MODIS era in particular and introduced a series of enhancements along these topics:

- This release uses daily VIIRS L2G data (500m and 1km) as the primary input
- We currently generate three different vegetation indices: NDVI, EVI and EVI2. While EVI and EVI2 are interchangeable and identical, issues related to operational EVI generation (blue band noise, snow, sub-pixel clouds, and aerosols) required the use of an EVI backup algorithm which is based on only the red & NIR bands (EVI2, Jiang et al 2008)
- The Green and all SWIR bands are now included in the output files
- Monthly products use both Terra and Aqua like S-NPP VIIRS VI input streams
- Monthly 1km product now uses only the input pixels that actually overlap the month
- Product files are now output in HDF5-EOS5
- Improved the processing rules
- We introduced a static Land/Water mask for CMG products that minimize issues associated with the internal LA mask. The full VIIRS VI product suite will also start using an ancillary LW mask that bypasses the L2G pixel LW mask in future reprocessing.

7. VIIRS VI Product Suite Description

7.1. VIIRS VI Suite Production Plan

Figure 18 shows the current Algorithm/Product suite. Three VIs (NDVI, EVI2, and EVI) along with their input surface reflectance, QA, Viewing geometry, and ancillary info, at 500 m, 1 km, and a climate modeling grid resolution (0.05°,5.6km), and at 16 days (VIIRS ground-track repeat cycle), monthly are generated. The blue band at 750 m will be resampled to 500m in order to generate the 500m EVI3, as was done with EOS-MODIS EVI3. These production choices are made in support of and to promote continuity with the EOS-MODIS VI record and to simplify the transition.
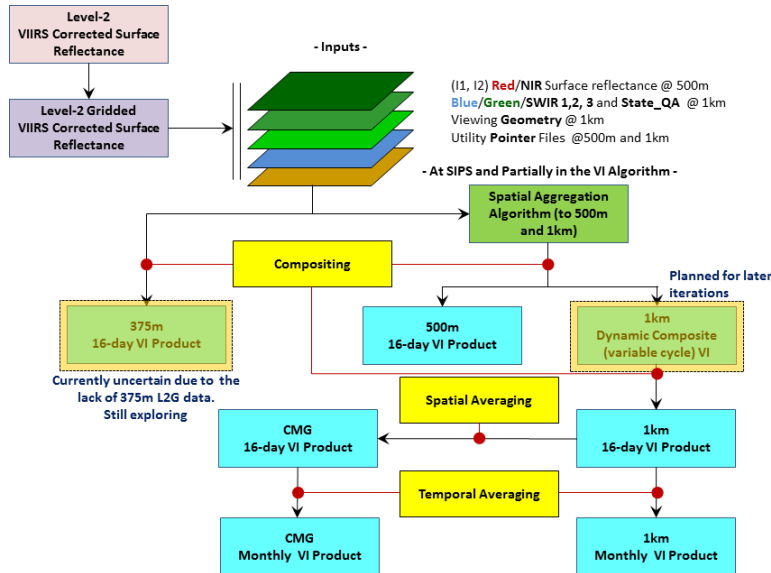
Figure 18: Production algorithms and dependencies. Some of these production choices will change with subsequent reprocessing.

This production scheme is an EOS-MODIS heritage that may change. The products are output in tile units that are approximately 10° x 10° in the sinusoidal grid projection, while the CMG product will be output in global geographic projection. When mosaicked, all tiles cover the globe. Each VI output file contain multiple Science Data Sets representing the per pixel, physical, viewing, and other information (NDVI, EVI3, EVI2, QA, red, NIR, blue, SWIR1-3, view angle, sun angle, and relative azimuth angle, pixel reliability, and composite DOY). All products will be stored in the HDF5-EOS format.

The S-NPP VIIRS Vegetation Index product suite is composed of:

1. **VNP13A1**: 16-day 500m VI (2 streams that are 8 days apart)
2. **VNP13A2**: 16-day 1km VI (2 streams that are 8 days apart)
3. **VNP13A3**: Monthly 1km VI
4. **VNP13C1**: 16-day 0.05deg VI (2 streams that are 8 days apart)
5. **VNP13C2**: Monthly 0.05deg VI

The first two products directly ingest daily level 2 gridded (L2G) product surface reflectance (daily VNP09A1/A2 series). The last three products are all based on the Vegetation Index VNP13A2 tiled data and uses aggregation schemes in time and/or space (Figure 18). The CMG products use a spatial averaging and reprojecting scheme from the tiled sinusoidal product suite to geographic lat/lon.

7.2. Terra and Aqua like Phased Production

While there is a single S-NPP VIIRS sensor and data stream, we are generating the 16-day VIIRS VI products 8 days apart to create identical streams to MODIS Terra and Aqua and assist the users during the transition period. In general, we follow the sensor/satellite repeat cycle of 16 days, however producing Terra and Aqua on the same composite day forces users to select one stream only given their high similarity. To separate the two streams (T & A) the EOS MODIS VI generates the product suite 8 days apart to help increase their temporal frequency. In production this scheme generates a Terra like time series on the usual DOY cycles (01/01, 01/17, 02/02, etc.). Aqua like VIIRS data is then generated on DOY 01/09, 01/25, 02/10, etc. To accommodate this processing arrangement (Fig. 19), the production rules are:

- For VIIRS 500m/1km
  - Start January 1st and process all days till January 16th (16 days) and get one product output on DOY 01/01 (Terra like stream)
  - Then process data between January 9th till Jan. 24th (16 days) and get another product output DOY 01/09 (Aqua like stream)
  - Repeat the process moving 8 days forward
  - At the end of the year and to complete the 16-day composite period supplement the last 16-day cycles with data from the new year
- For the 1km monthly and since it is a calendar month:
  - Process all 16-day products for that calendar month and generate one VIIRS monthly product
  - Each month will either ingest 5 or 6 16-day products
  - Only if the composite DOY of the pixel intersects the month will the pixel be used
- For the 16-day CMG, there will be two streams (8-days apart):
  - Start January 1st and process all 16-day tiles to get one product output on DOY 01/01
  - Ingest all 16-day tiles following the Jan. 9th, Jan. 25th, etc. to get one product output for DOY 01/09, 01/25, etc.
  - There will be one CMG each 8-day
- For the monthly CMG and since it is a calendar month, the rules are:
  - Process all the 16-day CMG products for the calendar month and generate one VIIRS monthly product
  - Each month will ingest 5 or 6x 16-day cycles
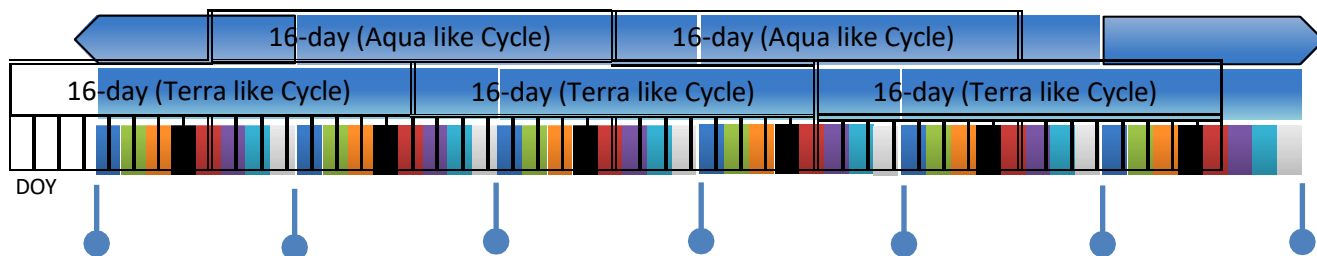
Figure 19: The 16-day VIIRS products are generated 8 days apart, a production scheme similar to the Terra/Aqua phased production approach while based on a single sensor. This improves the temporal frequency of the product record but also creates some bias and data repeat due to the overlap.

We evaluated the impact of this production scheme and the resulting overlap on the data and time series using daily surface reflectance processed in our Science Compositing Facility (SCF,

---

vip.arizona.edu) and the current (V2) versions of the VIIRS VI Algorithms.

	017	025	033	041	049	057		017	025	033	041	049	057
NDVI	6168	6168	6990	7096	7453	7453	NDVI	4485	4629	4629	4774	4774	4346
EVI	3641	3641	4074	3766	4311	4311	EVI	1880	1664	1664	1664	1664	1925
EVI2	3658	3658	4063	3760	4295	4295	EVI2	1850	1654	1654	1655	1655	1893
QA	2185	2185	2185	2116	2116	2116	QA	2116	2116	2116	2116	2116	2116
RED	650	650	487	413	403	403	RED	590	478	478	447	447	651
NIR	2743	2743	2749	2432	2762	2762	NIR	1550	1302	1302	1264	1264	1652
BLUE	303	303	239	201	200	200	BLUE	310	239	239	223	223	341
GREEN	714	714	653	550	554	554	GREEN	492	388	388	362	362	531
SWIR1	3257	3257	3056	2789	2968	2968	SWIR1	1776	1472	1472	1478	1478	1981
SWIR2	2765	2765	2369	2085	2056	2056	SWIR2	1600	1316	1316	1311	1311	1811
SWIR3	1676	1676	1353	1235	1151	1151	SWIR3	1154	938	938	916	916	1327
VZA	2941	2941	2975	1117	2993	2993	VZA	2353	2893	2893	2911	2911	2318
SZA	5766	5766	5049	4742	4474	4474	SZA	5344	4983	4983	4449	4449	4320
RAA	-638	-638	-2480	-2475	-2469	-2469	RAA	-624	-2471	-2471	-2463	-2463	-586
CDOY	27	27	45	55	61	61	CDOY	29	36	36	52	52	61
Rank	3	3	3	0	1	1	Rank	1	1	1	1	1	1
Pweight	0	0	0.5	0.5	0	0	Pweight	0	0.5	0	0.5	0	0

Figure 20: Compositing DOY resulting from the 8-day overlap between the two VIIRS-VI data streams. Data from Tile h08v05 and year 2017. On average 50% of the data repeats (considering only at a limited data set in space and time). However, there are temporal gains by salvaging good observations that would have been otherwise discarded when compositing every 16 days only.
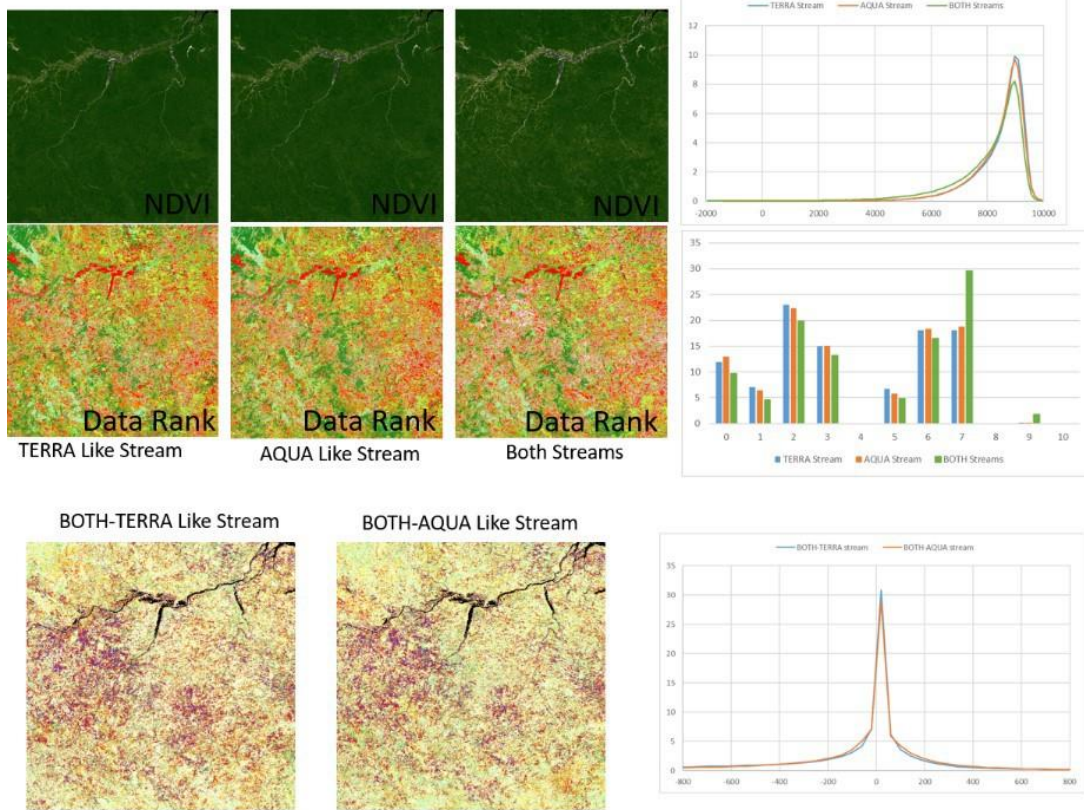
Figure 21: Impact of VIIRS phased production on the monthly VI Data record (Tile h12v09 Amazon, 2017). Top images show the NDVI and data Rank, a measure of quality, the bottom images show the differences between the VI when using both data streams vs a single stream. Minor differences exist but there is no bias. The minor rank drop in the monthly product when using both data streams resulted from the Algorithm use of the worst-case scenario approach with QA.

While limited in space and time these test results show:

- Improved temporal frequency and potential benefits over areas with generally less clouds
- Around 50% redundancy (repeated days)
- The approach minimizes data losses (discarded with only 16-day composite)

Data records form these production schemes are labeled "Regular production" (in the metadata) and are compositing following the 1-16, 17-32, 33-48, etc and "Phased production" compositing following the 9-24, 25-40, 41-56, etc intervals.

All output products carry identical Science Data set layers that are quite similar to the EOS MODIS data record. Each VI product contains three vegetation indices (NDVI, EVI, EVI2), seven surface reflectance's (Red, NIR, Blue, Green, SWIR1, SWIR2 and SWIR3), view geometry (Sensor Zenith Angle, Sun Zenith angle, and Relative Azimuth) and quality information layers (Rank and State QA). Example images of these layers are shown in Figure 22.

NDVI	EVI	EVI2	Red (600-680 nm)
NIR (846-885 nm)	Blue (478-498 nm)	Green (545-565 nm)	SWIR1 (1230-1250 nm)
SWIR2 (1580-1640 nm)	SWIR3 (2225-2275 nm)	View Zenith Angle (Vza)	Sun Zenith Angle (Sza)

| Relative Azimuth Angle (RAA) | Pixel Reliability (Rank) | VI Quality (QA) | Composited Day |
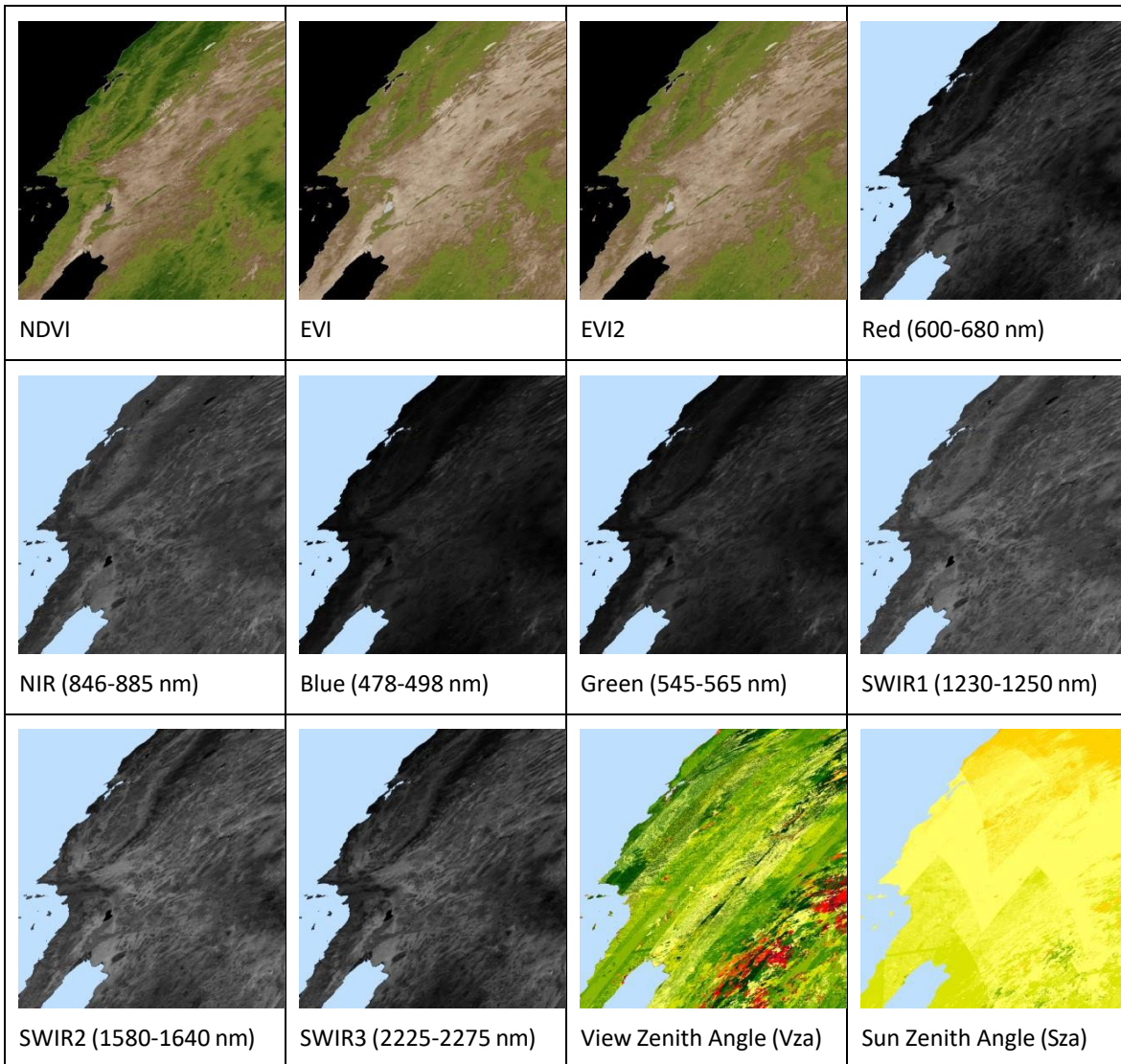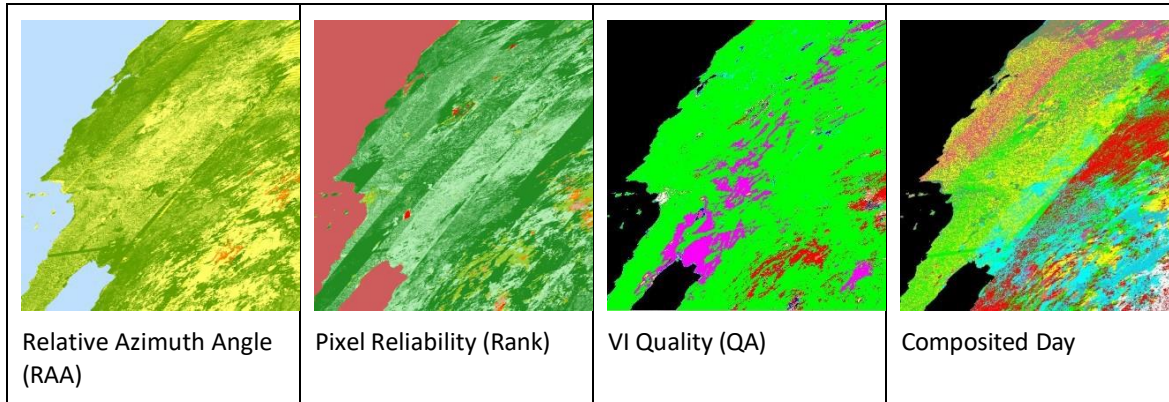
Figure 22. Example images of each of the science datasets in the S-NPP VIIRS VI product.

7.3.   File Format

The S-NPP VIIRS Vegetation Index product files are stored in the Hierarchical Data Format-Earth Observing System (HDF5-EOS5) structure, which is the newer standard archive format for NASA EOS Data Information System (EOSDIS) products. Files contain two separate structures:

- Scientific data sets (SDS) which are actually 2-D data arrays (Row x Column or Latitude x longitude)
- And four metadata structures
  - Structural metadata that describes the content of the file,
  - Core metadata that describes the projection and grid name,
  - Archive metadata that describes miscellaneous aspects of the data and product such as dates, times, statistics about quality, etc.. that are useful for archiving and searching the products.
  - A limited set of information from the Core and Archive metadata is repeated and stored as Global file attributes, allowing easy access to and parsing of information to identify the product and contents.

All VIIRS VI products are either in tile format (10x10 degrees grids, Fig 23) that are projected and fixed-areas. The use of metadata enhances the self-describing nature of HDF5 files and is useful to the end user, facilitating the archiving and searching of files. This metadata provides the users with general information about the file contents, its characteristics and general quality, which aids in deciding if a particular day/file is useful. There are two types of metadata attributes:

- Global attributes common to all VIIRS products, and
- Product specific attributes

7.4.   Tiled and Global Production

While the S-NPP VIIRS collects data at 375m and 750m, the VIIRS Land team decided to keep the production spatially consistent with the EOS MODIS (Justice et al. 2013). All VIIRS VI products are generated at 3 resolutions 500m, 1km, and a Climate Modeling Grid (CMG) at 0.05 deg. (~5.6km), and in 2 projections. VI Products are generated and distributed in adjacent non-overlapping tile units that are approximately 10 degrees square (true at the equator), called the sinusoidal tile grid. There are a total of 460 tiles that are arranged into a global 36x18 grid, with horizontal (0-17) and vertical (0-17) tile numbers. Tile (0,0) is at the upper left corner of the grid and tile (35,17) at the lower right corner (Fig. 23).
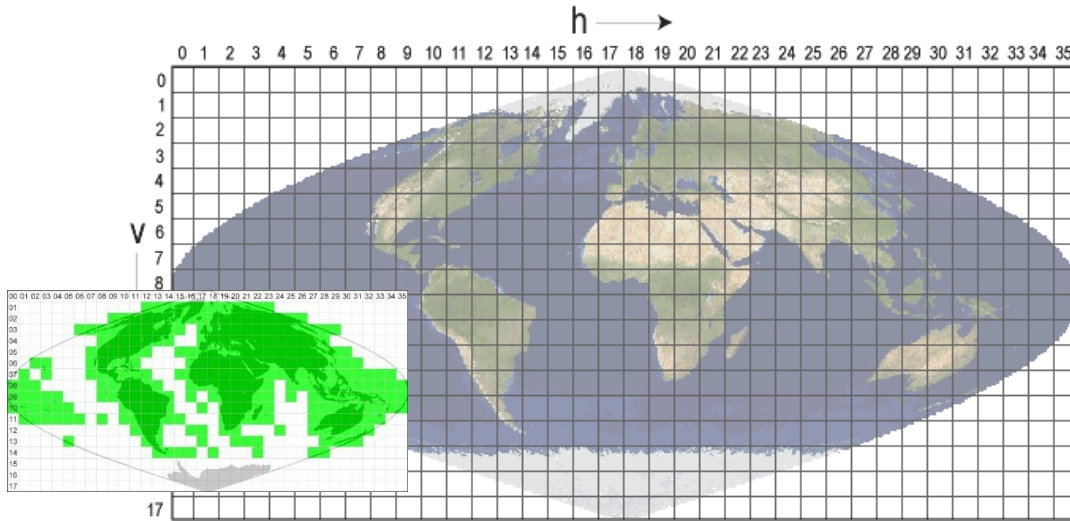
Figure 23: Sinusoidal Tile Grid system. Each square is approximately 10x10 degrees and production takes place over tiles that contain land only (highlighted green in the inset). In the winter the top two tile rows are either not produced or partially produced (due to sun angle considerations).

The coarser resolution CMG products are generated in the Geographic Lat/Lon projection (Fig. 24) and combine and reproject the tiles into a single global view.
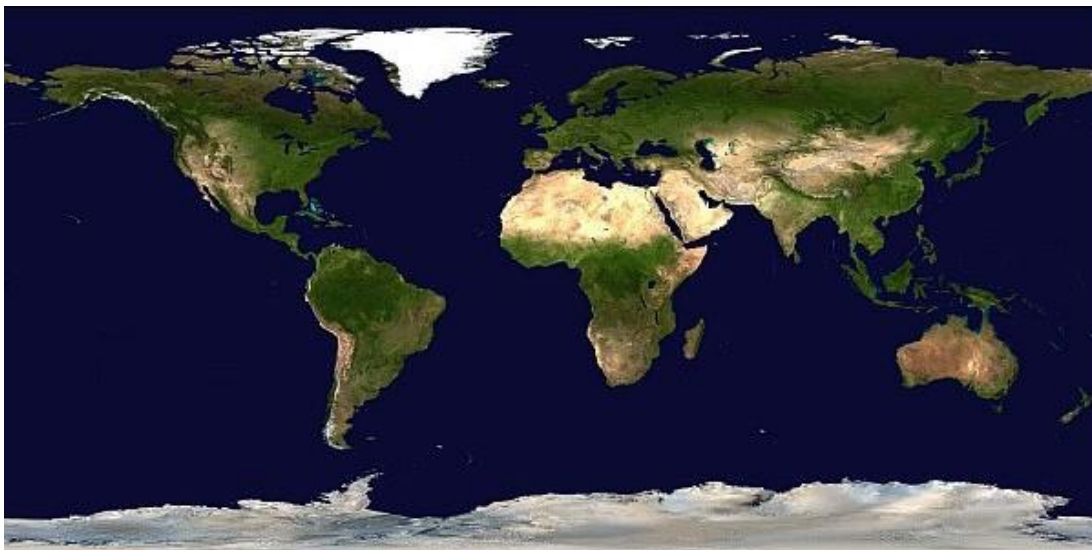
Figure 24: Global Geographic projection. These product files are generated by aggregating and reprojecting all titles.

7.5.   File Naming Convention

There are two types of VIIRS VI products, Tiled and Global. The file naming convention for the VIIRS products suite is similar to the file naming used for MODIS and other EOS products. The file names are structured left to right following this nomenclature per product type:

7.5.1. Tiled Products

The VIIRS VI series contains 3 tiled products from different temporal and spatial resolutions, they all use the following filename convention, adopted to facilitate their identification, search, and order:

VNP13AX.A2015190.hXXvXX.001.2015195220005.h5

Table 2. Tiled product files standard name description

Sequence	Description
VNP	Identifies the product as a VIIRS S-NPP product
13	Identifies the dataset as vegetation index
AX	Indicates the spatial and temporal resolution (2 digits)
	A1 = 500m, 16days
	A2 = 1km,16days
	A3 = 1km, monthly
A2015190	Observation year (4-digits) followed by the first acquisition day of period (3-digits)
hXX	Horizontal tile number (00 to 35)
vXX	Vertical tile number (00 to 17)
001	Identifies the data product version
2015195	Is the year the file was processed followed by the day of year
220005	Is the hour (2 digits), minute (2 digits)and second (2 digits)the file was processed
.h5	Indicates that output file is in HDF5-EOS5 format

7.5.2. Global CMG Products

The VI suite also contains two global products (VNP13C1 and VNP13C2), with a pixel resolution of 0.05° (~5.5km) in a geographical projection. The file name follows this format:

VNP13CX.A2014190.001.2015190220005.h5

Table 3. Global products standard name description

Sequence	Description
VNP	Identifies the product as a VIIRS product
13	Identifies the dataset as vegetation index
CX	Indicates the temporal and spatial resolution (2 digits)
	C1 = 0.05deg, 16days
	C2 = 0.05deg, monthly
A2015190	Observation year (4-digits) followed by the first acquisition day of period (3-digits)
001	Identifies the data product version
2015195	Is the year the file was processed followed by the day of year
220005	Is the hour, minute and second the file was processed
.h5	Indicates that output file is in HDF-EOS5 format

8. VNP13A1 (16-day 500m)/VNP13A2 (16-day 1km) VI Products

VNP13A1 and VNP13A2 are generated from the 500m and 1km daily land surface reflectance input files using the same science algorithm, since they share and need the same input data (State QA, Viewing geometry data, Pointer files). Depending on the input files listed in the process control file (PCF, a file that parameterize the algorithm) the algorithm identifies the desired output resolution. These products ingest daily VIIRS Level-2G (L2G) surface reflectance, pointer file, geo-angle file and 1-km state file (Fig. 25). Input filenames are based on current VIIRS surface reflectance files naming convention, listed in table 4.

Table 4. VIIRS VI input files

Input file	Description, resolution
VNPPTHKDI	Pointer file, 500m
VNPPT1KDI	Pointer file, 1km
VNP09GHKI	Surface reflectance, 500m (with HK denoting half kilometer)
VNP09G1KI	Surface reflectance and quality flags, 1km
VNPMGGAD1I	Geo-angle file, 1km
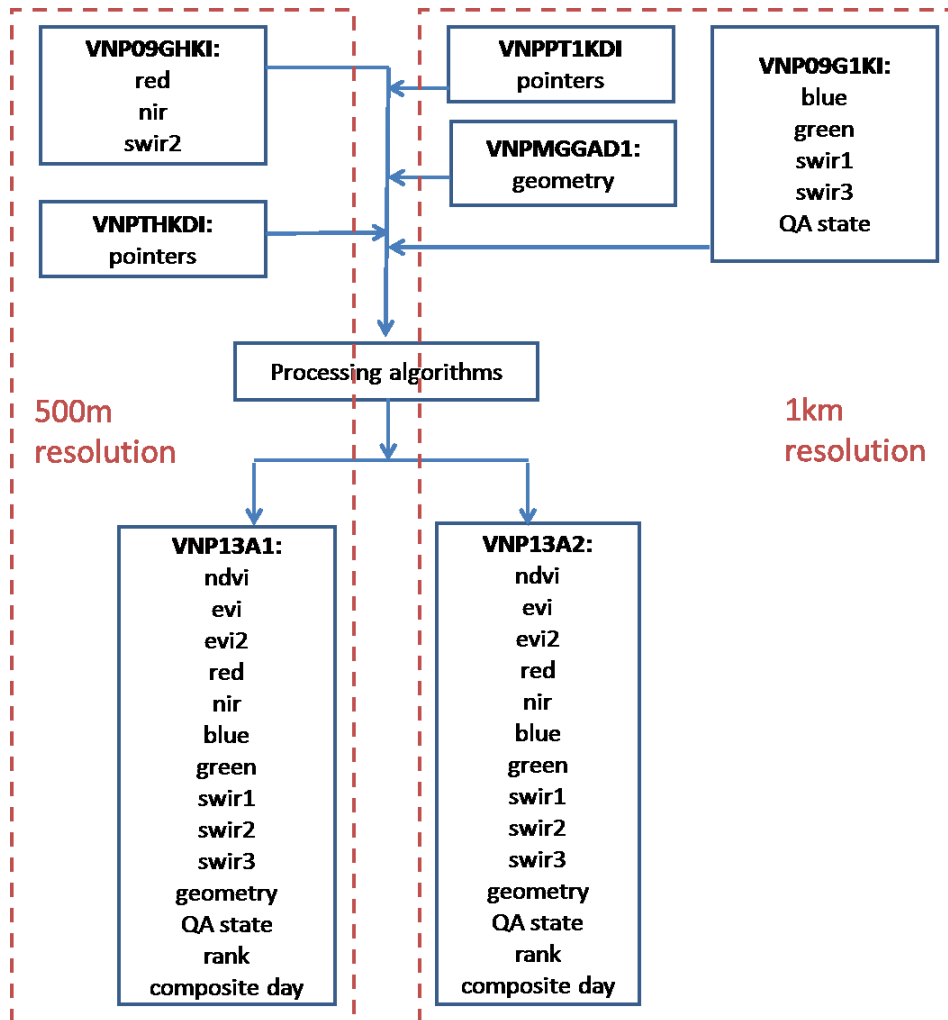
Figure 25. 500m/1km VIIRS VI production data processing flow diagram

8.1. Compositing Algorithm Theoretical and Practical Considerations

NDVI and EVI2 vegetation indices algorithms are calculated using the red and NIR surface reflectance, EVI requires the use of the blue band, following the science algorithms described earlier. Only reflectance values between 0-1.0 (scaled by 10,000) are retained and used during processing. Resulting VI values are also scaled by 10,000 and range from -10,000 to 10,000 (we note the slight deviation from MODIS VI data range being -2000 to 10000). This change was implemented to deal with the VI algorithm forced to select cloudy data instead of negative VI values below the -0.2 threshold, which was observed over inland water. While both values are still of no practical use (filtered out or negative) avoiding cloudy observations is always desirable. If no valid VI value could

be obtained (i.e. red or NIR outside the normal range, gaps between orbits, bad VI values, etc…) we assign a fill value. In addition, each output pixel is characterized by a set of QA flags, to assist and help automate the post-processing. To further simplify the data post-processing, and evaluate the quality of an observation, all pixels are ranked (Fig. 26) based on data usefulness, derived from the QA flags and the viewing geometry. This pixel reliability (a term used to describe how reliable and useful an observation would be for research), or rank (Didan and Huete, 2006), summarizes the pixel quality based on its overall quality flags and how likely it will serve the end user. The categories of this ranking scheme are listed in table 5.

Table 5. VI rank classes

Rank	Label	Rank	Label
0	Excellent	8	Snow/Ice
1	Good	9	Cloud
2	Acceptable	10	Estimated (For CMG products)
3	Marginal	11	LTAVG (for CMG product)
4	Pass	-1	NO_DATA
5	Questionable	-2	NO_DATA High latitude
6	Poor	-3	Antarctica (no production
7	Cloud Shadow	-4	Water/Ocean
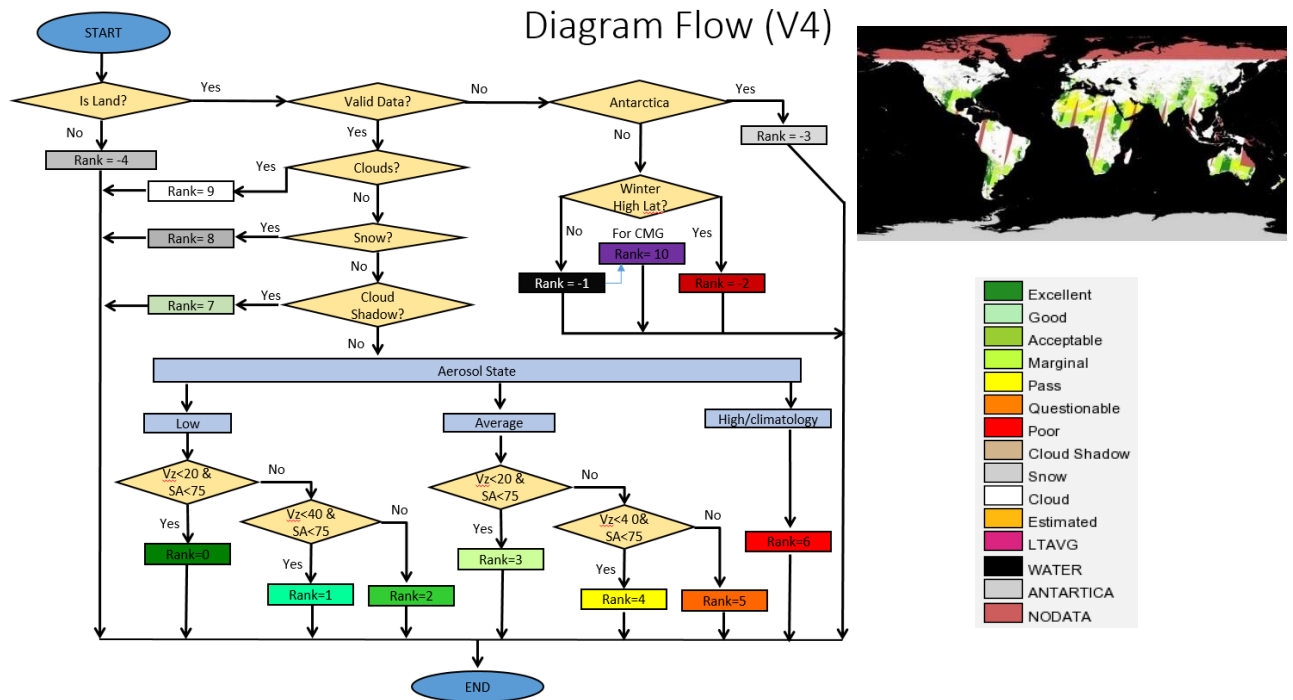
Figure 26. Data raking algorithm flow diagram and example Rank image (DOY 001, inset)

The VI processing algorithms chain (Fig. 18) operates on a per-pixel basis and requires multiple observations (days) to generate a composited VI value. Due to orbital overlap, multiple observations may exist for one pixel per day (especially at high latitude where orbits overlap the most due to the polar orbiting nature of the satellites). In theory, this can result in more than 16 observations during the 16-day composite cycle, however, due to the presence of clouds, atmosphere contaminants, sensor orbits arrangements, the actual number is practically less.

Using a method similar to EOS MODIS VI, the NPP13A1/A2 algorithm separates all observations

by their orbits, a process needed to maintain the consistency of the viewing geometry, as observation from different orbits are collected under different illumination conditions. The NPP VI algorithm starts by discarding all observations that cannot support the generation of a valid VI value, this usually concerns out of range surface reflectances (0- 1), cases where the generated VI value it outside the acceptable boundaries (-1 to 1). The remaining observation are filtered using the various QA flags, cloud status, and viewing geometry (Fig. 27). Cloud-contaminated pixels and extreme off-nadir observations are the least desirable, and will only be used as output in case other observation are not present. Although outputting a cloudy pixel is counterintuitive and likely useless, the S-NPP VIIRS Land science team, as was the case with the MODIS land science team, adopted a strategy of outputting an observation under all conditions unless impossible (out of range). The QA and rank will identify the quality and status of the pixel and users will likely discard it, but there are instances where the cloud flag is wrong and the pixel is actually useful (a post process decision) or simply the pixel could be ignored and gap filled using the end user strategy. Eliminating all cloudy pixels and Gap filling the finer resolution products is of course possible, as in the case of the CMG product suite, but the science team feels that leaving that decision to the product users is more prudent at this stage. In later iterations and reprocessing of the algorithms this decision may be changed to eliminate completely cloudy pixels and gap fill the product.

The general objective of the compositing strategy is to generate gap free, cloud-free, close to nadir observations, with minimum atmospheric contamination (especially aerosols loads, since correction remains challenging. Only the highest quality, cloud free, filtered observations are retained for further consideration by the compositing algorithm. In practice, this strict process results in few acceptable observations over a 16-day compositing period, especially when one considers a mean global cloud cover of ~60% and the long slash and burn season in the tropics. The goal of the compositing methodology is to select a single value from the remaining data that will represent in 16-day period. The VI compositing technique uses very rigorous criteria under normal-to-ideal observations conditions, but lowers the selection criteria when conditions are less than ideal. There are two compositing sequences:

1. Main: Constrained View Angle - Maximum Value Composite (CV-MVC, Huete et al. 2002)
2. Backup: Maximum Value Composite (MVC, Holben 1986)
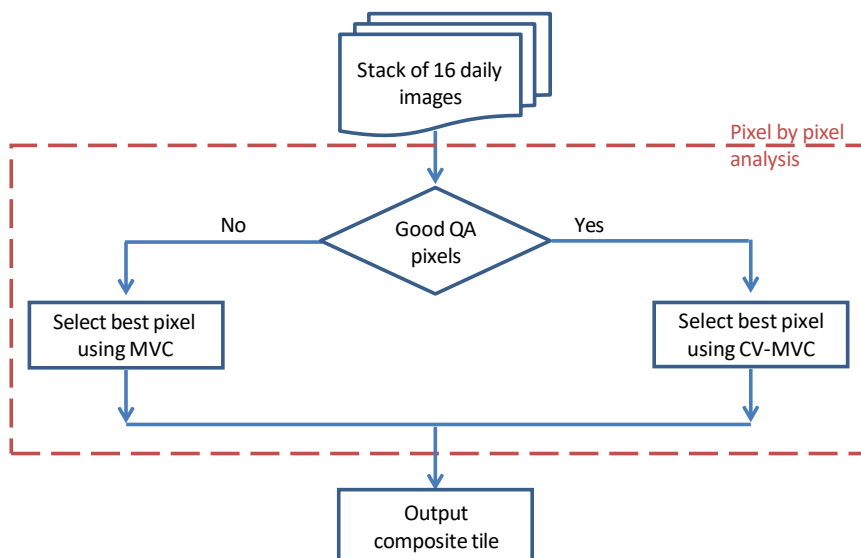
Figure 27. VIIRS VI compositing algorithm

The technique employed depends on the number and quality of observations. The MVC is

similar to that used in the AVHHR-NDVI product (Holben 1986), in which the observation with the highest NDVI value is selected to represent the entire period (16 days) based on the assumption that clouds, aerosols and other issues lower the NDVI value, and searching for the highest values will minimize those issues (Huete et al. 2002). The CV-MVC is an enhanced MVC technique. The algorithm is similar to the one used with MODIS, however it has been slightly modified for the S-NPP VIIRS to bin all observations with view angles below 30 degrees and select based on the maximum NDVI value within that bin. If no pixels are found within the 30 degrees then the algorithm relies on the original technique in which the observations with the two (or three) highest NDVI values are compared and the observation with the smallest view angle is selected to represent the 16-day composite cycle.

All compositing methodologies lead to spatial discontinuities, which are inevitable and result from the fact that disparate days can always be chosen for adjacent pixels over the 16-days period. Thus, adjacent selected pixels may originate from different days, with different sun-pixel-sensor viewing geometries and different atmospheric and residual cloud/smoke contamination. While VI ratioing tend to minimize these artefacts the spatial issues continue to be quite visible sometimes but usually less in the VI domain.

To illustrate how the compositing algorithm performs and manipulates the daily observations we will show examples from two key biomes, the high latitude (ex: Siberia) and the Tropics (ex: Amazon). Each of these examples illustrate a different aspects of the algorithm performance. High latitude tend to be prone to snow/ice and unstable surface reflectance due to the bright nature of the land, and are usually covered by many observations. The tropics usually have a smaller numbers of observations and are prone to persistent clouds and heavy aerosols.

8.1.1. Compositing steps for a high latitude pixel

In this example we illustrate the process of compositing with a pixel from the high latitude region, in Siberia:

Step 1.

Extract raw observations from the multiple orbits and assign a ranking quality value for each observation. High latitude pixels are characterized by multiple observations from multiple orbits due to overlap. Table 6 shows a series of observations from high latitude. Day of the year (DOY), ORBIT-NUM and OBS_COV are used to reconstruct the observations per orbit. The GROUP column is a summary of the quality of all observations based on clouds and aerosols loads. Observations are grouped into categories ranging from 0 to 9, with 0 (G-0) being the highest quality group and 9 (G-9) being the worst.

Table 6. Raw observations for a pixel from high latitude location (Siberia)

DOY	NDVI	EVI	EVI2	VZ	SZ	RED	NIR	BLUE	MIR	ORBIT NU	OBS_COV	GROUP
231	160	165	165	4993	6630	6633	6850	6385	3998	19730	34	G9
231	144	128	128	2821	6167	4395	4524	4666	2386	19731	50	G9
231	298	290	290	2125	6009	5481	5818	5669	1994	19732	53	G9
231	98	105	105	5926	6208	7670	7823	7549	3226	19733	22	G9
231	78	84	84	5926	6208	7672	7794	7587	3180	19733	21	G9
231	-26	-95	-28	4032	8170	7633	7592	7020	3387	19742	43	G9
231	163	194	194	4032	8171	12214	12619	9285	5959	19742	45	
231	158	126	126	5315	7451	3408	3518	3956	1903	19743	44	G9
232	282	330	330	5170	6773	10662	11282	10189	7140	19744	27	
232	200	199	199	3432	6265	5939	6182	6028	3844	19745	41	G9
232	405	412	412	1116	6045	6079	6593	5874	2799	19746	32	G9
232	446	446	446	1110	6044	5728	6264	5471	2468	19746	55	G9
232	455	443	443	1110	6044	5286	5791	5471	2468	19746	46	G9
232	163	178	178	5430	6177	8194	8466	7790	4282	19747	36	G9
232	-26	-384	-25	3553	8330	5865	5834	6534	5328	19756	30	G9
232	1141	767	767	5203	7616	2110	2654	2275	960	19757	30	G4
232	1217	813	813	5203	7616	2063	2635	2343	1103	19757	29	G4
233	807	832	832	5294	6921	5875	6907	5396	3988	19758	43	G9
233	694	722	722	5294	6921	6208	7134	5702	4221	19758	34	G9
233	563	585	585	3936	6373	6350	7108	4912	2889	19759	41	G9
233	1174	953	953	78	6093	3016	3819	3534	2015	19760	49	G9
233	630	594	594	4845	6158	4707	5340	4876	2740	19761	39	G9
233	137	165	165	2965	8487	12885	13243	10523	8850	19770	40	
233	103	124	124	2965	8487	12669	12935	10523	8850	19770	33	
233	898	850	850	5039	7782	4540	5436	4543	5172	19771	23	G9
234	417	433	433	5373	7075	6520	7088	6303	5185	19772	43	G9
234	411	428	428	5373	7075	6558	7121	6327	5118	19772	47	G9
234	688	675	675	4343	6491	5198	5967	5202	4751	19773	36	G9
234	1046	950	950	916	6153	3984	4915	3949	2757	19774	54	G9
234	1075	999	999	4158	6153	4191	5201	3998	3983	19775	29	G9
234	285	306	306	6820	6497	7480	7920	7110	5567	19776	21	G9
234	-1002	-619	-619	4814	7949	2421	1980	3582	532	19785	18	G9
234	19	21	21	5407	7232	8936	8971	8951	5287	19786	23	G9
234	39	44	44	5406	7232	9054	9126	9110	5481	19786	41	G9
234	26	29	29	5406	7233	8628	8674	8777	5429	19786	37	G9
235	176	199	199	4669	6616	9437	9776	8242	4886	19787	29	G9
235	121	140	140	1813	6225	10804	11069	10513	5479	19788	42	
235	117	136	136	1813	6225	10710	10965	10513	5479	19788	52	
235	65	74	74	3360	6159	9735	9864	9591	5234	19789	32	G9
235	132	147	147	6473	6443	8918	9157	8525	5778	19790	26	G9
235	83	92	92	6476	6444	8831	8979	8571	5706	19790	30	G9
235	4384	3448	3448	4529	8115	1572	4027	1363	1737	19799	35	G8
235	805	894	894	5397	7394	7559	8883	5498	5288	19800	38	G9
236	174	190	190	4924	6750	8293	8587	8005	5110	19801	42	G9
236	353	340	340	2590	6309	5249	5634	5284	4141	19802	48	G9
236	578	535	535	2452	6179	4537	5094	4418	4240	19803	47	G9
236	491	471	471	2446	6178	5052	5574	5873	5259	19803	48	G9
236	4937	3948	3677	6072	6399	1264	3730	760	1680	19804	23	G8
236	5303	3397	3397	4171	8279	912	2972	438	1119	19813	26	G4
236	4923	3738	3371	5344	7558	1106	3251	739	1685	19814	40	G0
237	5213	3880	3616	5119	6890	1055	3353	650	1575	19815	37	G0
237	5142	3147	2985	3242	6403	819	2553	492	1423	19816	42	G0
237	5031	3087	2999	1451	6210	873	2641	475	1555	19817	31	G0
237	4975	3702	3549	5602	6367	1167	3478	650	2085	19818	36	G0
237	4964	3662	3418	5605	6368	1105	3284	672	1993	19818	25	G0
237	4946	3441	3406	3725	8441	1110	3283	554	966	19827	48	G4
237	3627	1517	1430	5245	7724	651	1392	412	588	19828	22	G0
237	4278	1780	1584	5245	7723	535	1335	441	675	19828	23	G0
238	5452	3830	3801	5259	7037	1003	3408	497	1497	19829	23	G0
238	5328	3547	3490	5260	7038	938	3078	483	1356	19829	30	G0
238	5296	3095	3083	3781	6509	793	2579	388	1198	19830	40	G0
238	5033	2923	2868	417	6254	817	2473	428	1418	19831	50	G0
238	5000	3365	3348	5053	6347	1049	3147	514	1844	19832	32	G0
238	4771	4103	3818	5100	7891	1487	4201	878	1656	19842	22	G1

Observations highlighted red are removed because of the poor quality, while the green and white background are observations considered potential candidates for output. This information is also shown in Figure 28 as a plot. The X-axis shows the DOY sequence.
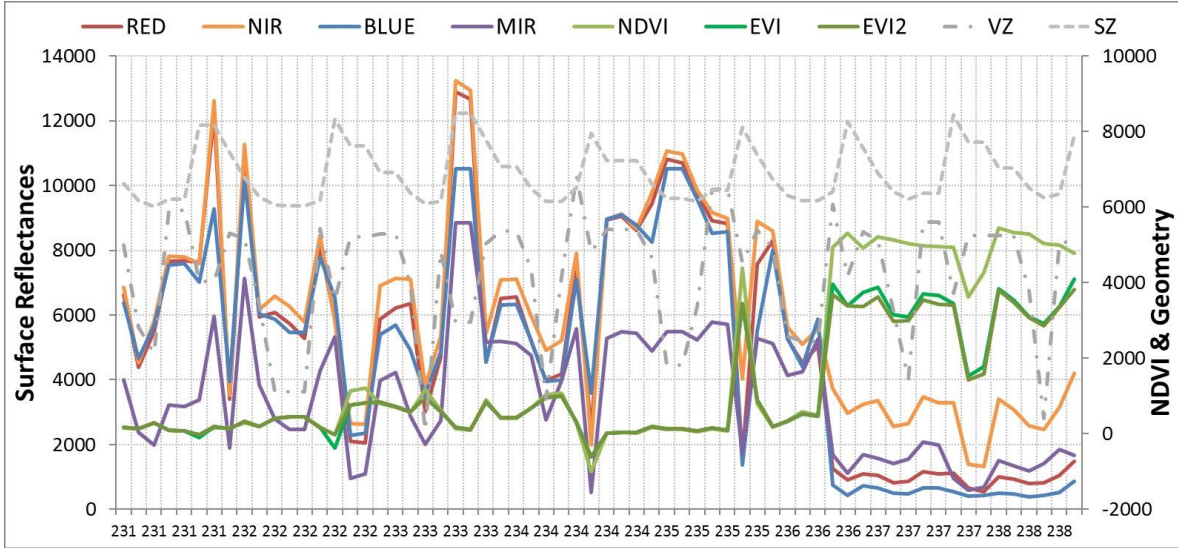
Figure 28. Single pixel (high latitude) sequence of observations considered for compositing.

Step 2.

Reconstruct observations per orbit. In this step all observations from the same orbit and same quality group are combined to generate an average observation.

Obs #	DOY	NDVI	EVI2	VZ	SZ	RED	NIR	BLUE	MIR	GP
1	236	4923	3371	5344	7558	1106	3251	739	1685	G0
2	237	5213	3616	5119	6890	1055	3353	650	1575	G0
3	237	5142	2985	3242	6403	819	2553	492	1423	G0
4	237	5031	2999	1451	6210	873	2641	475	1555	G0
5	237	4972	3496	5603	6367	1141	3398	659	2047	G0
6	237	3947	1508	5245	7723	591	1362	426	632	G0
7	238	5385	3627	5259	7037	966	3221	489	1417	G0
8	238	5296	3083	3781	6509	793	2579	388	1198	G0
9	238	5033	2868	417	6254	817	2473	428	1418	G0
10	238	5000	3348	5053	6347	1049	3147	514	1844	G0
11	238	4771	3818	5100	7891	1487	4201	878	1656	G1
12	232	1179	790	5203	7616	2086	2644	2308	1030	G4
13	236	5303	3397	4171	8279	912	2972	438	1119	G4
14	237	4946	3406	3725	8441	1110	3283	554	966	G4
15	235	4384	3448	4529	8115	1572	4027	1363	1737	G8
16	236	4937	3677	6072	6399	1264	3730	760	1680	G8
17	231	160	165	4993	6630	6633	6850	6385	3998	G9
18	231	144	128	2821	6167	4395	4524	4666	2386	G9
19	231	298	290	2125	6009	5481	5818	5669	1994	G9
20	231	89	95	5926	6208	7670	7808	7567	3203	G9
21	231	-26	-28	4032	8170	7633	7592	7020	3387	G9
22	231	158	126	5315	7451	3408	3518	3956	1903	G9
23	232	200	199	3432	6265	5939	6182	6028	3844	G9
24	232	439	436	1111	6044	5659	6179	5567	2547	G9
25	232	163	178	5430	6177	8194	8466	7790	4282	G9
26	232	-26	-25	3553	8330	5865	5834	6534	5328	G9
27	233	756	782	5294	6921	6022	7007	5531	4090	G9
28	233	563	585	3936	6373	6350	7108	4912	2889	G9
29	233	1174	953	78	6093	3016	3819	3534	2015	G9
30	233	630	594	4845	6158	4707	5340	4876	2740	G9
31	233	898	850	5039	7782	4540	5436	4543	5172	G9
32	234	414	431	5373	7075	6539	7105	6315	5150	G9
33	234	688	675	4343	6491	5198	5967	5202	4751	G9
34	234	1046	950	916	6153	3984	4915	3949	2757	G9
35	234	1075	999	4158	6153	4191	5201	3998	3983	G9
36	234	285	306	6820	6497	7480	7920	7110	5567	G9
37	234	-1002	-619	4814	7949	2421	1980	3582	532	G9
38	234	30	33	5406	7232	8871	8925	8951	5417	G9
39	235	176	199	4669	6616	9437	9776	8242	4886	G9
40	235	65	74	3360	6159	9735	9864	9591	5234	G9
41	235	105	117	6474	6443	8871	9061	8549	5739	G9
42	235	805	894	5397	7394	7559	8883	5498	5288	G9
43	236	174	190	4924	6750	8293	8587	8005	5110	G9
44	236	353	340	2590	6309	5249	5634	5284	4141	G9
45	236	531	501	2448	6178	4797	5336	5153	4754	G9

Table 7. Observations per orbit.

Raw observations are reconstructed into single orbit values per day by using the observation coverage weight and orbit number. Figure 29 shows the information summary of this process.
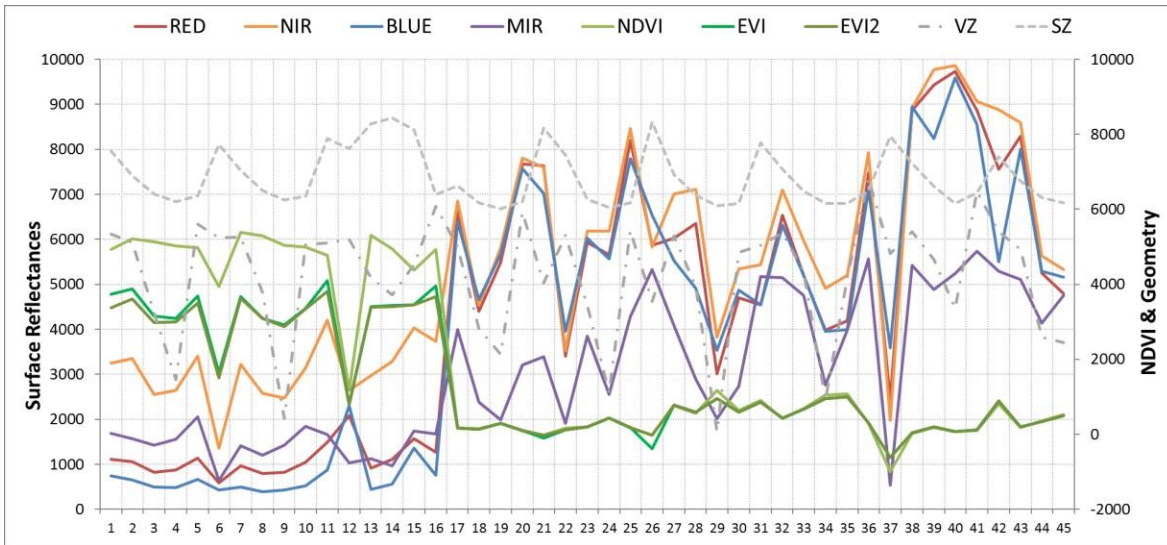
Figure 29. Earlier orbital observations are combined into a single value per orbit.

Step 3.

Remove all low quality observations and run the compositing algorithm to select the best observation. Using the ranking index, observation with low quality information are filtered (removed) leaving only the best group of observations. Table 8 and Figure 30 show the result of this process.

Table 8. Selected observations for compositing

Obs #	DOY	NDVI	EVI	EVI2	VZ	SZ	RED	NIR	BLUE	MIR
1	237	5142	3147	2985	3242	6403	819	2553	492	1423
2	237	5031	3087	2999	1451	6210	873	2641	475	1555
3	238	5296	3095	3083	3781	6509	793	2579	388	1198
4	238	5033	2923	2868	417	6254	817	2473	428	1418
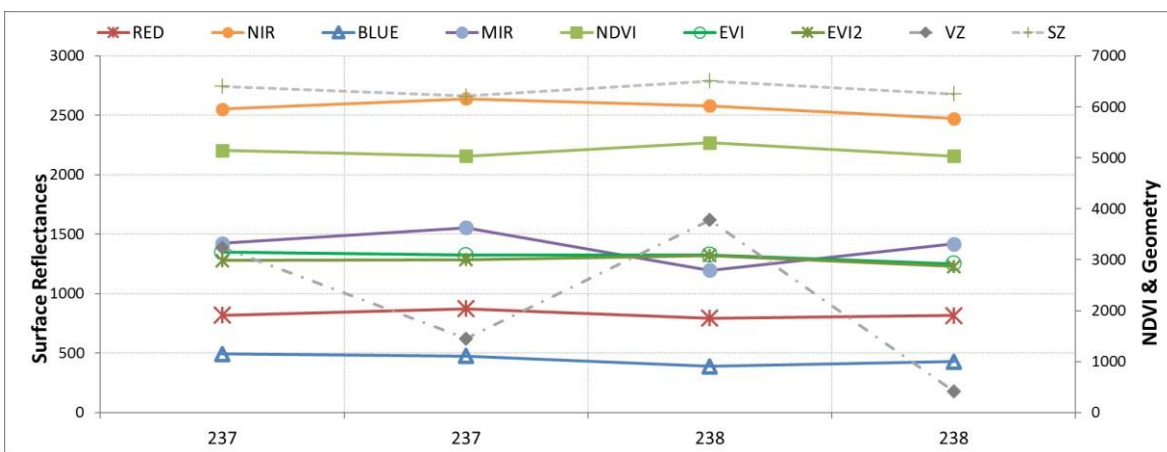
Figure 30. Selected observation

The compositing algorithm will first attempt to use observations with view angle below 30°. If observations are available the MCV will be applied to this subgroup, otherwise the CV-MCV will be applied to any retained data with any view angle. For this particular case, 2 observations have a

view angle below 30º (observation #2 and #4). However, observation #4 has the highest NDVI value and also happens to have the lowest view angle. Therefore observation #4 from DOY=238 is selected to represent the 16-day compositing period.

Note that with the MVC algorithm, observation #3 would have been selected given that it has the highest NDVI value from the preselected input observations. However, because of the view angle outside of the 30deg this observation was not selected.

8.1.2. Compositing steps for a pixel in the tropics

Table 9 and Figure 31 show observations values for a single pixel in the Amazon. Pixels close to the equator are characterized by a smaller number of observations because orbits do not overlap at the equator. In addition over the Amazon clouds are present more than 75% of the time, making it difficult to get cloud free pixels and forcing the algorithm to use poor quality data sometimes.

Table 9. Raw observations for a pixel in Brazil

DOY	NDVI	EVI	EVI2	VZ	SZ	RED	NIR	BLUE	MIR	ORBIT NU	OBS_COV	GX
230	8779	5616	5498	1383	2765	210	3231	139	480	19725	64	G8
231	8657	4768	4658	4498	2420	189	2626	131	345	19739	49	G2
232	2944	2011	2011	6282	2122	1628	2987	1938	1163	19753	46	G9
232	2955	2009	2009	6280	2122	1614	2968	1874	1090	19753	42	G9
232	1790	1534	1534	6998	4030	3055	4388	2871	2376	19754	19	G9
233	259	299	299	5720	3608	10090	10627	10143	5030	19768	43	
234	3580	2550	2550	3523	3197	1558	3296	1791	1614	19782	39	G9
235	8433	1707	1669	75	2801	68	800	65	213	19796	35	G5
236	1860	1734	1734	3633	2428	3663	5337	4436	2757	19810	46	G9
237	1584	1460	1460	5794	2091	3746	5157	3309	2098	19824	52	G9
238	405	447	447	6214	3699	8060	8742	7324	4077	19839	37	G9
239	1173	1195	1195	4397	3274	5280	6684	5276	3686	19853	46	G9
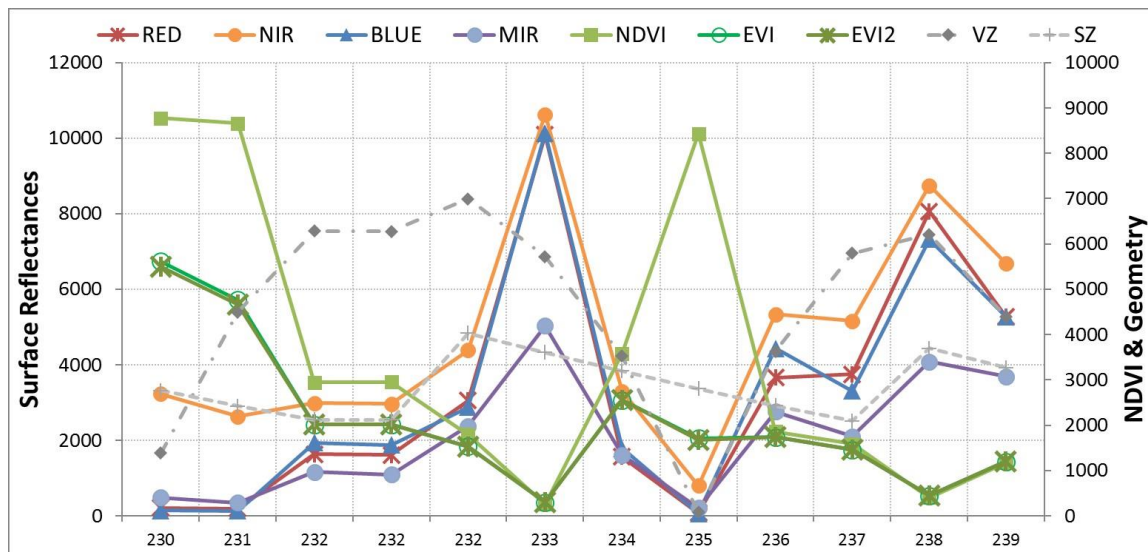
Figure 31 Raw observations time series

Step 1.

Reconstruct observations per orbit: All the raw observations are reduced to only 10 after orbit reconstruction (Table 10 and Figure 32).

Table 10. Single observation per orbit

Obs #	DOY	NDVI	EVI	EVI2	VZ	SZ	RED	NIR	BLUE	MIR	GX
1	231	8657	4768	4658	4498	2420	189	2626	131	345	G2
2	235	8433	1707	1669	75	2801	68	800	65	213	G5
3	230	8779	5616	5498	1383	2765	210	3231	139	480	G8
4	232	2949	2009	2009	6281	2122	1621	2977	1907	1128	G9
5	232	1790	1534	1534	6998	4030	3055	4388	2871	2376	G9
6	234	3580	2550	2550	3523	3197	1558	3296	1791	1614	G9
7	236	1860	1734	1734	3633	2428	3663	5337	4436	2757	G9
8	237	1584	1460	1460	5794	2091	3746	5157	3309	2098	G9
9	238	405	447	447	6214	3699	8060	8742	7324	4077	G9
10	239	1173	1195	1195	4397	3274	5280	6684	5276	3686	G9
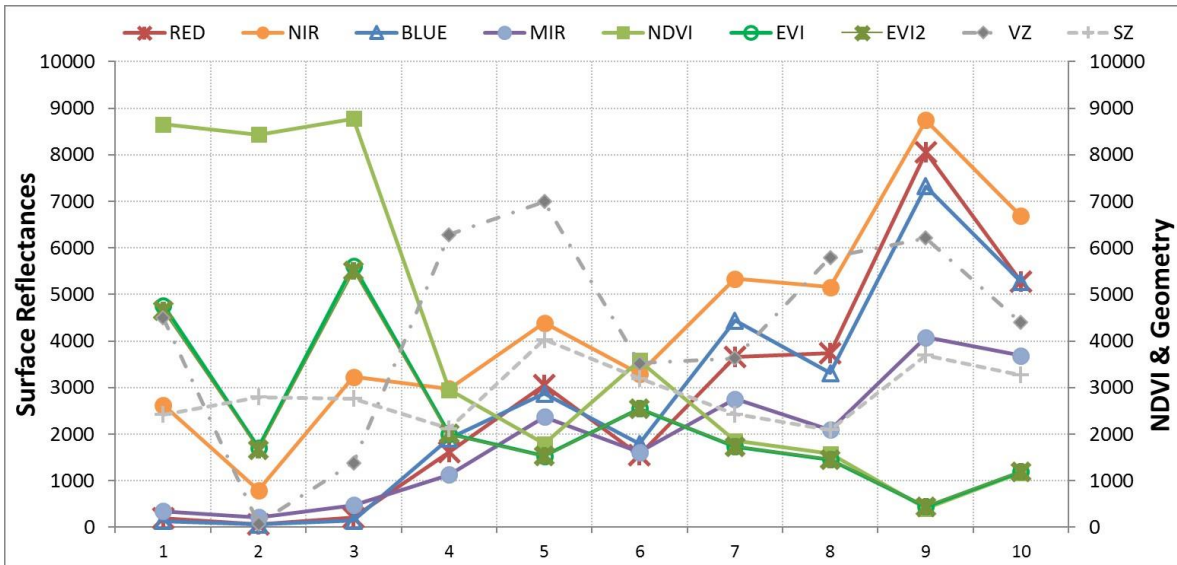
Figure 32. Single observation per orbit

Step 3.

Remove low quality observations and run compositing algorithm

Table 11. Only one observation was retained

DOY	NDVI	EVI2	VZ	SZ	RED	NIR	BLUE	MIR
231	8657	4658	4498	2420	189	2626	131	345

After removing all low quality observations, only 1 observation was retained. And while this was not a high quality pixel, it was nonetheless the best possible observation with no clouds (Group 2). The pixel output rank will capture and relay the quality of this selected observation.

8.2.   Output Scientific Data Sets

8.2.1. SDS Structure

The 500m and 1km 16-day VI product contain the following scientific data (output layers)

Table 12. VNP13A1/VNP13A2 SDS structure

Science Data set	Units	Data Type	Valid Range	Fill *	Scale
500m 16 days NDVI	NDVI	INT16	-10,000 - 10,000	-15,000	10,000
500m 16 days EVI	EVI	INT16	-10,000 – 10,000	-15,000	10,000
500m 16 days EVI2	EVI2	INT16	-10,000 – 10,000	-15,000	10,000

500m 16 days VI Quality	bits	UINT16	0 - 65534	65535	N/A
500m 16 days red reflectance	Reflectance	INT16	0 – 10,000	-1000	10,000
500m 16 days NIR reflectance	Reflectance	INT16	0 – 10,000	-1000	10,000
500m 16 days blue reflectance	Reflectance	INT16	0 – 10,000	-1000	10,000
500m 16 days green reflectance	Reflectance	INT16	0 – 10,000	-1000	10,000
500m 16 days SWIR1 reflectance	Reflectance	INT16	0 – 10,000	-1000	10,000
500m 16 days SWIR2 reflectance	Reflectance	INT16	0 – 10,000	-1000	10,000
500m 16 days SWIR3 reflectance	Reflectance	INT16	0 – 10,000	-1000	10,000
500m 16 days view zenith angle	Degree	INT16	0 – 18,000	-20,000	100
500m 16 days sun zenith angle	Degree	INT16	0 – 18,000	-20,000	100
500m 16 days relative azimuth angle	Degree	INT16	-18,000 - 18,000	-20,000	100
500m 16 days composite day of the	Day	INT16	1 – 366	-1	1
500m 16 days pixel reliability	Rank	INT8	0 - 11	-4	N/A

500m (VNP13A1) is replaced by 1km for VNP13A2.

*: For the VIs there are more than one unique Fill value to capture the different LW statuses. For the tiled products, the VI Fill is -15,000 over ocean/water, -13,000 over land, and in addition for CMG products it is -12,000 over high latitude during the dark winter, and -14,000 over Antarctica (which is never produced). For the Rank the Fill is -4 over ocean (all products), -3 for Antarctica (CMG products), -2 over high latitude during the dark winter (CMG only), -1 over land (all products).

8.2.2. Pixel Reliability SDS Description

While a comprehensive VI Quality SDS is provided with each product and for each pixel, the complexity of the bit layout (inherited from MODIS) is usually difficult and inaccessible to average users looking for a quick method to evaluate the data quality and decide what to reject for their specific applications. To simplify this information, the S-NPP VIIRS VI product, and similarly to MODIS, implemented a pixel reliability metric that uses a simple decimal scale and provides an easy approach to assess the quality of the pixel and its usefulness (Didan and Huete, 2006). This metric provides a simple and direct mask for automating filtering the product (Table 5).

8.2.3. Quality Assurance

The quality of each VI product is stored in Quality Assessment (QA) metadata objects and QA science data sets (SDS). The QA metadata objects summarize global level file or product quality with single words and numeric values, and thus are useful for data ordering and screening. The QA SDS (layer), on the other hand, documents the product quality on a pixel-by-pixel basis and thus is useful for data analyses and application.

Table 13. VIIRS VI quality assurance description

Bit #	Description	Values
0-1	MODLAND_QA	00: VI produced, good quality
		01: VI produced, but check other QA
		10: Pixel produced, but most probably cloudy
		11: Pixel not produced due to other reasons than clouds
2-5	VI usefulness	0000: Highest quality
		0001: Lower quality
		0010...1010: Decreasing quality
		1100: Lowest quality
		1101: Quality so low that it is not useful

		1110: L1B data faulty
		1111: Not useful for any other reason/not processed
6-7	Aerosol quantity	00: Climatology
		01: Low
		10: Average
		11: High
8	Adjacent cloud detected	1: Yes
		0: No
9	Atmosphere BRDF correction performed	1: Yes
		0: No
10	Mixed clouds	1: Yes
		0: No
11-13	Land/Water Flag	000: land & desert
		001: land no desert
		010: inland water
		011: sea water
		101: coastal
14	Possible snow/ice	1: Yes
		0: No
15	Possible shadow	1: Yes
		0: No

Bits are listed from MSB (bit 15) to the LSB (bit 0)

8.3.   QA Metadata

The metadata fields used in the S-NPP VIIRS VI product suite are listed below. They provide a summary of the file overall quality based on a frequency analysis of the reliability rank.

Table 14. Metadata fields for QA evaluation of VNP13A1/VNP13A2

Inventory Metadata fields for all VI products (searchable)		
QAPERCENTINTERPOLATEDDATA QAPERCENTMISSINGDATA QAPERCENTOUTOFBOUNDSDATA QAPERCENTCLOUDCOVER QAPERCENTGOODQUALITY QAPERCENTOTHERQUALITY QAPERCENTNOTPRODUCEDCLOUD QAPERCENTNOTPRODUCEDOTHER		
Product specific metadata (searchable)		
Product	Specific metadata variable name (best quality)	
VNP13A1	NDVI500M16DAYQCLASSPERCENTAGE	
VNP13A1	EVI500M16DAYQCLASSPERCENTAGE	
VNP13A1	EVI2500M16DAYQCLASSPERCENTAGE	
VNP13A2	NDVI1KM16DAYQCLASSPERCENTAGE	
VNP13A2	EVI1KM16DAYQCLASSPERCENTAGE	
VNP13A2	EVI21KM16DAYQCLASSPERCENTAGE	
Archived Metadata (not searchable)		
Product	Metadata variable name (Array of QA usefulness histogram)	
VNP13A1	QAPERCENTPOOR500M16DAYNDVI	

VNP13A1	QAPERCENTPOOR500M16DAYEVI
VNP13A1	QAPERCENTPOOR500M16DAYEVI2
VNP13A2	QAPERCENTPOOR1KM16DAYNDVI
VNP13A2	QAPERCENTPOOR1KM16DAYEVI
VNP13A2	QAPERCENTPOOR1KM16DAYEVI2

8.4.   Global and Local Metadata Attributes

All S-NPP VIIRS VI products contain local and global metadata that is written during the product generation. The local metadata is written as attributes of the SDS within the HDF file. This global metadata is useful for archiving, searching, and ordering the product and describe other key attributes about the file.

8.4.1. Global Metadata Attributes

Each HDF file contains a series of attribute objects structure (slightly abridged for space). The list of the actual metadata structure is in **Appendix-I**

8.4.2. Global File Attributes

Each HDF file contains a minimum set of attributes to identify the product, written as global file attributes and listed in a key - value format. The following list apply to 500m and 1km datasets:

- AlgorithmType
- AlgorithmVersion
- DataResolution
- DayNightFlag
- DayNumbers
- EastBoundingCoord
- EndTime
- GRingLatitude
- GRingLongitude
- HorizontalTileNumber
- InputPointer
- LocalGranuleID
- LongName
- NorthBoundingCoord
- NumberofInputGranules
- PGENumber
- PGEVersion
- PGE_EndTime
- PGE_Name
- PGE_StartTime
- PlatformShortName
- ProcessVersion
- ProcessingCenter
- ProcessingEnvironment
- ProductionTime
- RangeBeginningDate
- RangeBeginningTime
- RangeEndingDate

- RangeEndingTime
- SensorShortName
- ShortName
- SouthBoundingCoord
- StartTime
- TileID
- VersionID
- VerticalTileNumber
- WestBoundingCoord
- identifier_product_doi
- identifier_product_doi_authority.

9. VNP13A3 (monthly 1km) Vegetation Index Product

This product is generated using the 16-day 1km VIIRS VI tiled products using a temporal compositing algorithm based on a weighted average scheme to create a true calendar-month composite. The output file contains 15 SDS's (Table 19)

9.1. Monthly Compositing Algorithm Description

The algorithm for S-NPP VIIRS monthly VI differs from the one used in the MODIS VI suite (Huete et al. 2002). The VIIRS algorithm was designed to generate a true monthly composite that only retains and average observations within the considered month and not an average of what the compositing period represents. It also uses the two 16-day VIIRS streams that are produced 8-days apart. This algorithm operates on a per-pixel basis and ingest "Normal" and "Phased" production data from the two 16-day 1km VI products that overlap the calendar month (Fig 33). The use of both data streams allows for a quasi-8-day compositing periodicity thus increasing the number of observations per month. This gain in observations allows for a better representation of the month and helps generate a true average monthly value. Since both streams are from the same S-NPP VIIRS sensor, observations may at times repeat (especially for areas with limited good quality pixels) for a particular month, however the algorithm was designed to identify and to avoid using repeated values to minimize bias.

Because the 16-day composite periods extend beyond the limits of the calendar month, only observations within the month, based on the composite day, will be used to compute the monthly pixel value; this is achieved by looking at each pixel Composite Day of Year SDS layer from the 1km input product.
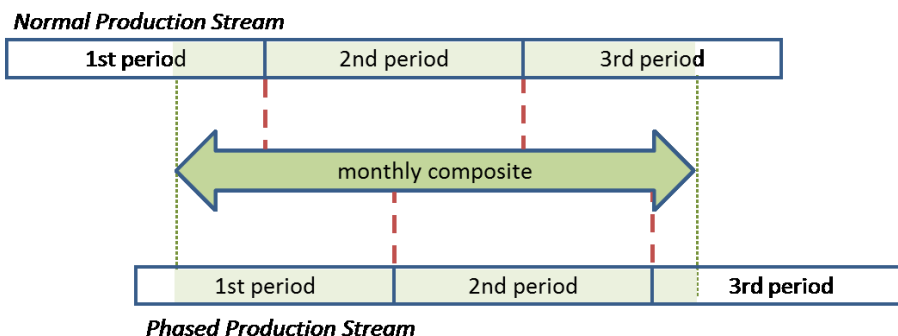
Figure 33. Monthly and the two 16-day composite periods overlap

Once all observations from the 16-day composites are collected, a quality analysis is performed to decide the method to calculate the monthly VI value and which 16-day observations to use. Clouds, cloud shadow and snow quality flags are extracted for each pixel, then observations are grouped in quality categories from best to lowest quality using a scheme that follows the pixel rank approach. The subset of observations to be used for the monthly pixel is selected following Fig 34. The algorithm starts by identifying if there are pixels that are cloud free, cloud shadow free and snow free. If there is a single observation that meets that criteria, that pixel will be used to represent the whole month. If there are more than one, their surface reflectance values are averaged (red, NIR, blue, green, SWIR1, SWIR2, SWIR3) and the VIs are recalculated from these average reflectance. If no pixels meet these conditions, the next QA subset will be created by limiting QA flags to cloud free and cloud shadow free. If one or more observations are found, the same averaging procedure is used to generate the monthly value. If no observations meet this criteria, the algorithm looks into Cloud free and snow free observations and the process continues as before. If only cloudy pixels are found, then the Maximum Composited Value (MCV) method will be used and only the observation with the highest NDVI is selected assuming that maximizing the NDVI will minimize the cloud impact.

In assigning the output pixel QA, the worst case scenario approach is used, and the pixel with the lowest quality dictates the final output QA when the averaging method for VI was used. If a single observation, the QA is passed directly from the input observation. We employ the worst case scenario to mitigate omission issues in assigning quality flag and favoring a conservative approach.
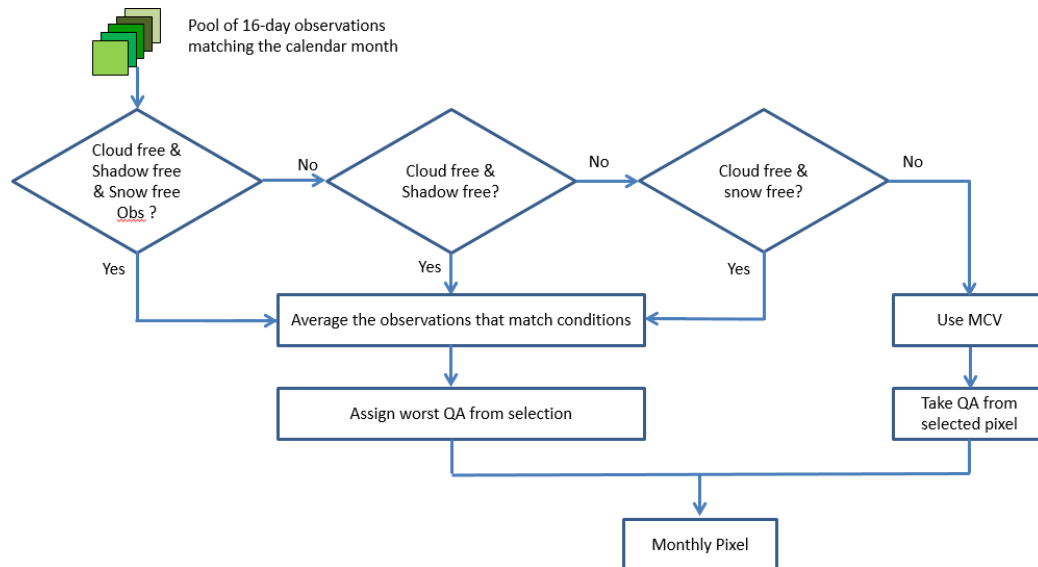
Figure 34. Monthly VIIRS VI pixel value estimation flow chart

9.1.1. Monthly Algorithm Operation Example

To illustrate the operation of the algorithm, we present here examples that show how to estimate a monthly pixel value from the 16-day data streams. The results are then compared to a

hypothetical old MODIS algorithm based value. 16-day 1km composites from VIIRS product VNP13A2 for the periods 017, 033, 049 (Normal Production) and 025, 041,057 (Phased Production) for the year 2017 were used. The monthly NDVI pixel value will be estimated for the calendar Month of February (DOY 32 to 59).

The first example is from a pixel (Row=1113 and Column=1085) in tile h08v05 (an area not prone to clouds or atmosphere issues and where usually high quality observations exist). Input from each 16day period and QA flags are shown in Table 15.

Table 15. 16-day 1km composite pixel observations

VNP13A2	017	025	033	041	049	057
NDVI	1558	1558	1452	1411	1386	1540
EVI	1018	1018	1007	989	983	1026
EVI2	1018	1018	998	987	982	1010
QA	2116	2116	2116	2116	2116	2120
RED	1888	1888	2095	2175	2236	1905
NIR	2585	2585	2807	2890	2956	2599
BLUE	908	908	1027	1051	1077	951
GREEN	1264	1264	1393	1445	1474	1285
SWIR1	3307	3307	3515	3623	3650	3211
SWIR2	3526	3526	3731	3846	3862	3392
SWIR3	2986	2986	3197	3258	3298	2828
VZA	1414	1414	294	1944	315	6263
SZA	4897	4897	4784	4554	4263	3801
RAA	-2450	-2450	-2481	-596	-2420	-2528
CDOY	31	31	36	46	52	60
Rank	0	0	0	0	0	2
Quality flags						
Clouds	no	no	no	no	no	no
Shadow	no	no	no	no	no	no
Snow/ice	no	no	no	no	no	no
Processing decision						
Use Pixel?	no	no	yes	yes	yes	no
Pweight	0	0	0.333333	0.333333	0.333333	0

Several good quality observations are available to work with. They are cloud free, cloud shadow free and snow/ice free. For the month of February 2017 (Day of the year 32 to 59) the 16day composited periods partially overlapping the month are 17-32,49-65 (Normal Production) and 25-41, 57-73 (Phased Production). From these periods only pixels with composite day of the year (CDOY) overlapping the month are used. Following tables 16, observations from the periods 17, 25 and 57 were eliminated because they correspond to a composite day of the year outside February month (CDOY were 31, 31 and 60 respectively). This leaves only 3 observations, and each contributes a third to the final monthly value.

Table 16. Comparisons of the new (VIIRS combined) and separate methods (old MODIS method) for generating monthly values.

Monthly values	Normal Production*	Phased Production*	Combined Streams
NDVI	1426	1468	1415
EVI	996	1002	992
EVI2	991	999	988
QA	2116	2116	2116
RED	2145	2054	2169
NIR	2859	2761	2884
BLUE	1043	994	1052
GREEN	1421	1370	1437
SWIR1	3562	3477	3596
SWIR2	3777	3695	3813
SWIR3	3230	3125	3251
VZA	294	1944	294
SZA	4784	4554	4784
RAA	-2481	-596	-2481
RANK	0	0	0

Normal Production and Phased Production monthly values were calculated using the old MODIS logic algorithm. They produced a higher NDVI value (1426 and 1468) compared to the 1415 obtained with the combined method. Even though all observations passed the quality test, three observations were avoided by the VIIRS algorithm because the pixel value came from outside the Month of February. These discarded observations had higher NDVI values, and were used by the older method, impacting the final computed value and giving a higher final VI value.

A second example is a pixel (row=403 and column=258) in the tile h12v09 (Tropics region, where good quality data is rare due to clouds). Input data values for each 16day period and QA flags are shown in Table 17, then Monthly output values are shown based on the new and old methodologies (Table 18).

Table 17. 16-day 1km composited pixel observations and processing decision Example 2

VNP13A2	017	025	033	041	049	057
NDVI	8553	7441	3141	6301	8392	8392
EVI	5454	4521	2350	4962	6303	6303
EVI2	5291	4311	2350	4962	6131	6131
QA	35037	3298	3102	3098	2116	2116
RED	246	408	1843	965	348	348
NIR	3155	2781	3531	4254	3982	3982
BLUE	173	281	2011	971	221	221
GREEN	454	512	2046	1264	674	674
SWIR1	2873	2591	3276	4009	3751	3751
SWIR2	1418	1390	2059	2231	2207	2207
SWIR3	557	712	1598	1170	974	974
VZA	6351	5873	4618	314	1012	1012
SZA	1823	1774	1709	1891	2018	2018
RAA	-2381	-2326	-2200	-1957	-9	-9
CDOY	20	25	35	55	60	60

Rank	7	9	9	9	0	0
Quality flags						
Clouds	yes	yes	yes	yes	no	no
Cloud	yes	no	no	no	no	no
Snow/Ice	no	no	no	no	no	no
Processing decision						
Used?	no	no	yes	yes	no	no
MVC -> DOY 55						

Four observations have cloud issues and 2 observations are cloud free. For the Month of February 2017 (DOY 32 to 59) the 16day composited periods partially overlapping the month are 17-32, 49-65 (Normal Production) and 25-41, 57-73 (Phased Production). From these periods only pixels where the composited day of the year fall within the month will be used. Therefore, observations from period 17, 25, 49 and 57 were eliminated because their CDOY were 20, 25, 60 and 60 respectively (outside the calendar month). Leaving only 2 observations to compute the month from. Because both observations were cloudy, the value representing the month will be selected using the MCV method, and in this case the observation selected was NDVI=6301 corresponding to DOY 55. Observation from DOY 60 was cloud free, but it was outside the month.

Table 18. Monthly values comparisons from old and new methods

Monthly values	Normal Production	Phased Production	Combined Streams
NDVI	8553	8392	6301
EVI	5454	6303	4962
EVI2	5291	6131	4962
QA	35037	2116	3098
RED	246	348	965
NIR	3155	3982	4254
BLUE	173	221	971
GREEN	454	674	1264
SWIR1	2873	3751	4009
SWIR2	1418	2207	2231
SWIR3	557	974	1170
VZA	6351	1012	314
SZA	1823	2018	1891
RAA	-2381	-9	-1957
RANK	7	0	9

Normal Production and Phased Production have very high values (8553 and 8392) and the new algorithm resulted in a value of 6301.

While very limited in space and time these two examples illustrate the performance of the algorithm, and in both cases the resulting NDVI values based on the new approach were lower than the ones obtained by the old algorithm. These results actually indicate that the old algorithm was overestimating the monthly values by overusing data from adjacent months (Extending as much as 15 days in the previous or next month sometimes) leading to this bias. VIIRS on the other hand minimizes this bias by only working with observations from the actual month.

When we look at the spatial distribution (tile h08v05) of the NDVI and at the NDVI histogram distribution of both algorithms (Figure 35) they show minor differences <0.3% (Fig 35d) and the NDVI difference histogram (Fig 35 e) shows that the majority of differences are within 1% VI unit with a slightly gain in higher values.
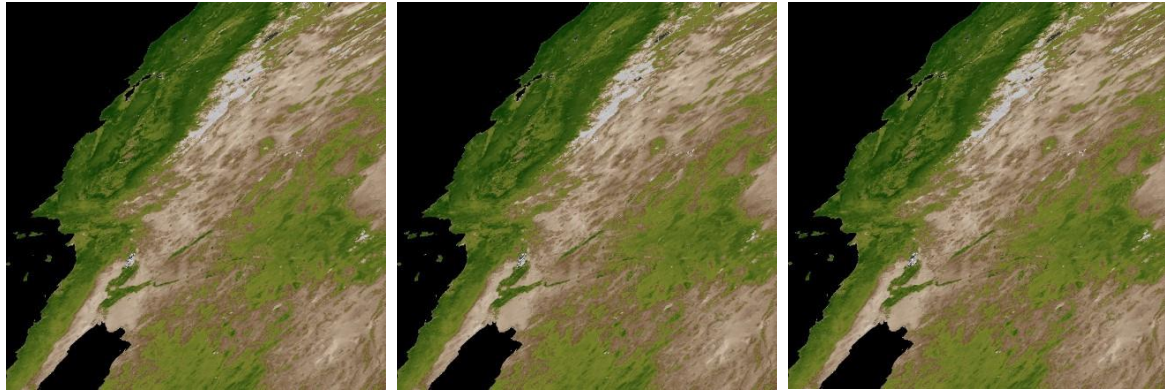
a) Month based on Normal Production

b) Month based on Phased Production

c) Month based on Combined streams
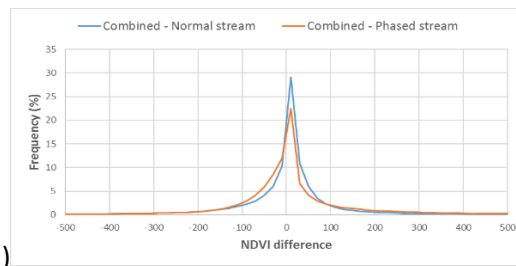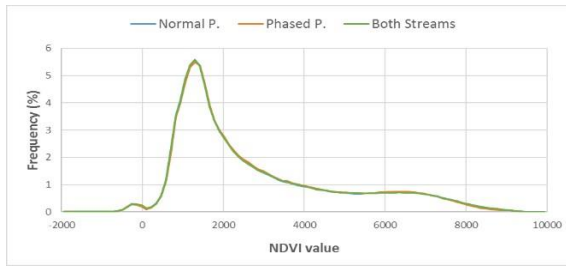
d) NDVI Histogram for Normal, Phased and Combined streams and e) NDVI difference between streams

Figure 35. Tile h08v05 Monthly NDVI results comparison
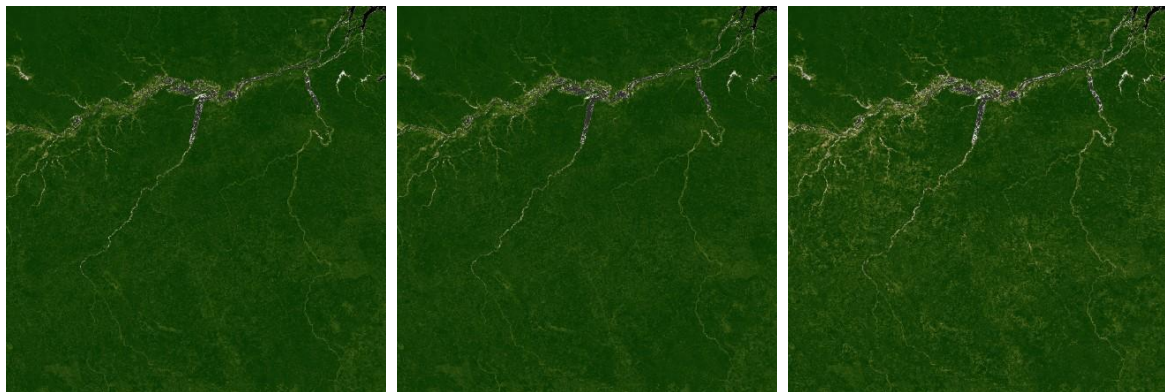
a) Normal Production

b) Phased Production

c) Combined stream
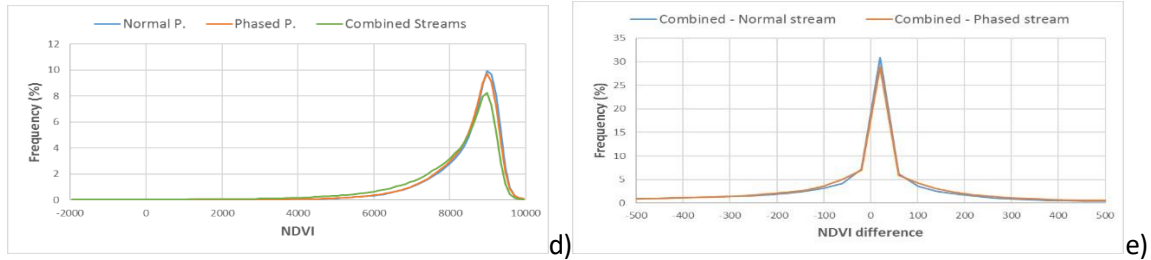
d) NDVI Histogram for Normal, Phased and Combined streams, e) NDVI difference
between streams

Figure 36. Tile h12v09 Monthly NDVI results comparison

The results for tile h12v09, show similar trends to tile h08v05. The majority of NDVI Differences between old method and new method are below 1% with slightly gain in high values over the whole range. However, when looking just at the >=8000 VI range, the NDVI values tend to be slightly lower from the new method. And while these difference are very small they are a direct result of the bias resulting from the old method overuse of data outside the month.

9.2. Scientific Datasets

9.2.1. SDS Structure

The monthly 1km VNP13A3 VI product has 15 SDSs (Table 19) that are identical to the 16-day VPN13A2 SDS list and at different temporal interval, and we note the absence of the composite day of the year.

Table 19. VNP13A3 File SDS structure

Science Data set	Units	Data Type	Valid Range	Fill*	Scale
1km monthly NDVI	NDVI	INT16	-10,000 - 10,000	-15,000	10,000
1km monthly EVI	EVI	INT16	-10,000 – 10,000	-15,000	10,000
1km monthly EVI2	EVI2	INT16	-10,000 – 10,000	-15,000	10,000
1km monthly VI Quality	bits	UINT16	0 - 65534	65535	N/A
1km monthly red reflectance	Reflectance	INT16	0 – 10,000	-1000	10,000
1km monthly NIR reflectance	Reflectance	INT16	0 – 10,000	-1000	10,000
1km monthly blue reflectance	Reflectance	INT16	0 – 10,000	-1000	10,000
1km monthly green reflectance	Reflectance	INT16	0 – 10,000	-1000	10,000
1km monthly SWIR1 reflectance	Reflectance	INT16	0 – 10,000	-1000	10,000
1km monthly SWIR2 reflectance	Reflectance	INT16	0 – 10,000	-1000	10,000
1km monthly SWIR3 reflectance	Reflectance	INT16	0 – 10,000	-1000	10,000
1km monthly view zenith angle	Degree	INT16	0 – 18,000	-20,000	100
1km monthly sun zenith angle	Degree	INT16	0 – 18,000	-20,000	100
1km monthly relative azimuth angle	Degree	INT16	-18,000 - 18,000	-20,000	100
1km monthly pixel reliability	Rank	INT8	0 - 11	-4	N/A

*: See Fill additional notes in Table 12 page 43

9.2.2. Pixel reliability & Quality Assurance

Each VNP13A3 output pixel has a pixel reliability index (rank) that summarizes the data quality (Table 5), and a single QA SDS for all VIs (NDVI, EVI,EVI2) quality assurance (Table 13).

9.3. Product Specific Metadata

A listing of the metadata fields used for QA evaluation of the VNP13A3 VI product is below (Table 20).

Table 20. Metadata fields for QA evaluation of VNP13A3

Inventory Metadata fields for all VI products (searchable)		
QAPERCENTINTERPOLATEDDATA QAPERCENTMISSINGDATA QAPERCENTOUTOFBOUNDSDATA QAPERCENTCLOUDCOVER QAPERCENTGOODQUALITY QAPERCENTOTHERQUALITY QAPERCENTNOTPRODUCEDCLOUD QAPERCENTNOTPRODUCEDOTHER		
Product specific metadata (searchable)		
Product	Specific metadata variable name (best quality)	
VNP13A3	NDVI1KMMONTHQCLASSPERCENTAGE	
VNP13A3	EVI1KMMONTHQCLASSPERCENTAGE	
VNP13A3	EVI21KMMONTHQCLASSPERCENTAGE	
Archived Metadata (not searchable)		
Product	Metadata variable name (Array of QA usefulness histogram)	
VNP13A3	QAPERCENTPOOR1KM16MONTHNDVI	
VNP13A3	QAPERCENTPOOR1KM16MONTHEVI	
VNP13A3	QAPERCENTPOOR1KM16MONTHEVI2	

9.4. Global and Local Metadata Attributes

VNP13A3 Metadata attributes are identical to the VNP13A2 (16-day 1km VI), see **Appendix I**.

10. VNP13C1 (16days 0.05deg) Vegetation Index product

The S-NPP VIIRS VI CMG series is a seamless global 3600x7200 pixel data product with 18 data layers, SDSs. Each file is approximately 120 MB per composite period (using internal compression). This is a higher quality climate product useful for modeling and long term global spatial analysis of Earth surface processes (Justice et al 2003). The algorithm employs a QA filter scheme that removes lower quality and cloud-contaminated pixels during aggregation and reprojection of the input 1-km data into the 0.05° geographic (lat/lon) grid. It uses a spatial gap filling scheme based on historic long term average data records, to produce a continuous, gap free and high quality product for ready ingestion by biogeochemical, carbon, and climate models.

In addition, this product uses a true static Land/Water mask that is not based on input data LW mask status, rather it uses an external fixed ancillary LW mask. Due to the complex process of orbital data gridding (L2 to L2 Grid) that bins sensor raw data into fixed Earth grid locations (bins)

and due to the size of the sensor foot print at the edge of each scan (observations that tend to grow with the view angle), the process in addition of the slight Geolocation errors (Wolfe et al. 2002) result in slight spatial inconsistencies especially at the edge of water bodies, coastlines, and areas where the land cover changes. To minimize the impact we use a static external LW mask and bypass the internal per pixel LW mask status.

10.1. Algorithm Description

Global VNP13C1 data are cloud free spatial composites of the gridded 16-day 1-km VNP13A2, and are provided as a level-3 product projected on a 0.05 degree (5600-meter) Geographic Climatic Modeling Grid (CMG) map. Figure 37 shows the processing steps of the CMG algorithm.
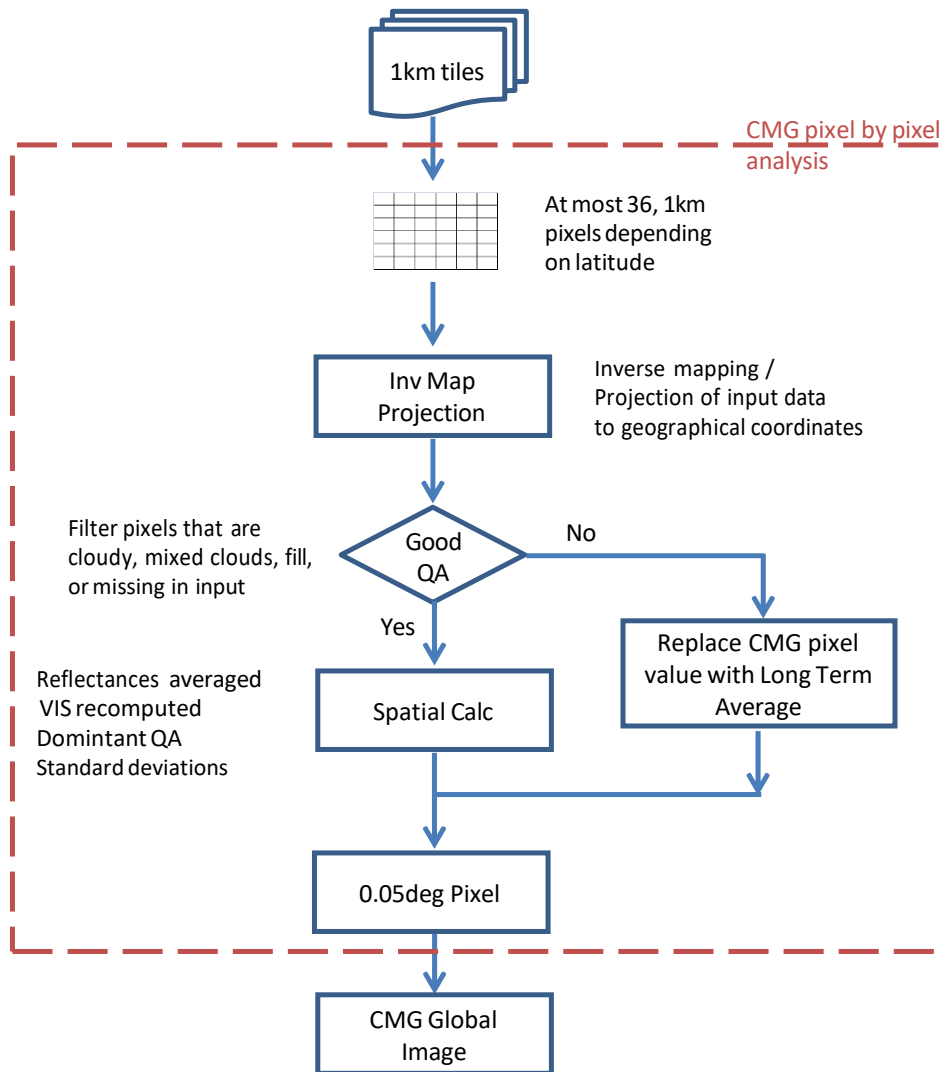
Figure 37. VNP13C1 Algorithm and data processing flow

The algorithm eliminates all cloudy observations from the input and the remaining pixels are averaged using three different schemes. All input 1-km pixels (nominal 6x6) will either be all clear, all cloudy, or mixed. These averaging schemes work as shown in Fig. 38: If all input pixels are clear,

they will be all averaged to produce one output value. If all input pixels are cloudy, the pixel will be estimated from the gap filling historical long term average; and If the input pixels are mixed, only the clear pixels are averaged to produce one output value.

1

Clear	Clear	Clear	Clear	Clear	Clear
Clear	Clear	Clear	Clear	Clear	Clear
Clear	Clear	Clear	Clear	Clear	Clear
Clear	Clear	Clear	Clear	Clear	Clear
Clear	Clear	Clear	Clear	Clear	Clear
Clear	Clear	Clear	Clear	Clear	Clear

→ Average all Pixels

2

Cloud	Cloud	Cloud	Cloud	Cloud	Cloud
Cloud	Cloud	Cloud	Cloud	Cloud	Cloud
Cloud	Cloud	Cloud	Cloud	Cloud	Cloud
Cloud	Cloud	Cloud	Cloud	Cloud	Cloud
Cloud	Cloud	Cloud	Cloud	Cloud	Cloud
Cloud	Cloud	Cloud	Cloud	Cloud	Cloud

→ Use long term VI value

3

Cloud	Cloud	Cloud	Cloud	Cloud	Cloud
Cloud	Clear	Clear	Cloud	Cloud	Cloud
Clear	Clear	Clear	Cloud	Cloud	Cloud
Clear	Clear	Clear	Cloud	Cloud	Cloud
Clear	Clear	Clear	Cloud	Cloud	Cloud
Clear	Clear	Cloud	Cloud	Cloud	Cloud

→ Average only clear values

Figure 38. VI Spatial averaging

An essential part of CMG processing is the presence of a global long term average dataset. This dataset will not only be used to fill pixels where the input cannot be used but also used to replace gaps in case of no data due to instrument error, orbit gaps, etc. In few instances even full tiles are replaced from this long term average database. The database consists of NDVI, EVI and EVI2 data layers and the static land water mask. The resulting global products will always be gap free for VIs, but not the surface reflectance layers and other SDSs (Figure 37). The Pixel reliability layer (Rank) has a specific value (11=LTAVG) to indicate the pixel value was taken from the database.

This database of fill values is calculated from the average of the good data from all previous years CMGs for that composite period. As of V1, VIIRS VI values from 2012 to 2015 were used to generate this long term average databases. The input values from 1KM 16 days VI datasets were resampled to CMG and reprojected to lat/lon coordinates. This database will be regularly updated with new data. And while this works fine for most pixels, it does have serious disadvantages in case of disturbances as the pixel will be replaced with data from a long term average prior to the disturbance.

Certain highly dynamic Land covers may show sudden change when filled from the long term database. However, for pixels missing due to cloud contamination, the fill strategy performs well on average. The algorithm only gap fills the three VI layers, all other layers remain empty with fill values, except for the data layer '#1 km pix used', which is set to 0, i.e. no good input data.
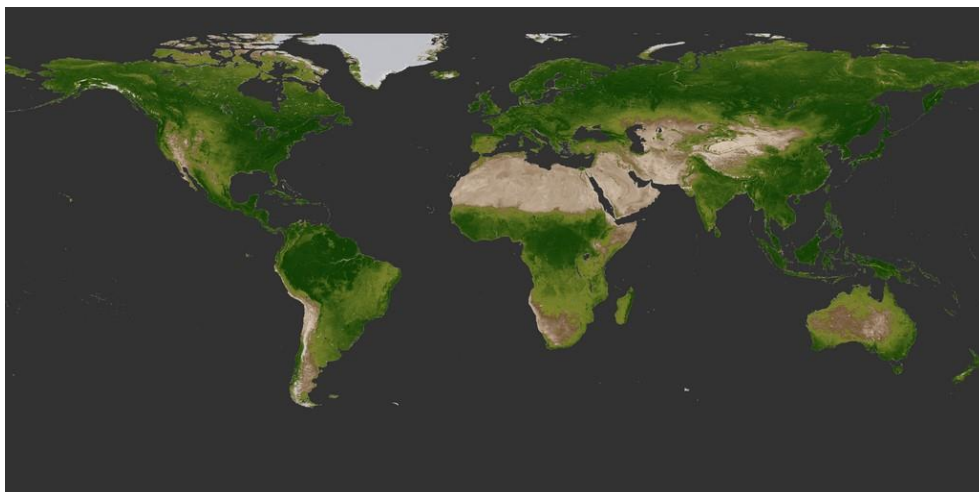
Figure 39. Global Gapfilled NDVI from Long Term Average

10.2. Scientific Datasets

10.2.1. SDS Structure

The 16-day 0.05 deg VNP13C1 VI product has 18 SDS's, as listed in Table 21.

Table 21. List of SDS's from 16-day 0.05 deg VNP13C1 VI

Science Data set	Units	Data Type	Valid Range	Fill*	Scale
CMG 0.05deg 16 days NDVI	NDVI	INT16	-10,000 - 10,000	-15,000	10,000
CMG 0.05deg 16 days EVI	EVI	INT16	-10,000 – 10,000	-15,000	10,000
CMG 0.05deg 16 days EVI2	EVI2	INT16	-10,000 – 10,000	-15,000	10,000
CMG 0.05deg 16 days VI Quality	bits	UINT16	0 - 65534	65535	N/A
CMG 0.05deg 16 days red reflectance	Reflectance	INT16	0 – 10,000	-1000	10,000
CMG 0.05deg 16 days NIR reflectance	Reflectance	INT16	0 – 10,000	-1000	10,000
CMG 0.05deg 16 days blue reflectance	Reflectance	INT16	0 – 10,000	-1000	10,000
CMG 0.05deg 16 days green reflectance	Reflectance	INT16	0 – 10,000	-1000	10,000
CMG 0.05deg 16 days SWIR1 reflectance	Reflectance	INT16	0 – 10,000	-1000	10,000
CMG 0.05deg 16 days SWIR2 reflectance	Reflectance	INT16	0 – 10,000	-1000	10,000
CMG 0.05deg 16 days SWIR3 reflectance	Reflectance	INT16	0 – 10,000	-1000	10,000
CMG 0.05deg 16 days Avg sun zen angle	Degree	INT16	0 – 18,000	-20,000	100
CMG 0.05deg 16 days NDVI std dev	NDVI	INT16	0 - 10,000	-15,000	10,000
CMG 0.05deg 16 days EVI std dev	EVI	INT16	0 - 10,000	-15,000	10,000
CMG 0.05deg 16 days EVI2 std dev	EVI2	INT16	0 - 10,000	-15,000	10,000
CMG 0.05deg 16 days #1km pix used	Pixels	UINT8	0 - 36	255	1
CMG 0.05deg 16 days #1km pix +-30deg VZ	Pixels	UINT8	0 - 36	255	1
CMG 0.05deg 16 days pixel reliability	Rank	INT8	0 - 1	-4	N/A

*: See Fill additional notes in Table 12 page 43

10.2.2. Pixel Reliability & Quality Assurance

Each VNP13C1 output pixel has a Rank summary SDS (Table 5), and a single QA SDS for all VIs (NDVI,EVI,EVI2) quality assurance (Table 13). Pixel reliability SDS will show value of 11 (LTAVG) if a

pixel was replaced from the long term average database. Users can use this Rank value to mask and remove the long term average values from this product if not desired.

The VI Usefulness rank (bits 2-5 in the QA SDS) computation is performed for VNP13C1 according to the criteria showed in Table 13. Detailed QA bit 0-13 are kept the same as for VNP13A2;

bits 14-15 are replaced as shown in Table 22.

Table 22. Bits 14-15 of the VNP13C1 VI Quality Assessment SDS

Bits Parameter Name	Value	Description
14-15 Geospatial quality	00	≤ 25% of the finer 1km resolution contributed to this
	01	> 25% and ≤ 50% of the finer 1km resolution
	10	>50% and ≤ 75% of the finer 1km resolution
	11	> 75% of the finer 1km resolution contributed to this

10.2.3. QA Metadata

A listing of the QA metadata fields used in the VNP13C1 VI product is shown in Table 23.

Table 23. Metadata fields for QA evaluation of VNP13C1

Inventory Metadata fields for all VI products (searchable)		
QAPERCENTINTERPOLATEDDATA		
QAPERCENTMISSINGDATA		
QAPERCENTOUTOFBOUNDSDATA		
QAPERCENTCLOUDCOVER		
QAPERCENTGOODQUALITY		
QAPERCENTOTHERQUALITY		
QAPERCENTNOTPRODUCEDCLOUD		
QAPERCENTNOTPRODUCEDOTHER		
Product specific metadata (searchable)		
Product	Specific metadata variable name (best quality)	
VNP13C1	NDVICMG16DAYQCLASSPERCENTAGE	
VNP13C1	EVICMG16DAYQCLASSPERCENTAGE	
VNP13C1	EVI2CMG16DAYQCLASSPERCENTAGE	
Archived Metadata (not searchable)		
Product	Metadata variable name (Array of QA usefulness histogram)	
VNP13C1	QAPERCENTPOORCMG16DAYNDVI	
VNP13C1	QAPERCENTPOORCMG16DAYEVI	
VNP13C1	QAPERCENTPOORCMG16DAYEVI2	

10.3.   Global and Local Metadata Attributes

All VIIRS VI products contain local and global metadata that is written during the product generation. The local metadata is written as attributes of the SDS within the HDF file. This global metadata is useful for archiving, searching, and ordering the product and provides other key attributes about the file.

10.3.1. Global Metadata Attributes

Each HDF file contains a long list of attribute object structure (slightly abridged for this documentation). The list of this structure is in **Appendix - II**

10.3.2. Global File Attributes

The Global file attributes of VNP13C1 provide useful information about the Algorithm, processing center, and other aspects of the product, and are:

- AlgorithmType
- AlgorithmVersion
- DataResolution
- DayNightFlag
- DayNumbers
- EastBoundingCoord
- EndTime
- InputPointer
- LocalGranuleID
- LongName
- NorthBoundingCoord
- NumberofInputGranules
- PGENumber
- PGEVersion
- PGE_EndTime
- PGE_Name
- PGE_StartTime
- PlatformShortName
- ProcessVersion
- ProcessingCenter
- ProcessingEnvironment
- ProductionTime
- RangeBeginningDate
- RangeBeginningTime
- RangeEndingDate
- RangeEndingTime
- SensorShortName
- ShortName
- SouthBoundingCoord
- StartTime
- VersionID
- WestBoundingCoord
- identifier_product_doi

- identifier_product_doi_authority

11.   VNP13C2 (monthly 0.05deg) Vegetation Index ESDR

Global VNP13C2 data are cloud-free temporal composites of the 16-day VNP13C1 products. VNP13C2 is a level-3 product projected on a 0.05 degree (5600-meter) Geographic (lat/lon) Climate Modeling Grid (CMG). Cloud-free coverage is achieved by replacing clouds with historical VIIRS VI time series climatology record during the generation of the input 16-day VNP13C1 CMG product.

11.1.   Algorithm description

This algorithm operates (Figure 40) on a per-pixel basis and ingest all 16-day VI products that overlap with the calendar month. Once all 16-day composites are present, a weight factor based on the degree of temporal overlap is applied to each input. In assigning the pixel QA, a worst case scenario is used, whereby the pixel with the lowest quality determines the final pixel QA. Once again, Normal Production and Phased Production streams are used together to increase the potential number of observations. However, this is different from the 1KM monthly VI product (VNP13A3) as the data does not permit the filtering based on the exact DOY of the observation, since the input data (VNP13C1) does not include a SDS layer indicating the composite day of the pixel. However, given that the CMG pixel was generated from a pool of 36 1km observations, the probability of observations from a day that intersects the month increases. And because the weights are directly proportional to the overlapping period, the second period (that falls the most in the month) contributes the highest to the final monthly pixel value. This minimize any biases associated with using data from outside the month.
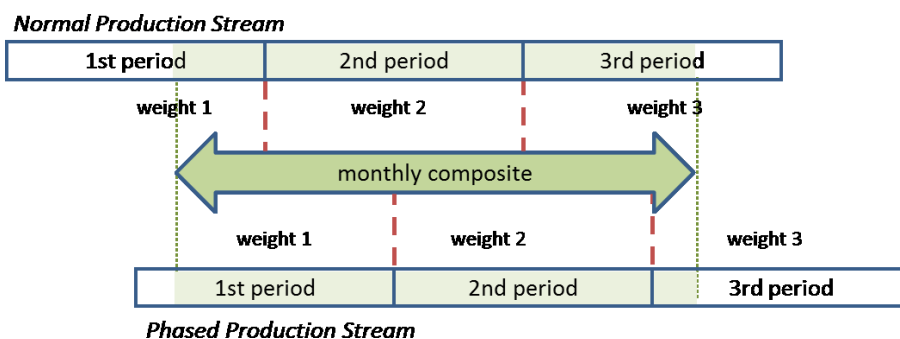
Figure 40. Monthly CMG VIIRS VI flow diagram

11.2.   Scientific Datasets

11.2.1. SDS Structure

VNP13C2 VI product has 18 SDSs, listed on 24

Table 24. List of SDS's from monthly 0.05-deg VNP13C2 VI

Science Data set	Units	Data Type	Valid Range	Fill*	Scale
CMG 0.05 Deg monthly NDVI	NDVI	INT16	-10,000 - 10,000	-15,000	10,000
CMG 0.05 Deg monthly EVI	EVI	INT16	-10,000 – 10,000	-15,000	10,000

CMG 0.05 Deg monthly EVI2	EVI2	INT16	-10,000 – 10,000	-15,000	10,000
CMG 0.05 Deg monthly VI Quality	bits	UINT16	0 - 65534	65535	N/A
CMG 0.05 Deg monthly red reflectance	Reflectance	INT16	0 – 10,000	-1000	10,000
CMG 0.05 Deg monthly NIR reflectance	Reflectance	INT16	0 – 10,000	-1000	10,000
CMG 0.05 Deg monthly blue reflectance	Reflectance	INT16	0 – 10,000	-1000	10,000
CMG 0.05 Deg monthly green reflectance	Reflectance	INT16	0 – 10,000	-1000	10,000
CMG 0.05 Deg monthly SWIR1 reflectance	Reflectance	INT16	0 – 10,000	-1000	10,000
CMG 0.05 Deg monthly SWIR2 reflectance	Reflectance	INT16	0 – 10,000	-1000	10,000
CMG 0.05 Deg monthly SWIR3 reflectance	Reflectance	INT16	0 – 10,000	-1000	10,000
CMG 0.05 Deg monthly Avg sun zen angle	Degree	INT16	0 – 18,000	-20,000	100
CMG 0.05 Deg monthly NDVI std dev	NDVI	INT16	0 - 10,000	-15,000	10,000
CMG 0.05 Deg monthly EVI std dev	EVI	INT16	0 - 10,000	-15,000	10,000
CMG 0.05 Deg monthly EVI2 std dev	EVI2	INT16	0 - 10,000	-15,000	10,000
CMG 0.05 Deg monthly #1km pix used	Pixels	UINT8	0 - 36	255	1
CMG 0.05 Deg monthly #1km pix +-30deg	Pixels	UINT8	0 - 36	255	1
CMG 0.05 Deg monthly pixel reliability	Rank	INT8	0 - 11	-4	N/A

*: See Fill additional notes in Table 12 page 43

11.2.2. Pixel reliability & Quality Assurance

Like with all VIIRS VI products, the VNP13C1 also generates a pixel reliability and QA SDSs documenting the quality of each pixel and thus useful for data post analysis and applications. Each VNP13C2 output pixel has a rank summary (Table 5) and a single QA SDS for NDVI, EVI and EVI2 quality assurance.

11.3. QA Metadata

A listing of the QA metadata fields used in the VNP13C2 VI product is shown in Table 25.

Table 25. Metadata fields for QA evaluation of VNP13C2 products

Inventory Metadata fields for all VI products (searchable)
QAPERCENTINTERPOLATEDDATA
Product specific metadata (searchable)
Product   Specific metadata variable name (best quality)
Archived Metadata (not searchable)
Product   Metadata variable name (Array of QA usefulness histogram)

11.4. Global and Local Metadata Attributes

VNP13C2 and VNP13C1 share the same structural metadata, with slight differences that capture the temporal resolution.

12. S-NPP VIIRS VI Record Error and Characterization

All S-NPP VI products, as was the case with EOS-MODIS and AVHRR (Nemani et al 2003, Myneni et al. 1997, Huete et al. 2006 & 2008) are suitable for the study of land surface vegetation short, medium, and long term patterns, trends and anomalies and are capable of supporting various ecosystem, biogeochemical, and climate models by providing key information about land the surface and vegetation cover. However, the error and uncertainty associated with these Vegetation Index products are sometimes quite large, complex, and time and space dependent. VI products need to be well characterized in order to promote accurate and proper use of the time series. It is however practically impossible to directly quantify the error in a vegetation index product due to the nature of the index itself, the underlying remote sensing data, and the spatial and temporal context.

One can still explore other quasi-quantitative methods that aim to simply characterizing these records and elicit their general error and uncertainty. Here we are proposing a simple framework (Fig. 41) and set of metrics to help characterize and capture the error and uncertainty in these products. In addition, a global spatially explicit statistical analysis is also proposed to help establish the error and characterize the data record. The methods proposed and discussed here are quasi-quantitative and meant to help characterize the product suite error and not validate the product.
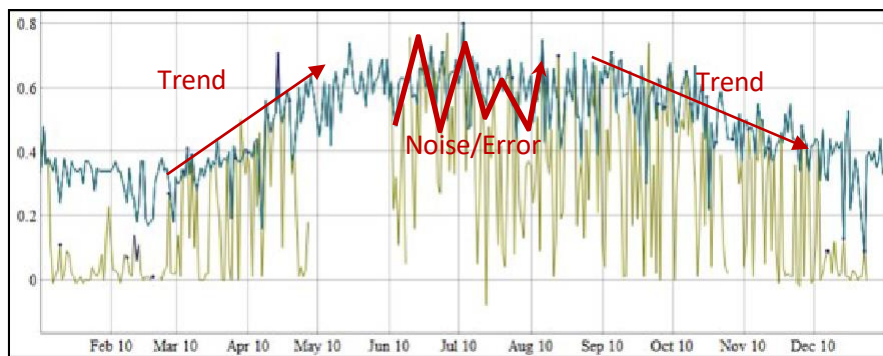
Figure 41. Error and Uncertainty model framework

12.1.   Global VI data record Error Framework

The proposed framework should be spatially and temporally explicit, and is designed to capture key features of these data records:

- **Impact and quality of the atmosphere correction:** This is a key characteristic, and while current atmosphere correction algorithms are capable of addressing and correcting a host of atmosphere issues (water vapor, ozone, Rayleigh scattering, and light to medium aerosols, viewing geometry) their performance is always an issue. In many situations the correction actually exacerbates the problems due to ingesting poor quality ancillary data needed to drive the atmosphere correction algorithm.
- **Departure from the long term average:** The departure although can result from natural factors (growing season or response to drivers), is in many cases the result of noise and error in the data. The departure will be measured by the absolute distance from the long term average. To separate the noise from natural change, the error related departures are identified by examining their persistence. A sustained departure is most likely the result of a natural change/disturbance and not an error in the data.
- **Temporal profile noise:** Although, the VI temporal profiles capture and reflect the natural cycle of vegetation dynamic, they can also result from noise and error in the underlying input data.

Random and large oscillation about the long term average are most likely the result of error in the data and cannot be attributed to natural and gradual vegetation dynamic.

Using this framework, the error is portioned into three categories (Fig. 42):

1. Error related to input (1): Which could be estimated from accurate atmospherically corrected data over validation sites (ex: Aeronet/Sunphotometer sites, Holben et al. 2006).
2. Departure from normal/stable profile (2): Based on long term standard deviations and statistical analyses of the records.
3. Temporal profile noise/stability (3): Will be based on change about normal/mean. This indicates noise in data records and inhibits the profile characterization especially in the context of phenology metrics extraction.
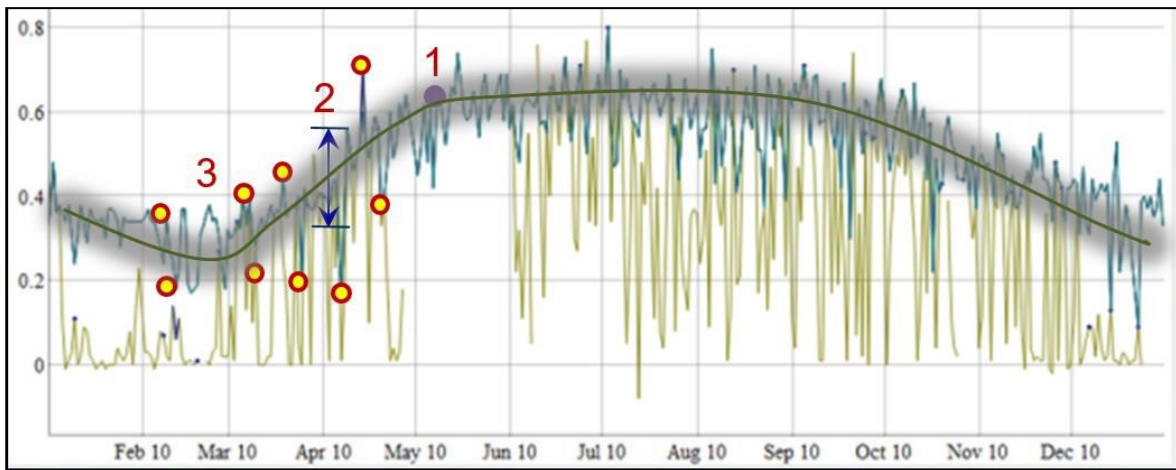
Figure 42. Error model

12.1.1. LSR Input Related Error

Herein, we're not concerned with the VI formulation, but the error in the input to the VI equation and how it translates into a VI error (envelope). This measures how close to the actual top of canopy the reflectance values are (TOC), which is an indication of the ability to remove all atmosphere contamination by the atmosphere correction algorithm.

To estimate this error, we use Surface Reflectance data from validation sites (ex: sunphotometers measurements over EOS Core validation sites, work maintained by the Land Product Validation group, LPV). The LSR error was estimated (EOS MODIS LPV website, http://landval.gsfc.nasa.gov/ and https://lpvs.gsfc.nasa.gov/) to average about 2-5% in the Red & NIR for high quality data (Vermote et al, https://landval.gsfc.nasa.gov/ProductStatus.php?ProductID=MOD09). This corresponds to the general error in estimating the surface reflectance under no clouds, no residual clouds, no to minimum aerosol, and ideal atmosphere conditions. Using an ad-hoc approach we can then model a maximum error, assuming the presence of residual to medium aerosols loads, of about ±10% in the Red/NIR reflectance. This means an assumption of double the error reported over sunphotometer sites in estimating the land surface reflectance under less than ideal conditions, or 10% error. Using a simple and direct transfer function we can estimate the impact of this surface reflectance error on the VI using the equation (Fig. 43).
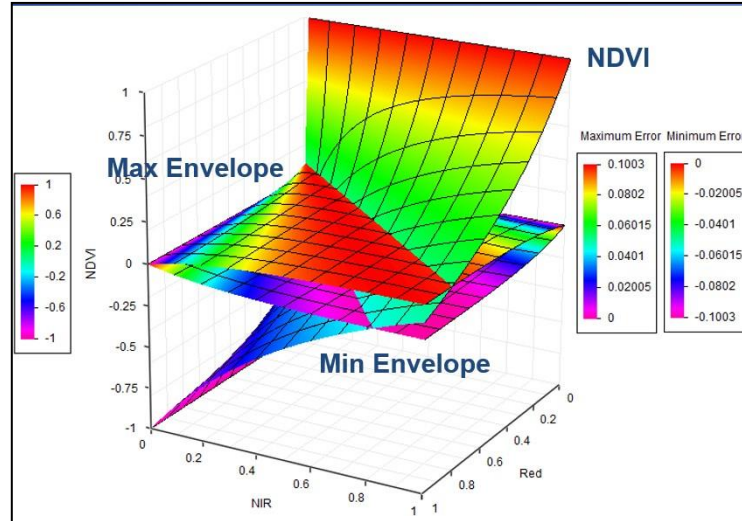
Figure 43. Input surface reflectance error impact on estimating NDVI. The NDVI error envelop range between -0.1 to 0.1 VI units.

Using this simple transfer model, the resulting maximum VI error was estimated to:
- For vegetated areas (High NDVI values) ~= 0.04-0.05 VI Units (~1-5-% relative)
- For sparsely and non-vegetated areas (Low NDVI values) ~= 0.11 VI Units (~100% relative)

12.1.2. Spatial Error Modeling

To model the input error spatially and estimate its impact on the resulting VI data we can further translate the VI error values from the model in Fig. 43 to a long term annual average map of red and NIR. Each pair of red and NIR corresponds to a unique VI value and error envelope and a spatial error distribution map can easily be constructed (Figs. 44 &45).
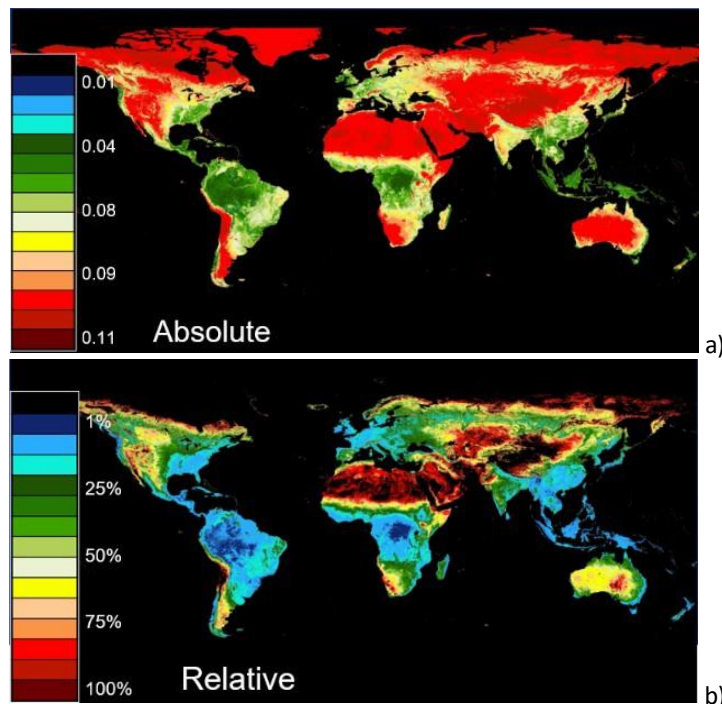
Figure 44. Spatial map of the absolute and Relative NDVI Error using the model from Fig. 43.
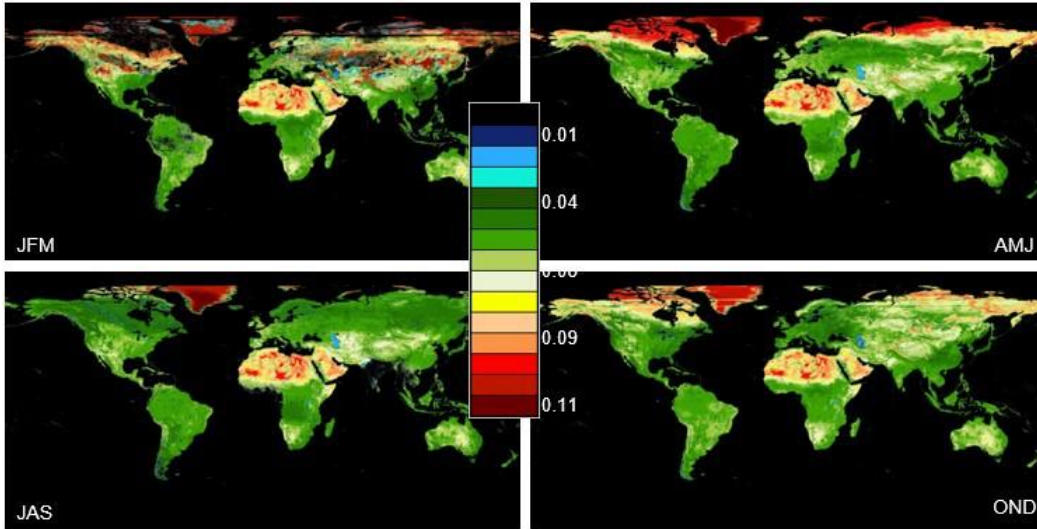
Figure 45. Similar to NDVI an EVI (EVI2) seasonal error spatial distribution can be estimated following the same model.

12.1.3. Standard Deviation of the VI ESDRs

In statistics the standard deviation depicts the departure from normal/average, or how spread the data about its average. In the context of the VI data record the standard deviation captures the impact of both natural processes and noise related error on the time series. This error is estimated by statistical analysis of the long term standard deviation of the VI profiles and is readily and explicitly estimated in space (Fig. 46).
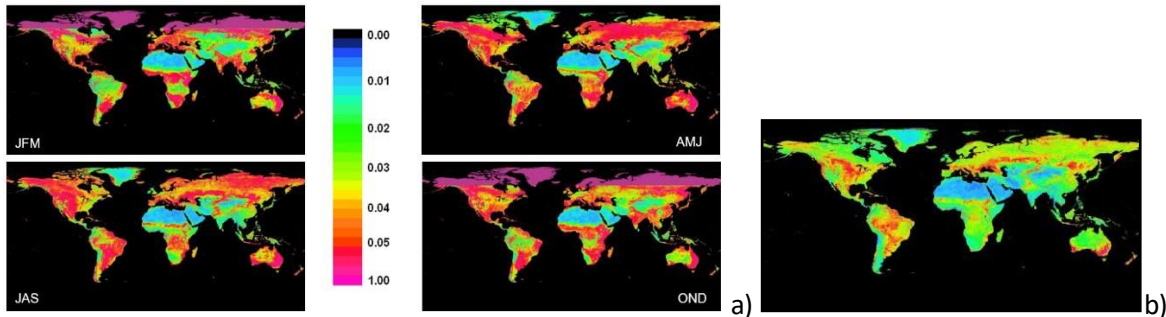
Figure 46. VI Standard deviation (error) or departure from long term average. (a) The seasonal NDVI error, and (b) the EVI standard deviation error shows a smaller range.

Using this statistical approach, the overall global average error is:

- 0.05 (VI Units) for vegetated and 0.005 (VI Units) for sparse or non-vegetated areas
- With largest error observed over vegetated areas and during spring/summer (peak growing season)

With this framework we computed spatially explicit annual error metrics for each pixel. The resulting global maps elucidate the spatial coherency and error in these ESDRs. The results can aid end users assess these records and associate a spatial and seasonal per-pixel estimate of error and uncertainty. Post analysis results using these records can be constrained and their significance established. Overall the error due to the surface reflectance input uncertainty, under ideal observing conditions, was rather small with an absolute max value of ~0.05, except for sparsely vegetated areas where it becomes relatively high up to 100% due to the signal (VI<=0.1) being small and overwhelmed by noise. The impact on EVI and EVI2 was larger than that of NDVI. The error

was also largest during the winter due to the presence of snow/ice which introduces more noise in the input data and inhibits atmosphere correction.

12.1.4. Accuracy Precision and Uncertainty (APU) of the VI record

The nature of the VI data makes assessing error, uncertainty, precision very challenging and not readily possible. Traditionally remote sensing measurements were characterized and validated using:

1. **A variety of ground truth and field data**
   - To establish the ground truth by perfectly correcting the data over the field site
   - Compare against the field data using QA filtered highest possible observations

But this usually leads to limited representation and scaling issues and challenges. Moreover, this is a validation of the actual algorithm under ideal conditions rather than real validation of actual data under normal observation conditions. These limitations suggest assessing the products using:

2. **Statistical approaches**

Using a variety of metrics to establish the product's APU characteristics, including:

   - Calculate AVG and STDEV, then estimate the **Uncertainty** as the range between AVG ± STDEV
   - Compute the **Precision** as STDEV /AVG
   - And compute the **Accuracy** as the difference between the AVG and a "true measurement". But since there is not spatially explicit ground truth data record to be used to derive the precision, one can use approximation by TM (Gao et al. 2003) or use a longer more established data record like Aqua or Terra MODIS VI record.

To compute the global NDVI, EVI, and EVI2 APU metrics we used long term data clustered by Land Cover to estimate average and standard deviation (Table 26).

Table 26: Global land cover dependent APU estimates using long term sensor time series and MODIS land cover maps. These estimates can then be transferred back to a LC map (Fig. 47).

	VIIRS NDVI						TERRA NDVI					AQUA NDVI				
Land Cover	AVERAGE	STDEV	UNCERTAINTY		PRECISION (%)	ACCURACY	AVERAGE	STDEV	UNCERTAINTY		PRECISION (%)	AVERAGE	STDEV	UNCERTAINTY		PRECISION (%)
Snow/Ice	-0.029	0.001	-0.030	-0.028	-3.34	-0.013	-0.042	0.015	-0.057	-0.027	-36.10	-0.060	0.027	-0.087	-0.033	-41.41
Evergreen needleleaf forest	0.832	0.017	0.814	0.849	2.10	-0.028	0.803	0.042	0.761	0.846	5.28	0.383	0.028	0.355	0.411	2.96
Deciduous needleleaf forest	0.802	0.059	0.743	0.861	7.34	-0.028	0.774	0.044	0.730	0.819	5.74	0.386	0.029	0.358	0.415	4.73
Open Shrublands	0.196	0.062	0.133	0.258	31.81	0.008	0.204	0.047	0.157	0.251	23.17	0.137	0.026	0.111	0.163	24.71
Deciduous neededleleaf forest	0.892	0.024	0.868	0.916	2.66	-0.012	0.880	0.028	0.852	0.907	3.15	0.587	0.037	0.550	0.624	4.10
Barren or sparsely vegetated	0.075	0.007	0.068	0.082	9.03	0.025	0.100	0.008	0.091	0.108	8.50	0.073	0.010	0.064	0.083	8.20
Croplands	0.323	0.066	0.257	0.390	20.58	0.003	0.327	0.102	0.225	0.429	31.22	0.220	0.094	0.128	0.315	51.44
Deciduous broadleaf forest	0.882	0.026	0.856	0.908	2.96	-0.036	0.846	0.034	0.812	0.880	4.06	0.479	0.030	0.449	0.508	3.97
Grasslands	0.550	0.049	0.501	0.599	8.85	0.004	0.554	0.044	0.510	0.598	7.89	0.290	0.028	0.262	0.317	7.908
Deciduous broadleaf forest	0.793	0.022	0.771	0.815	2.72	-0.022	0.771	0.058	0.713	0.829	7.52	0.441	0.059	0.382	0.501	13.95
Woody Savannas	0.416	0.057	0.359	0.473	13.77	0.009	0.425	0.051	0.374	0.476	12.09	0.196	0.033	0.160	0.233	13.44
Savannas	0.297	0.018	0.280	0.315	5.91	0.032	0.329	0.017	0.312	0.346	5.29	0.193	0.009	0.184	0.202	5.18
Open Shrublands	0.195	0.014	0.181	0.209	7.35	0.021	0.216	0.011	0.205	0.227	5.02	0.102	0.008	0.094	0.109	4.89

	VIIRS EVI						TERRA EVI					AQUA EVI				
Land Cover	AVERAGE	STDEV	UNCERTAINTY		PRECISION (%)	ACCURACY	AVERAGE	STDEV	UNCERTAINTY		PRECISION (%)	AVERAGE	STDEV	UNCERTAINTY		PRECISION (%)
Snow/Ice	-0.055	0.012	-0.067	-0.043	-21.850	0.003	-0.052	0.030	-0.082	-0.022	-57.00	-0.060	0.027	-0.087	-0.033	-45.16
Evergreen needleleaf forest	0.408	0.031	0.377	0.439	7.589	-0.019	0.389	0.026	0.363	0.415	6.67	0.383	0.028	0.355	0.411	7.23
Deciduous neededleleaf forest	0.415	0.028	0.387	0.443	6.703	-0.034	0.381	0.031	0.350	0.412	8.07	0.386	0.029	0.358	0.415	7.408
Open Shrublands	0.133	0.032	0.101	0.165	24.387	0.000	0.133	0.024	0.109	0.157	18.28	0.137	0.026	0.111	0.163	18.674
Deciduous neededleleaf forest	0.642	0.030	0.613	0.672	4.610	-0.085	0.557	0.044	0.514	0.601	7.87	0.587	0.037	0.550	0.624	6.314
Barren or sparsely vegetated	0.061	0.008	0.053	0.069	13.163	0.014	0.074	0.010	0.064	0.084	13.61	0.073	0.010	0.064	0.083	13.003
Croplands	0.248	0.055	0.194	0.303	22.071	-0.024	0.224	0.069	0.154	0.293	31.028	0.220	0.094	0.128	0.315	42.892
Deciduous broadleaf forest	0.524	0.029	0.495	0.554	5.566	-0.051	0.473	0.024	0.449	0.497	5.16	0.479	0.030	0.449	0.508	6.252
Grasslands	0.312	0.030	0.282	0.342	9.596	-0.030	0.282	0.026	0.256	0.309	9.39	0.290	0.028	0.262	0.317	9.61
Deciduous broadleaf forest	0.435	0.020	0.415	0.455	4.646	-0.036	0.399	0.033	0.366	0.432	8.168	0.441	0.059	0.382	0.501	13.478
Woody Savannas	0.209	0.034	0.171	0.239	16.692	-0.022	0.183	0.032	0.151	0.215	17.355	0.196	0.033	0.160	0.233	18.069
Savannas	0.183	0.008	0.175	0.192	4.460	0.000	0.183	0.009	0.175	0.192	4.82	0.193	0.009	0.184	0.202	4.722
Open Shrublands	0.097	0.007	0.090	0.104	7.358	0.002	0.100	0.007	0.092	0.107	7.362	0.102	0.008	0.094	0.109	7.444

	VIIRS EVI2						TERRA EVI2					AQUA EVI2				
Land Cover	AVERAGE	STDEV	UNCERTAINTY		PRECISION (%)	ACCURACY	AVERAGE	STDEV	UNCERTAINTY		PRECISION (%)	AVERAGE	STDEV	UNCERTAINTY		PRECISION (%)
Snow/Ice	-0.032	0.001	-0.033	-0.031	-3.467	-0.010	-0.042	0.012	-0.054	-0.029	-29.536	-0.054	0.015	-0.069	-0.038	-28.666
Evergreen needleleaf forest	0.406	0.029	0.377	0.435	7.099	-0.014	0.392	0.027	0.365	0.418	6.799	0.382	0.028	0.354	0.410	7.217
Deciduous needledleaf forest	0.399	0.036	0.363	0.435	9.058	-0.020	0.379	0.031	0.348	0.410	8.099	0.385	0.029	0.356	0.414	7.538
Open Shrublands	0.136	0.027	0.109	0.163	20.078	0.007	0.143	0.023	0.120	0.166	15.819	0.142	0.023	0.119	0.165	16.301
Deciduous needledleaf forest	0.634	0.030	0.604	0.664	4.726	-0.078	0.555	0.044	0.511	0.599	7.909	0.582	0.038	0.544	0.621	6.609
Barren or sparsely vegetated	0.063	0.010	0.053	0.073	16.189	0.018	0.081	0.013	0.068	0.094	16.410	0.078	0.012	0.066	0.091	15.722
Croplands	0.220	0.052	0.167	0.272	23.817	0.004	0.224	0.069	0.154	0.293	31.037	0.220	0.094	0.126	0.315	42.892
Deciduous broadleaf forest	0.522	0.022	0.500	0.545	4.283	-0.050	0.473	0.024	0.448	0.497	5.144	0.477	0.030	0.448	0.507	6.202
Grasslands	0.306	0.028	0.278	0.335	9.299	-0.015	0.291	0.027	0.264	0.318	9.293	0.290	0.028	0.262	0.318	9.588
Deciduous broadleaf forest	0.424	0.019	0.405	0.444	4.563	-0.029	0.395	0.033	0.363	0.428	8.322	0.438	0.062	0.376	0.499	14.047
Woody Savannas	0.194	0.033	0.162	0.227	16.765	-0.014	0.181	0.032	0.149	0.212	17.536	0.193	0.035	0.157	0.228	18.283
Savannas	0.176	0.009	0.167	0.185	4.944	0.007	0.183	0.010	0.173	0.193	5.321	0.190	0.009	0.181	0.199	4.854
Open Shrublands	0.106	0.008	0.098	0.114	7.367	0.007	0.113	0.009	0.104	0.122	8.163	0.113	0.010	0.104	0.123	8.405

AVERAGE

STDEV

Global NDVI APU

ACCURACY

PRECISION

AVERAGE

STDEV

Global EVI APU

ACCURACY

PRECISION

Figure 47: Statistically modeled Accuracy Precision and Uncertainty of the VI data record. These maps were estimated based on the statistical analysis of long term VI data over clustered land cover. Then results were transferred back to a MODIS LC map.

13. S-NPP VIIRS VI Record Continuity Considerations

Whereas single mission or sensor specific measurements of vegetation index exist, the length of these records is usually limited due to the mission life expectancy, usually few years, engineering and technological changes which necessitates new designs and improvements, and changes in data processing methods and approaches which render the older data undesirable and hard to integrate with newer data. In practice, these limitations impose a restriction on the data usefulness, in particular when addressing long-term phenomenon and trends because they lack representation, or in statistical context, they cannot support the generation of an accurate and representative long-term normal. Extending these records beyond the life span of a single sensor is crucial to remote sensing data.

Three global daily synoptic imagers; AVHRR, MODIS and VIIRS are the current work horse of global land surface vegetation imaging. Up to 1998/2000 AVHHR (N-7, 9, 11, 14) remained the only synoptic remote sensing work horse of Earth Observation, and starting 2000/2002 the records were augmented by data from the much improved EOS MODIS Terra and Aqua (Justice and Townshend 2002; Huete et al. 2002) and to a lesser extend SPOT-VEGETATION (VGT). These records are now being replaced by the operational S-NPP VIIRS and eventually by the *Joint Polar Satellite System* (*JPSS*) VIIRS instrument (Fig. 48). The merits of these systems lie in their time-series of daily multi-spectral observations, which are used to characterize and monitor the land surface at regional to global scales. While not all land products have their heritage in the NOAA-AVHRR, the Vegetation Index data record dates back to 1981 when NOAA's Advanced Very High Resolution Radiometer (AVHRR) started this continuum (Tucker et al. 2005; Brown et al. 2006). This vital VI Earth science record supports monitoring, detecting, and quantifying global land vegetation properties.
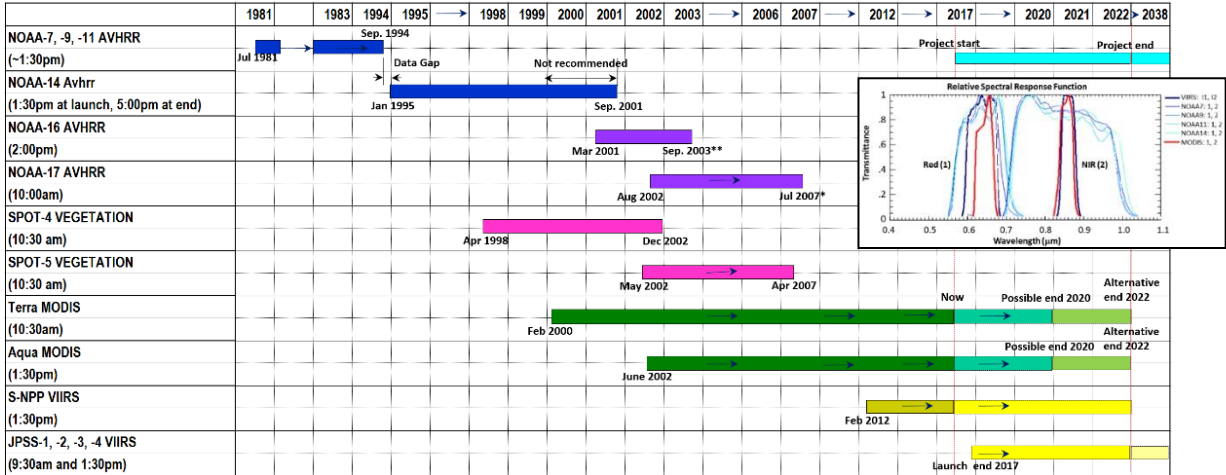
Figure 48: Current single sensor data records, including S-NPP and JPSS (1-4) VIIRS, while providing a 35+ year long time series remain quite disparate and continuity across these sensors need to be accounted for in order to use the record as a single time series. Inset: AVHRR, MODIS, and VIIRS spectral band passes.

To support across sensor data continuity, VIIRS VI data was compared to AVHRR and MODIS records. Figure 49 shows the data histogram distributions with minor differences across the three sensors.
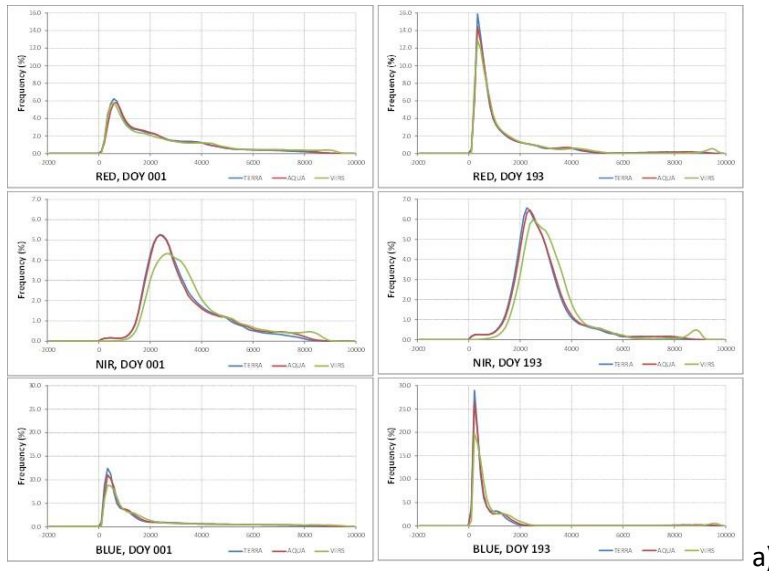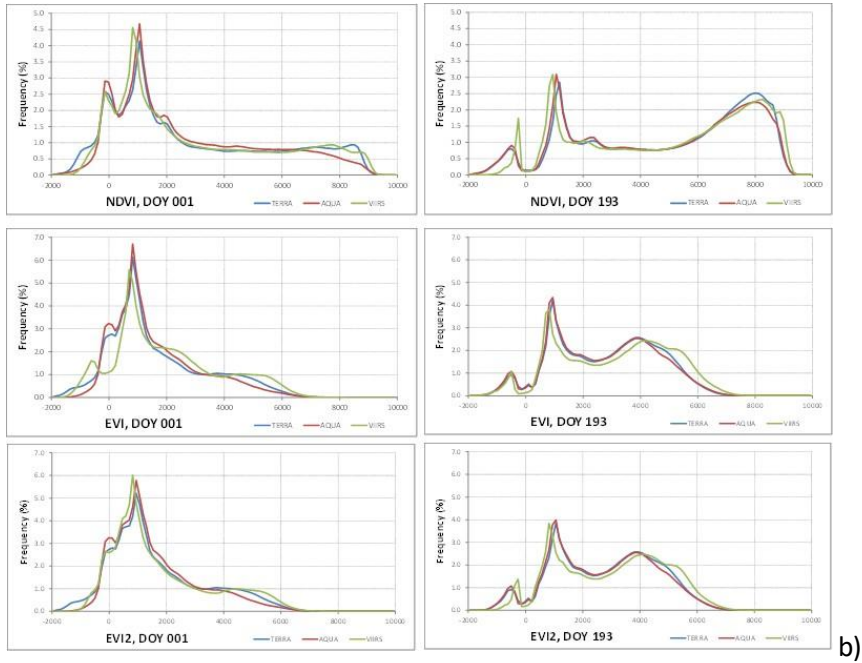
Figure 49: Red, NIR, Blue, and VIs Histogram distributions of T/A MODIS and S-NPP VIIRS. Largest differences in the NIR and blue bands (b) and Largest VI differences at the low and high ends of the range (b) (Tropics, Deserts, Snow/Ice) with VIIRS being higher at the higher end lower at the lower end.

The surface reflectance and VI differences between VIIRS-AVHRR and VIIRS-MODIS are shown in Fig. 50
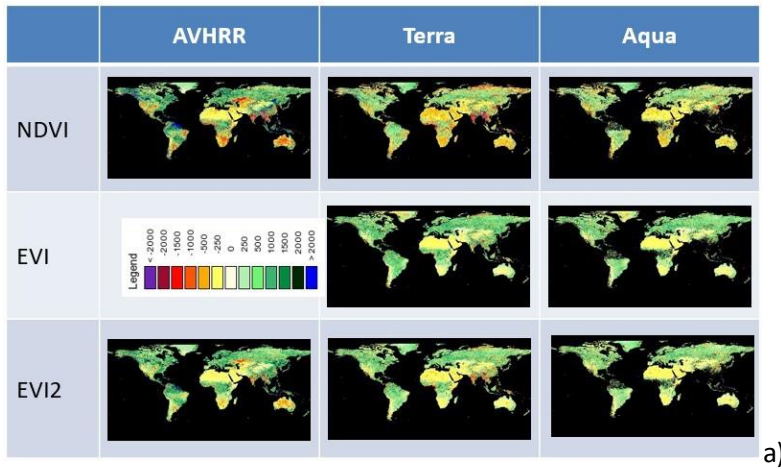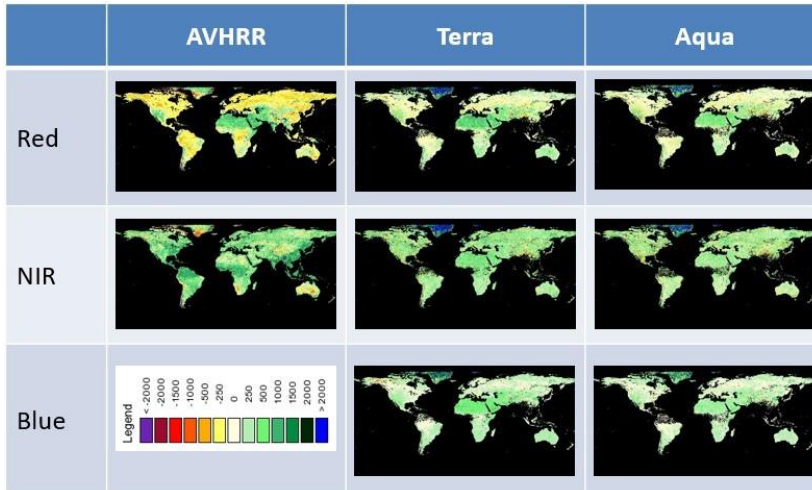
Figure 50: VIs spatial distribution of the difference between VIIRS, AVHRR and MODIS. Globaly the difference is 2-5% and is larger with NDVI than EVI/EVI2. Similarly the average difference in surface reflectance is < 5% with a 2.5% mean.

The sensor land cover based data cross correlations show strong and consistent linearity (R^2>95%., Fig 51), which indicates that VI are for the most part readily interchangeable requiring minor continuity adjustment (Didan et al. 2016).
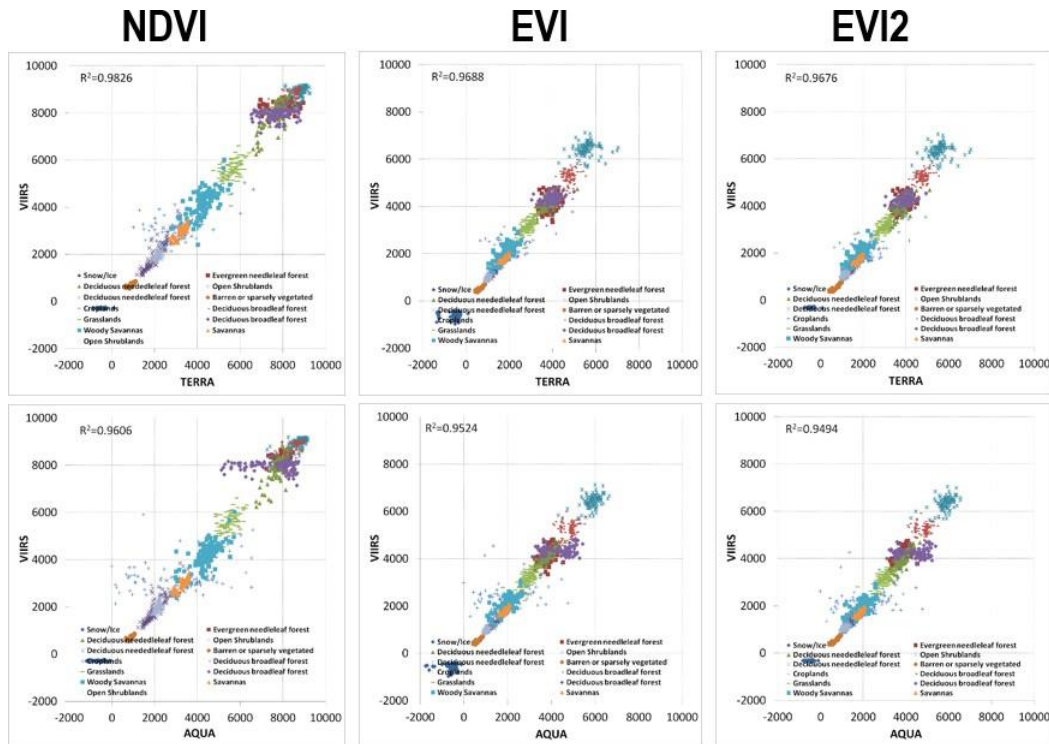
Figure 51: Land cover dependent across sensors VIs correlation. Data form the three sensors are highly correlated (R^2>95%) which should permit translation and continuity.
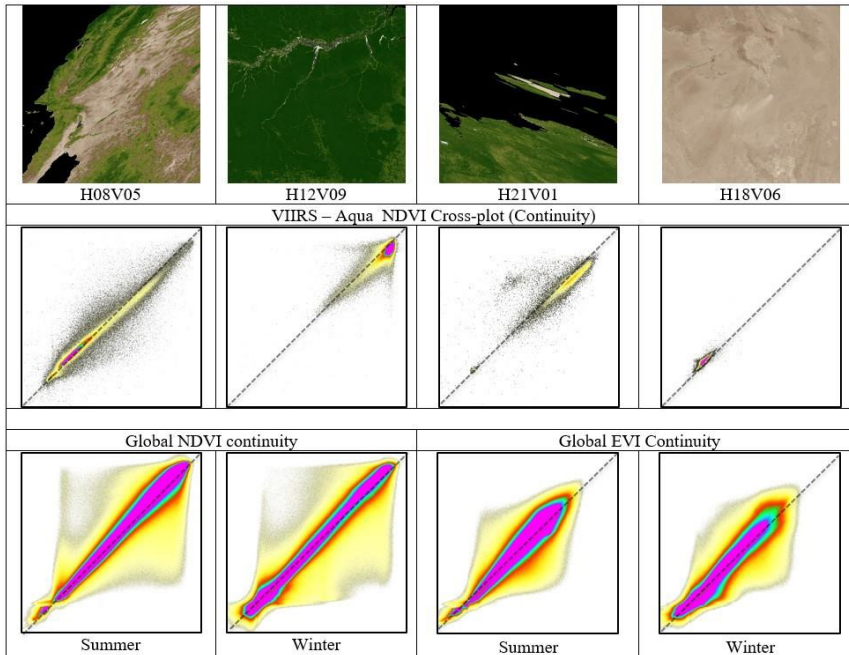
Figure 52: Regional VIIRS and MODIS VI continuity analysis. These correlations could be used to design the transfer functions for the data translation across the two sensors.

Using the above information, and VIIRS/MODIS 2012-2015 overlap data a prototype explicit pixel based monthly continuity transfer maps were developed (Fig. 53) between VIIRS and MODIS (and AVHRR not shown). These transfer maps can be used to translate the VI data cross the two sensors, following equation:

$$VIIRS_{VI} = \alpha(AVHRR_{VI} \text{ or } MODIS_{VI}) + \beta$$
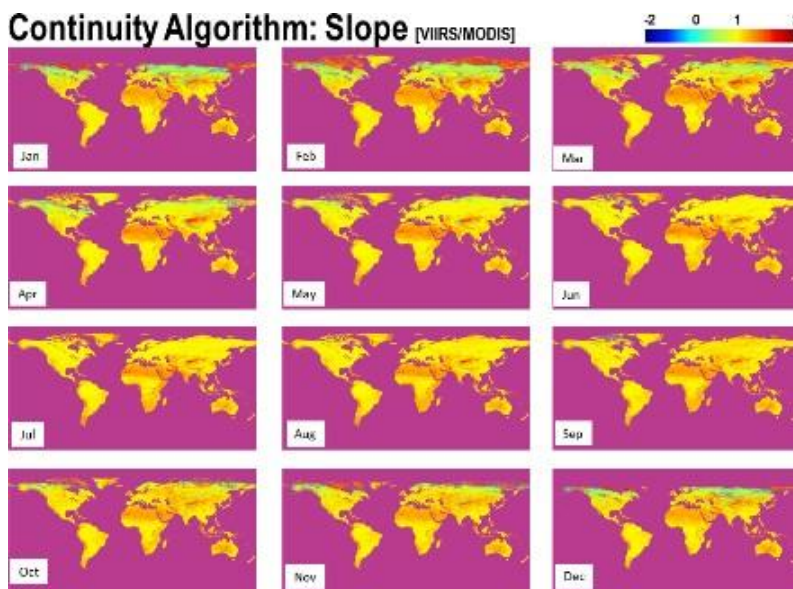
Figure 53. Prototype explicit seasonally dependent per pixel transfer function/map continuity algorithms for VIIRS to MODIS (using data from 2012- 2015).

Any sensor data from AVHRR, MODIS, or VIIRS can be standardized to any other sensor domain

using these transfer maps. Here we are proposing VIIRS as the reference sensor based on practical and contextual reasons, since this work concerns VIIRS, the data record is the most recent, and VIIRS will likely be the longest (considering JPSS plans).

This prototype empirical continuity approaches suggest that VIIRS will perform as good as MODIS (Vargas et al. 2013) and that the VIIRS data record will provide for the extension of this VI time series. Prior work (by the VIP group, vip.arizona.edu, Didan et al. 2016) has shown that empirical and explicit per pixel continuity regionally calibrated approach performs extremely well in addressing the ancillary sources of issues in the data records. This provides a solid and necessary foundation to extending the VI time series across these major sensors.

14. Summary and Conclusions

Continuous acquisition of global satellite imagery over the years has contributed to the creation of a long VI time series from AVHRR, MODIS, TM, SPOT-VGT and other sensors. These records now account for more than 35 years of synoptic Earth surface observation. As these archives grow, they are becoming an invaluable tool for environmental monitoring, resources management, and climate studies from local, to regional, to global scales.

This S-NPP effort is building upon the EOS-MODIS legacy and methods. In this document we presented a set of methodologies and science algorithms for the creation of a consistent multi-spatial and temporal resolution Vegetation Index product suite from the S-NPP VIIRS Sensor. While adapting the various EOS MODIS science algorithms to ingest and process VIIRS data was the primary goal of this project and document, other objectives and opportunities ranging from continuity, data processing strategies, and the longer goal of sustaining the generation of a long term time series data record were also discussed. In addition, we presented and discussed an initial framework for a spatially explicit per-pixel error characterization approach.

The S-NPP VIIRS VI data are public and will be available from the LP-DAAC (lpdaac.usgs.gov) distribution center and via an interactive online tool at the science team's facility (the VIP Data Explorer (vip.arizona.edu/viplab_data_explorer.php) with focus on value addition and on demand time series services.

The S-NPP VIIRS Vegetation Index product suite is building upon the MODIS legacy and shows strong correlation and capabilities to sustain the VI time series for many years.

15. Acknowledgements

References

Agbu, P.A., and James, M.E., 1994. The NOAA/NASA Pathfinder AVHRR Land Data Set User's Manual. Goddard Distributed Active Archive Center, NASA, Goddard Space Flight Center, Greenbelt.

Ahl, D. E., Gower, S. T., Burrows, S. N., Shabanow, N. V., Myneni, R. B., & Knyazikhim, Y. (2006). Monitoring spring canopy phenology of a deciduous broadleaf forest using MODIS. *Remote Sensing of Environment*, *104*, 88-95.

Archard, F., JP. Malingreau, T. Phulpin, G. Saint, B. Saugier, B. Seguin, D. Vidal Madjar, 1994. A mission for global monitoring of the continental biosphere. VEGETATION International Users Committee Secretariat, Joint Research Centre, Institute for Remote Sensing Applications, I-21020 ISPRA (Va) Italy. http://www-vegetation.cst.cnes.fr:8050/.

Asner G, Townsend A, Braswell B (2000). Satellite observations of El Nino effects on Amazon forest phenology and productivity. Geophysical Research Letters, 27, 981-984.

Asrar, G., Fuchs, M., Kanemasu, E.T. and Hatfield, J.L., 1984, Estimating absorbed photosynthetic radiation and leaf area index from spectral reflectance in wheat, Agron. J., 76:300—306.

Baldocchi D, Falge E, Gu L, Olson R, Hollinger D, Running S, Anthoni P, Bernhofer C, Davis K, Evans R, Fuentes J. FLUXNET: A new tool to study the temporal and spatial variability of ecosystem-scale carbon dioxide, water vapor, and energy flux densities. Bulletin of the American Meteorological Society. 2001 Nov;82(11):2415-34.

Beaubien, E.G., and Hall-Beyer, M. (2003) Plant phenology in Western Canada: Trends and links to the view from space. *Environmental Monitoring and Assessment* 88(1-3): 419-429

Begue, A., 1993, Leaf area index, intercepted photosynthetically active radiation, and spectral vegetation indices: a sensitivity analysis for regular-clumped canopies, Remote Sens. Environ. 46:45-59.

Bogaert J, Zhou L, Tucker CJ, Myneni RB, Ceulemans R. Evidence for a persistent and extensive greening trend in Eurasia inferred from satellite vegetation index data. Journal of Geophysical Research: Atmospheres (1984–2012). 2002 Jun 16;107(D11):ACL-4.

Bonan, G.B., Pollard, D. & Thompson, S.L. (1992) ffects of boreal forest vegetation on global climate. *Nature*, 359, 716–718.

Braswell, B. H., Schimel, D. S., Privette, J. L., Moore, B., Emery, W. J., Sulzman, E. W., & Hudak, A. T. (1996). Extracting ecological and biophysical information from AVHRR optical data: An integrated algorithm based on inverse modeling. *Journal of Geophysical Research-Atmospheres*, 101, 23335-23348.

Brown, M. E., Pinzón, J. E., Didan, K., Morisette, J. T., & Tucker, C. J. (2006). Evaluation of the consistency of long-term NDVI time series derived from AVHRR, SPOT-Vegetation, SeaWiFS, MODIS, and Landsat ETM+ sensors.*Geoscience and Remote Sensing, IEEE Transactions on*, *44*(7), 1787-1793.

Cao C, Xiong J, Blonski S, Liu Q, Uprety S, Shao X, Bai Y, Weng F. Suomi NPP VIIRS sensor data record verification, validation, and long-term performance monitoring. Journal of Geophysical Research: Atmospheres. 2013a Oct 27;118(20).

Cao C, Xiong X, Wolfe R, De Luccia F, Liu Q, Blonski S, Lin G, Nishihama M, Pogorzala D, Oudrari H, Hillger D. Visible Infrared Imaging Radiometer Suite (VIIRS) Sensor Data Record (SDR) User's Guide. NOAA Technical Report NESDIS: College Park, MD, USA. 2013b Sep.

Chen, J., Jönsson, P., Tamura, M., Gu, Z., Matsushita, B. and Eklundh, L. (2004): A simple method for reconstructing a high-quality NDVI time-series dataset based on the Savitzky-Golay filter.* Remote Sensing of Environment, 91 332-344.

Churkina G, Schimel D, Braswell BH, Xiao X. Spatial analysis of growing season length control over net ecosystem exchange. Global Change Biology. 2005 Oct 1;11(10):1777-87.

Cihlar, J., Manak, D., and D'Iorio, M., 1994b. Evaluation of Compositing Algorithms for AVHRR Data over Land. IEEE Trans. Geosc. Remote Sens., 32:427-437.

Cihlar, J., Manak, D., and Voisin, N., 1994a. AVHRR Bidirectional Reflectance Effects and Compositing. Remote Sens. Environ., 48:77-88

Cihlar, J.C., H. Ly, Z. Li, J. Chen, H. Pokrant, and F. Huang, 1997. Multi temporal, Multichannel AVHRR data sets for Land Biosphere Studies— Artifacts and Corrections. Remote Sens. Environ. 60:35-57.

Claussen, M. (1994) On coupling global biome models with climate models. *Climate Research*, 4, 203–221.

Cochrane MA, Alencar A, Schulze MD, Souza CM, Nepstad DC, Lefebvre P, Davidson EA. Positive feedbacks in the fire dynamic of closed canopy tropical forests. Science. 1999 Jun 11;284(5421):1832-5.

Colwell, J.E., 1974, Vegetation canopy reflectance, Remote sensing of environment. 1974 Jan 1;3(3):175-83.

Cooke JE, Weih M. Nitrogen storage and seasonal nitrogen cycling in Populus: bridging molecular physiology and ecophysiology. New Phytologist. 2005 Jul 1;167(1):19-30.

Daughtry, C.S.T., Gallo, K.P., Goward, S.N., Prince, S.D., Kustas, W.P., 1992, Spectral estimates of absorbed radiation and phytomass production in corn and soybean canopies, Remote Sens. Environ. 39:141-152.

de Beurs, K.M., and Henebry, G.M. (2005) Land surface phenology and temperature variation in the IGBP high-latitude transects. *Global Change Biology* 11, 779-790.

Deering, D.W., 1978, Rangeland reflectance characteristics measured by aircraft and spacecraft sensors. Ph.D. Dissertation, Texas A & M University, College Station, TX, 338 pp.

Dickinson, R.E. & Henderson-Sellers, A. (1988) Modelling tropical deforestation: a study of GCM land-surface parameterizations. *Quarterly Journal of theRoyal Meteorological Society*, 114, 439– 462.

Didan K., (2010). Multi-Satellite Earth Science Data Record For Studying Global Vegetation Trends And Changes: Phase I Vegetation Index Continuity. *2010 IEEE International Geoscience and Remote Sensing Symposium, 25-30 July 2010, Honolulu, Hawaii, USA*.

Didan K., Barreto A., Miura T., Tsend-Ayush J., Zhang X., Friedl M., Gray J., Van Leeuwen W., CZapla-Myers J., Jenkerson C., Maiersperger T. and Meyer D. (2016). Algorithm Theoretical Basis Document & Users Guide. Version 4.0. Vegetation Index and Phenology Lab. https://vip.arizona.edu/VIP_ATBD_UsersGuide.php

Didan K., Huete R. A., 2006. MODIS VI Product suite, Collection 4.0 to Collection 5.0 changes. On LDOPE. Web (http://landweb.nascom.nasa.gov/QA_WWW/forPage/MOD13_VI_C5_Changes_Document_06_28_06.pdf)

Dungan JL, Peterson DL, Curran PJ. Alternative approaches for mapping vegetation quantities using ground and image data. Environmental information management and analysis: ecosystem to global scales. 1994 Aug 8:237-61.

Eidenshink, J. (2006). A 16-year time series of 1 km AVHRR satellite data of the conterminous United States and Alaska. *Photogrammetric Engineering and Remote Sensing*, 72, 1027-1035.

Eidenshink, J.C. and Faundeen, J.L., 1994, "The 1km AVHRR global land data set: first stages in implementation," Int. J. Remote Sensing, 15(17), pp. 3443-3462.

Epstein PR, Rogers DJ, Slooff R. Conference: Satellite imaging and vector-borne disease. The Lancet. 1993 May 29;341(8857):1404.

Fensholt, R., Sandholt, I., & Stisen, S. (2006). Evaluating MODIS, MERIS, and VEGETATION vegetation indices using in situ measurements in a semiarid environment. *Geoscience and Remote Sensing, IEEE Transactions on*, *44*(7), 1774-1786.

Friedl M., et. al. Land Surface Phenology White Paper, 2006, lcluc.umd.edu/products/Land_ESDR/index.asp

Fung, Y., Tucker, C.J. and Prentice, K.C., 1987. Application of Advanced Very High Resolution Radiometer Vegetation Index to Study Atmosphere-Biosphere Exchange of CO_2. J. Geoph. Res., 92, 2999-3015.

Gallo K, Ji L, Reed B, Eidenshink J, Dwyer J. Multi-platform comparisons of MODIS and AVHRR normalized difference vegetation index data. Remote Sensing of Environment. 2005 Nov 30;99(3):221-31.

Gamon JA, Field CB, Goulden ML, Griffin KL, Hartley AE, Joel G, Penuelas J, Valentini R. Relationships between NDVI, canopy structure, and photosynthesis in three Californian vegetation types. Ecological Applications. 1995 Feb 1;5(1):28-41.

Gedney N, Valdes PJ. The effect of Amazonian deforestation on the northern hemisphere circulation and climate. Geophysical Research Letters. 2000 Oct 1;27(19):3053-6.

Geng G, Wu J, Wang Q, Lei T, He B, Li X, Mo X, Luo H, Zhou H, Liu D. Agricultural drought hazard analysis during 1980–2008: a global perspective. International Journal of Climatology. 2016 Jan 1;36(1):389-99.

Gitelson, A. A. (2004). Wide dynamic range vegetation index for remote quantification of biophysical characteristics of vegetation. *Journal of plant physiology*, *161*(2), 165-173.

Goldberg, Mitchell D., James Gleason, Robert Murphy, Carl Hoffman, and John Furgerson. "NOAA's Joint Polar Satellite System and the NPP Satellite Delivering the Next Generation of Environmental Earth Observations." In*Hyperspectral Imaging and Sounding of the Environment*, p. HMA1. Optical Society of America, 2011.

Goward SN, Markham B, Dye DG, Dulaney W, Yang J. Normalized difference vegetation index measurements from the Advanced Very High Resolution Radiometer. Remote sensing of environment. 1991 Mar 31;35(2):257-77.

Goward, D.G., Turner, S., Dye, D.G., and Liang, J., 1994. University of Maryland improved Global Vegetation Index. Int. J. Remote Sensing, 15(17), 3365-3395.

Goward, S. N., Markham, B. L., Dye, D. G., Dulaney, W., and Yang, J. (1991), Normalized difference vegetation index measurements from the Advanced Very High Resolution Radiometer, *Remote Sens. Environ.*, 35:257-277.

Goward, S.N., and Huemmrich, K.F., 1992, "Vegetation canopy PAR absorptance and the normalized difference vegetation index: an assessment using the SAIL model", Remote Sens. Environ., 39:119-140.

Guan K, Pan M, Li H, Wolf A, Wu J, Medvigy D, Caylor KK, Sheffield J, Wood EF, Malhi Y, Liang M. Photosynthetic seasonality of global tropical forests constrained by hydroclimate. Nature Geoscience. 2015 Apr 1;8(4):284-9.

Gutman, G., 1991, "Vegetation indices from AVHRR: an update and future prospects", Remote Sens. Environ., 35:121-136.

Gutman, G., D. Tarpley, A. Ignatov and S. Olson, 1995, The enhanced NOAA Global Land datasets from the Advanced Very High Resolution Radiometer. *Bull. Amer. Meteorol. Soc.*, 76: 1141-1156.

Hansen J, Ruedy R, Sato M, Lo K. Global surface temperature change. Reviews of Geophysics. 2010 Dec 1;48(4).

Hay SI, Lennon JJ. Deriving meteorological variables across Africa for the study and control of vector-borne disease: a comparison of remote sensing and spatial interpolation of climate. Tropical Medicine & International Health. 1999 Jan 1;4(1):58-71.

Heimann M, Esser G, Haxeltine A, Kaduk J, Kicklighter DW, Knorr W, Kohlmaier GH, McGuire AD, Melillo J, Moore B, Otto RD. Evaluation of terrestrial carbon cycle models through simulations of the seasonal cycle of atmospheric CO2: First results of a model intercomparison study. Global

Biogeochemical Cycles. 1998 Mar 1;12(1):1-24.

Henderson-Sellers, A. (1993) Continental vegetation as a dynamic component of a global climate model: a preliminary assessment. *Climatic Change*, 23, 337–377.

Henderson-Sellers, A. (1995) Global climate models and 'dynamic' vegetation changes. *Global Change Biology*, 1, 63–75.

Herrmann SM, Didan K, Barreto-Munoz A, Crimmins MA. Divergent responses of vegetation cover in Southwestern US ecosystems to dry and wet years at different elevations. Environmental Research Letters. 2016 Nov 24;11(12):124005.

Herwitz SR. Interception storage capacities of tropical rainforest canopy trees. Journal of Hydrology. 1985 Apr 25;77(1):237-52.

Hogg EH, Price DT, Black TA. Postulated feedbacks of deciduous forest phenology on seasonal climate patterns in the western Canadian interior. Journal of Climate. 2000 Dec;13(24):4229-43.

Holben, Brent N. "Characteristics of maximum-value composite images from temporal AVHRR data." *International Journal of Remote Sensing* 7, no. 11 (1986): 1417-1434.

Hooker, S.B., W.E. Esaias, G.C. Feldman, W.W. Gregg, and C.R. McClain, 1992: An Overview of SeaWiFS and Ocean Color. NASA Tech. Memo. 104566, Vol. 1, S.B. Hooker and E.R. Firestone, Eds., NASA Goddard Space Flight Center, Greenbelt, Maryland, 24 pp.

Houborg, R., Soegaard, H., & Boegh, E. (2007). Combining vegetation index and model inversion methods for the extraction of key vegetation biophysical parameters using Terra and Aqua MODIS reflectance data. *Remote Sensing of Environment*, *106*(1), 39-58.

Huete A. R., Compton J. Tucker, Forrest Hall, Karl F. Huemmrich, Tomoaki Miura, Kamel Didan. 2006, Vegetation Index time series global data set for *NASA ESDR/CDR.* lcluc.umd.edu/products/Land_ESDR/index.asp

Huete A.R., T. Miura, Y. Kim, K. Didan, J. Privette, 2006, Assessments of multisensor vegetation index dependencies with hyperspectral and tower flux data, SPIE 6298-45, Proceedings on Remote Sensing and Modeling of Ecosystems for Sustainability III.

Huete AR, Liu HQ. An error and sensitivity analysis of the atmospheric-and soil-correcting variants of the NDVI for the MODIS-EOS. Geoscience and Remote Sensing, IEEE Transactions on. 1994 Jul;32(4):897-905.

Huete AR, Restrepo-Coupe N, Ratana P, Didan K, Saleska SR, Ichii K, Panuthai S, Gamo M. Multiple site tower flux and remote sensing comparisons of tropical forest dynamics in Monsoon Asia. Agricultural and Forest Meteorology. 2008 May 15;148(5):748-60.

Huete AR. A soil-adjusted vegetation index (SAVI). Remote sensing of environment. 1988 Aug 31;25(3):295-309.

Huete, A. R., N. Restrepo-Coupe, P. Ratana, K. Didan, S. R. Saleska, K. Ichii, S. Panuthai, and M. Gamo. "Multiple site tower flux and remote sensing comparisons of tropical forest dynamics in Monsoon Asia." *Agricultural and Forest Meteorology* 148, no. 5 (2008): 748-760.

Huete, A., Didan, K., Miura, T., Rodriguez, E. P., Gao, X., & Ferreira, L. G. (2002). Overview of the radiometric and biophysical performance of the MODIS vegetation indices. *Remote Sensing of Environment*, 83, 195-213.

Huete, A.R., Didan, K., Shimabukuro, Y.E., Ratana, P., Saleska, S.R., Hutyra, L.R., Yang, W., Nemani, R.R., and Myneni, R., Amazon rainforests green up with sunlight in dry season, 2006, Geophys. Res. Lett., 33, L06405, doi:10.1029/2005GL025583, 2006

Huete, A.R., et al. 2006, VI White Paper, lcluc.umd.edu/products/Land_ESDR/index.asp

Huete, A.R., Liu, H.Q., Batchily, K., and van Leeuwen, W., 1997, A comparison of vegetation indices over a global set of TM images for EOS-MODIS, Remote Sens. Environ., 59:440-451.

IGBP, 1992, The International Geosphere-Biosphere Programme: A Study of Global Change, Improved Global Data for Land Applications, IGBP Report No. 20, Stockholm, Sweden: IGBP Secretariat.

IPCC Reports, 2006. Solomon S, editor. Climate change 2007-the physical science basis: Working group I contribution to the fourth assessment report of the IPCC. Cambridge University Press; 2007 Sep 10.

Jackson, R.D. and Huete, A.R., 1991, Interpreting vegetation indices, Prev. Vet. Med. 11:185-200.

Jia GJ, Epstein HE, Walker DA. Greening of arctic Alaska, 1981–2001. Geophysical Research Letters. 2003 Oct 1;30(20).

Jiang, Z., Huete, A. R., Didan, K., & Miura, T. (2008). Development of a two-band enhanced vegetation index without a blue band. *Remote Sensing of Environment*, *112*(10), 3833-3845.

Jordan, C.F., 1969, Derivation of leaf area index from quality of light on the forest floor. Ecology 50:663-666.

Justice CO, Román MO, Csiszar I, Vermote EF, Wolfe RE, Hook SJ, Friedl M, Wang Z, Schaaf CB, Miura T, Tschudi M. Land and cryosphere products from Suomi NPP VIIRS: Overview and status. Journal of Geophysical Research: Atmospheres. 2013 Sep 16;118(17):9753-65.

Kaufman, Y.J. and Tanre, D., 1992, Atmospherically resistant vegetation index (ARVI) for EOS-MODIS, IEEE Trans. Geosci. Remote Sensing, 30:261-270.

Keeling C. D., Chin J.F.S, Whorf T.P. (1996). Increased activity of northern vegetation inferred from atmospheric CO2 measurements. Nature, 382, 146-149.

Keeling RF, Piper SC, Heimann M. Global and hemispheric CO2 sinks deduced from changes in atmospheric O2 concentration. Nature. 1996 May 16;381(6579):218-21.

Kelly JF, Horton KG, Stepanian PM, Beurs KM, Fagin T, Bridge ES, Chilson PB. Novel measures of continental-scale avian migration phenology related to proximate environmental cues. Ecosphere. 2016 Aug 1;7(8).

Kimes, D.S., Newcomb, W.W., Tucker, C.J., Zonneveld, I.S., Van Wijngaarden, W., De Leeuw, J., and Epema, G.F., 1985. Directional Reflectance Factor Distribution for Cover Types of Northern Africa. Remote Sens. Environ. 18:1-19.

Lambin EF, Geist HJ, Lepers E. Dynamics of land-use and land-cover change in tropical regions. Annual review of environment and resources. 2003 Nov;28(1):205-41.

Lassau SA, Cassis G, Flemons PK, Wilkie L, Hochuli DF. Using high-resolution multi-spectral imagery to estimate habitat complexity in open-canopy forests: can we predict ant community patterns?. Ecography. 2005 Aug 1;28(4):495-504.

Leeuwen van, W.J.D., A.R. Huete, J. Duncan, J. Franklin, 1994. Radiative transfer in shrub savanna sites in Niger -- preliminary results from HAPEX-II-Sahel: 3. Optical dynamics and vegetation index sensitivity to biomass and plant cover. Agricultural and Forest Meteorology 69, 267-288.

Liu X, Li X, Shi X, Huang K, Liu Y. A multi-type ant colony optimization (MACO) method for optimal land use allocation in large areas. International Journal of Geographical Information Science. 2012 Jul 1;26(7):1325-43.

Lyapustin AI, Wang Y, Laszlo I, Hilker T, Hall FG, Sellers PJ, Tucker CJ, Korkin SV. Multi-angle implementation of atmospheric correction for MODIS (MAIAC): 3. Atmospheric correction. Remote Sensing of Environment. 2012 Dec 31;127:385-393.

Lyapustin, A., Y. Wang, I. Laszlo, R. Kahn, S. Korkin, L. Remer, R. Levy, and J. S. Reid. "Multiangle implementation of atmospheric correction (MAIAC): 2. Aerosol algorithm." *Journal of Geophysical Research: Atmospheres (1984–2012)* 116, no. D3 (2011).

Marshall M, Okuto E, Kang Y, Opiyo E, Ahmed M. Global assessment of Vegetation Index and Phenology Lab (VIP) and Global Inventory Modeling and Mapping Studies (GIMMS) version 3 products. Biogeosciences. 2016 Feb 3;13(3):625-39

Meehl, G.A., T.F. Stocker, W.D. Collins, P. Friedlingstein, A.T. Gaye, J.M. Gregory, A. Kitoh, R. Knutti, J.M. Murphy, A. Noda, S.C.B. Raper, I.G. Watterson, A.J. Weaver and Z.-C. Zhao, 2007: Global Climate Projections. In: Climate Change 2007: The Physical Science Basis. Contribution of Working Group I to the Fourth Assessment Report of the Intergovernmental Panel on Climate Change [Solomon, S., D. Qin, M. Manning, Z. Chen, M. Marquis, K.B. Averyt, M. Tignor and H.L. Miller (eds.)]. Cambridge University Press, Cambridge, United Kingdom and New York, NY, USA. (www.ipcc.ch).

Melillo, J.M., Prentice, I.C., Farquhar, G.D., Schulze, E.-D. & Sala, O.E. (1996) Terrestrial biotic responses to environmental change and feedbacks to climate. *Climate change 1995. Contribution of WG I to the second assessment report of the intergovernmental panel on climate change* (ed. By J.T. Houghton, L.G. Meira Filho, B.A. Callander, N. Harris, A. Kattenberg & K. Maskell), pp. 445– 481. Cambridge University Press, Cambridge, UK.

Meyer, D., Verstraete, M. and Pinty, B., 1995. The effect of surface anisotropy and viewing geometry on the estimation of NDVI from AVHRR. Remote Sensing Reviews, 12:3-27.

Mintz, Y. (1984) The sensitivity of numerically simulated climates to land–surface boundary conditions. *The global climate* (ed. by J.T. Houghton), pp. 79–105. Cambridge University Press, Cambridge, UK.

Miura, T., Huete, A., & Yoshioka, H. (2006). An empirical investigation of cross-sensor relationships of NDVI and red/near-infrared reflectance using EO-1 hyperion data. *Remote Sensing of Environment*, 100, 223-236.

monitor global vegetation from satellites, Vegetatio 101:15-20.

Moore KE, Fitzjarrald DR, Sakai RK, Goulden ML, Munger JW, Wofsy SC. Seasonal variation in radiative and turbulent exchange at a deciduous forest in central Massachusetts. Journal of Applied Meteorology. 1996 Jan;35(1):122-34.

Morton, Douglas C., Jyoteshwar Nagol, Claudia C. Carabajal, Jacqueline Rosette, Michael Palace, Bruce D. Cook, Eric F. Vermote, David J. Harding, and Peter RJ North. "Amazon forests maintain consistent canopy structure and greenness during the dry season." *Nature* (2014). doi:10.1038/nature13006

Murphy RE, Barnes WL, Lyapustin AI, Privette J, Welsch C, DeLuccia F, Swenson H, Schueler CF, Ardanuy PE, Kealy PS. Using VIIRS to provide data continuity with MODIS. InGeoscience and Remote Sensing Symposium, 2001. IGARSS'01. IEEE 2001 International 2001 (Vol. 3, pp. 1212-1214). IEEE.

Myneni RB, Williams DL. On the relationship between FAPAR and NDVI. Remote Sensing of Environment. 1994 Sep 1;49(3):200-11.

Myneni, R.B., C.D Keeling, C.J Tucker, G Asrar, R.R Nemani Increased plant growth in northern high latitudes from 1981–1991. Nature, 386 (1997), pp. 698–702

Nagler, Pamela L., Russell L. Scott, Craig Westenburg, James R. Cleverly, Edward P. Glenn, and Alfredo R. Huete. "Evapotranspiration on western US rivers estimated using the Enhanced Vegetation Index from MODIS and data from eddy covariance and Bowen ratio flux towers." *Remote sensing of environment* 97, no. 3 (2005): 337-351.

Nakajima, T. Y., T. Nakajima, M. Nakajima, H. Fukushima, M. Kuji, A. Uchiyama, and M Kishino, 1998. Optimization of the Advanced Observing Satellite Global Imager channels by use of radiative transfer calculations. Applied Optics Vol. 37, No. 15.

Nemani, Ramakrishna R., Charles D. Keeling, Hirofumi Hashimoto, William M. Jolly, Stephen C. Piper, Compton J. Tucker, Ranga B. Myneni, and Steven W. Running. "Climate-driven increases in global terrestrial net primary production from 1982 to 1999." science 300, no. 5625 (2003): 1560-1563.

Nieto S, Flombaum P, Garbulsky MF. Can temporal and spatial NDVI predict regional bird-species richness?. Global Ecology and Conservation. 2015 Jan 31;3:729-35.

Ollinger SV, Richardson AD, Martin ME, Hollinger DY, Frolking SE, Reich PB, Plourde LC, Katul GG, Munger JW, Oren R, Smith ML. Canopy nitrogen, carbon assimilation, and albedo in temperate and boreal forests: Functional relations and potential climate feedbacks. Proceedings of the National Academy of Sciences. 2008 Dec 9;105(49):19336-41.

Pinter, P.J., Jr., 1993, Solar angle independence in the relationship between absorbed PAR and remotely sensed data for alfalfa, Remote Sens. Environ. 46:19-25.

Prince SD. Satellite remote sensing of primary production: comparison of results for Sahelian grasslands 1981-1988. International Journal of Remote Sensing. 1991 Jun 1;12(6):1301-11.

Prince, S.D., Justice, C.O., and Moore, B., 1994, Remote Sensing of NPP. IGBP DIS Working Paper #10, IGBP-DIS, Paris.

Rahman AF, Sims DA, Cordova VD, El-Masri BZ. Potential of MODIS EVI and surface temperature for directly estimating per-pixel ecosystem C fluxes. Geophysical Research Letters. 2005 Oct 1;32(19).

Rahman, H., Pinty, B. and Verstraete, M.M., 1993. Coupled surface-atmosphere reflectance (CSAR) model 2. Semiemperical surface model usable with NOAA AVHRR. J. Geophys. Res. 89(D11):20791-20801.

Raich, J.W., and Schlesinger, W.H., 1992, The global carbon dioxide flux in soil respiration and its relationship to vegetation and climate, Tellus 44B:81-99.

Randerson J, Field C, Fung I et al. (1999). Increase in early season ecosystem uptake explain recent changes in the seasonal cycle of atmospheric CO2 at high northern latitudes. Geophysical Research Letters, 26, 2765-2768.

Rao, C.R.N. and J. Chen, 1994: Post-launch calibration of the visible and near-IR channels of AVHRR on NOAA-7, -9, and -11 spacecraft. *NOAA Tech. Rpt. NESDIS 78*, US Dept. of Commerce, NOAA, 22 pp.

Reich PB, Borchert R. Changes with leaf age in stomatal function and water status of several tropical tree species. Biotropica. 1988 Mar 1:60-9.

Richardson AD, Braswell BH, Hollinger DY, Jenkins JP, Ollinger SV. Near-surface remote sensing of spatial and temporal variation in canopy phenology. Ecological Applications. 2009 Sep;19(6):1417-28.

Rouse, J.W., Haas, R.H., Schell, J.A., Deering, D.W., 1973. Monitoring vegetation systems in the Great Plains with ERTS. Proc. Third Earth Resources Technology Satellite-1 Symposium, Goddard Space Flight Center, NASA SP-351, Science and Technical Information Office, NASA, Washington, DC, pp. 309–317.

Rowntree, P.R. (1988) Review of general circulation models as a basis for predicting the effects of vegetation change on climate. *Forests, climate, and hydrology: regional impacts* (ed. by E.R.C. Reynolds & F.B. Thompson), pp. 162–196. The United Nations University, Tokyo.

Running SW, Justice CO, Salomonson V, Hall D, Barker J, Kaufmann YJ, Strahler AH, Huete AR, Muller JP, Vanderbilt V, Wan ZM. Terrestrial remote sensing science and algorithms planned for EOS/MODIS. International journal of remote sensing. 1994 Nov 1;15(17):3587-620.

Running SW, Nemani RR. Relating seasonal patterns of the AVHRR vegetation index to simulated photosynthesis and transpiration of forests in different climates. Remote Sensing of Environment. 1988 Mar 1;24(2):347-67.

Running, S.W., 1990, Estimating terrestrial primary productivity by combining remote sensing and ecosystem simulation, IN: Ecological Studies Vol "Remote Sensing of Biosphere Functioning". H. Mooney and R. Hobbs., eds. Springer-Verlag, pp. 65-86.

Saleska SR, Wu J, Guan K, Araujo AC, Huete A, Nobre AD, Restrepo-Coupe N. Dry-season greening of Amazon forests. Nature. 2016 Mar 17;531(7594):E4-5.

Saleska SR, Didan K, Huete AR, Da Rocha HR. Amazon forests green-up during 2005 drought. Science. 2007 Oct 26;318(5850):612-.

Samanta, Arindam, Sangram Ganguly, Hirofumi Hashimoto, Sadashiva Devadiga, Eric Vermote, Yuri Knyazikhin, Ramakrishna R. Nemani, and Ranga B. Myneni. "Amazon forests did not green-up during the 2005 drought."*Geophysical Research Letters* 37, no. 5 (2010).

Schaaf, Crystal B., Feng Gao, Alan H. Strahler, Wolfgang Lucht, Xiaowen Li, Trevor Tsang, Nicholas C. Strugnell et al. "First operational BRDF, albedo nadir reflectance products from MODIS." *Remote sensing of Environment* 83, no. 1 (2002): 135-148

Schwartz MD, Reed BC. Surface phenology and satellite sensor-derived onset of greenness: an initial comparison. International Journal of Remote Sensing. 1999 Jan 1;20(17):3451-7.

Seddon AW, Macias-Fauria M, Long PR, Benz D, Willis KJ. Sensitivity of global terrestrial ecosystems to climate variability. Nature. 2016 Mar 10;531(7593):229-32.

Sellers, P.J., 1985, Canopy reflectance, photosynthesis and transpiration, I International Journal of Remote Sensing, 6:1335-1372.

Shabanov NV, Zhou L, Knyazikhin Y, Myneni RB, Tucker CJ. Analysis of interannual changes in northern vegetation activity observed in AVHRR data from 1981 to 1994. Geoscience and Remote Sensing, IEEE Transactions on. 2002 Jan;40(1):115-30.

Sims DA, Rahman AF, Cordova VD, El-Masri BZ, Baldocchi DD, Flanagan LB, Goldstein AH, Hollinger DY, Misson L, Monson RK, Oechel WC. On the use of MODIS EVI to assess gross primary productivity of North American ecosystems. Journal of Geophysical Research: Biogeosciences (2005–2012). 2006 Dec 1;111(G4).

Sims, Daniel A., Abdullah F. Rahman, Vicente D. Cordova, Bassil Z. El-Masri, Dennis D. Baldocchi, Paul V. Bolstad, Lawrence B. Flanagan et al. "A new model of gross primary productivity for North American ecosystems based solely on the enhanced vegetation index and land surface temperature from MODIS." Remote Sensing of Environment 112, no. 4 (2008): 1633-1646.

Tucker CJ. Red and photographic infrared linear combinations for monitoring vegetation. Remote sensing of Environment. 1979 May 31;8(2):127-50.

Tucker, C. J., Pinzon, J. E., Brown, M. E., Slayback, D. A., Pak, E. W.,Mahoney, R., Vermote, E. F., & El Saleous, N. (2005). An extended AVHRR 8-km NDVI dataset compatible with MODIS and SPOT vegetation NDVI data. *International Journal of Remote Sensing*, 26, 4485-4498.

Tucker, C.J. and Sellers, P.J., 1986, Satellite remote sensing of primary productivity, International Journal of Remote Sensing, 7:1395-1416.

Tucker, C.J. Holben, B.N., Elgin, J.H. and McMurtrey, 1981, Remote sensing of total dry matter accumulation in winter wheat. Remote Sens. Environ. 11:171.

Tucker, C.J., P.J. Seller. Satellite remote sensing for primary production. Remote Sensing, 7 (1986), pp. 1395–1416

framework. *Geoscience and Remote Sensing, IEEE Transactions on*, *42*(7), 1575-1585.

Vaiopoulos D, Skianis GA, Nikolakopoulos K. The contribution of probability theory in assessing the efficiency of two frequently used vegetation indices. International Journal of Remote Sensing. 2004 Oct 1;25(20):4219-36.

Vargas, M., T. Miura, N. Shabanov, and A. Kato. "An initial assessment of Suomi NPP VIIRS vegetation index EDR." *Journal of Geophysical Research: Atmospheres* 118, no. 22 (2013): 12-301.

Vermote, E., & Kaufman, Y. J. (1995). Absolute calibration of AVHRR visible and near-infrared channels using ocean and cloud views. *International Journal of Remote Sensing*, 16, 2317-2340.

Vermote, Eric F., Nazmi Z. El Saleous, and Christopher O. Justice. "Atmospheric correction of MODIS data in the visible to middle infrared: first results." *Remote Sensing of Environment* 83, no. 1 (2002): 97-111.

Vierling, L.A., Deering, D.W., Eck, T.F., 1997. Differences in Arctic Tundra Vegetation Type and Phenology as Seen Using Bidirectional Radiometry in the Early Growing Season. Remote Sens. Environ. 60:71-82.

Viovy, N., Arino, O., and Belward, A.S., 1992, The best index slope extraction (BISE): a method for reducing noise in NDVI time series, International Journal of Remote Sensing, 13:1585-1590.

Walter-Shea, E. A., J. L. Privette, D. Cornell, M. A. Mesarch, and C. J. Hays, 1997, Relations between spectral vegetation indices and leaf area and absorbed radiation in alfalfa, Remote Sens. Environ., 61:162-177.

Wardlow, B. D., Egbert, S. L., & Kastens, J. H. (2007). Analysis of time-series MODIS 250 m vegetation index data for crop classification in the US Central Great Plains. *Remote Sensing of Environment*, *108*(3), 290-310.

Waring, R. H., Coops, N. C., Fan, W., & Nightingale, J. M. (2006). MODIS enhanced vegetation index predicts tree species richness across forested ecoregions in the contiguous USA. *Remote Sensing of Environment*, *103*(2), 218-226.

Watson, R.T., Zinyowera, M.C. & Moss, R.H., eds (1996) *Climate change 1995*. *Contribution of WG II to the second assessment report of the intergovernmental panel on climate change*. 878 pp. Cambridge University Press, Cambridge, UK.

Welsch C, Swenson H, Cota S, DeLuccia F, Haas JM, Schueler C, Durham RM, Clement JE, Ardanuy PE. VIIRS (Visible Infrared Imager Radiometer Suite): a next-generation operational environmental sensor for NPOESS. InGeoscience and Remote Sensing Symposium, 2001. IGARSS'01. IEEE 2001 International 2001 (Vol. 3, pp. 1020-1022). IEEE.

White MA, Nemani RR, Thornton PE, Running SW. Satellite evidence of phenological differences between urbanized and rural areas of the eastern United States deciduous broadleaf forest. Ecosystems. 2002 Apr 1;5(3):260-73.

White, Michael A., De BEURS, M. Kirsten, KAMEL DIDAN, DAVID W. INOUYE, ANDREW D. RICHARDSON, OLAF P. JENSEN et al. "Intercomparison, interpretation, and assessment of spring phenology in North America estimated from remote sensing for 1982–2006." *Global Change Biology*15, no. 10 (2009): 2335-2359.

Wiegand, C.L., Richardson, A.J., Escobar, D.E., Gebermann, A.H., 1991, Vegetation indices in crop assessments, Remote Sens. Environ. 35:105-119.

Wolfe. R.E., D.P., Roy, and E. Vermote. 1998. MODIS land data storage, gridding, and compositing methodology: Level 2 grid. IEEE Trans. Geosci. and Remote Sensing, vol. 36, no.4, pp1324-1338.

Wu J, Albert LP, Lopes AP, Restrepo-Coupe N, Hayek M, Wiedemann KT, Guan K, Stark SC, Christoffersen B, Prohaska N, Tavares JV. Leaf development and demography explain photosynthetic seasonality in Amazon evergreen forests. Science. 2016 Feb 26;351(6276):972-6.

Xiao X, Hagen S, Zhang Q, Keller M, Moore B. Detecting leaf phenology of seasonally moist tropical forests in South America with multi-temporal MODIS images. Remote Sensing of Environment. 2006 Aug 30;103(4):465-73.

Xiao X, Zhang Q, Braswell B, Urbanski S, Boles S, Wofsy S, Moore B, Ojima D. Modeling gross primary production of temperate deciduous broadleaf forest using satellite images and climate data. Remote Sensing of Environment. 2004 May 30;91(2):256-70.

Xiao, X., Zhang, Q., Saleska, S., Hutyra, L., De Camargo, P., Wofsy, S., Frolking, S., Boles, S., Keller, M., and Moore III, B. (2005), Satellite-based modeling of gross primary production in a sesonally moist tropical evergreen forest, *Remote Sens. Environ.*, *94*, 105-122.

Yang J, Ding Y, Chen R. Spatial and temporal of variations of alpine vegetation cover in the source regions of the Yangtze and Yellow Rivers of the Tibetan Plateau from 1982 to 2001. Environmental Geology. 2006 Jun 1;50(3):313-22.

Zhang X, Friedl MA, Schaaf CB, Strahler AH, Hodges JC, Gao F, Reed BC, Huete A. Monitoring vegetation phenology using MODIS. Remote sensing of environment. 2003 Mar 31;84(3):471-5.

Zhang X, Friedl MA, Schaaf CB. Global vegetation phenology from Moderate Resolution Imaging

Spectroradiometer (MODIS): Evaluation of global patterns and comparison with in situ measurements. Journal of Geophysical Research: Biogeosciences (2005–2012). 2006 Dec 1;111(G4).

Zhang Y, Song C, Band LE, Sun G, Li J. Reanalysis of global terrestrial vegetation trends from MODIS products: Browning or greening?. Remote Sensing of Environment. 2017 Mar 15;191:145-55.

Appendix – I - Global Metadata Attributes

```
GROUP=SwathStructure
END_GROUP=SwathStructure
GROUP=GridStructure
GROUP=GRID_1
        GridName="NPP_Grid_16Day_VI_500m"
        XDim=2400
        YDim=2400
        UpperLeftPointMtrs=(-10007554.677000,4447802.078667)
        LowerRightMtrs=(-8895604.157333,3335851.559000)
        Projection=HE5_GCTP_SNSOID
        ProjParams=(6371007.181000,0,0,0,0,0,0,0,0,0,0,0,0)
        SphereCode=-1
        GROUP=Dimension
        END_GROUP=Dimension
        GROUP=DataField
                OBJECT=DataField_1
                        DataFieldName="500 m 16 days NDVI"
                        DataType=H5T_NATIVE_SHORT
                        DimList=("YDim","XDim")
                        MaxdimList=("YDim","XDim")
                        CompressionType=HE5_HDFE_COMP_DEFLATE
                        DeflateLevel=5
                END_OBJECT=DataField_1
                OBJECT=DataField_2
                        DataFieldName="500 m 16 days EVI"
                        DataType=H5T_NATIVE_SHORT
                        DimList=("YDim","XDim")
                        MaxdimList=("YDim","XDim")
                        CompressionType=HE5_HDFE_COMP_DEFLATE
                        DeflateLevel=5
                END_OBJECT=DataField_2
                OBJECT=DataField_3
                        DataFieldName="500 m 16 days EVI2"
                        DataType=H5T_NATIVE_SHORT
                        DimList=("YDim","XDim")
                        MaxdimList=("YDim","XDim")
                        CompressionType=HE5_HDFE_COMP_DEFLATE
                        DeflateLevel=5
                END_OBJECT=DataField_3
                OBJECT=DataField_4
                        DataFieldName="500 m 16 days VI Quality"
                        DataType=H5T_NATIVE_USHORT
                        DimList=("YDim","XDim")
                        MaxdimList=("YDim","XDim")
                        CompressionType=HE5_HDFE_COMP_DEFLATE
                        DeflateLevel=5
                END_OBJECT=DataField_4
                OBJECT=DataField_5
                        DataFieldName="500 m 16 days red reflectance"
                        DataType=H5T_NATIVE_SHORT
                        DimList=("YDim","XDim")
                        MaxdimList=("YDim","XDim")
                        CompressionType=HE5_HDFE_COMP_DEFLATE
                        DeflateLevel=5
                END_OBJECT=DataField_5
                OBJECT=DataField_6
                        DataFieldName="500 m 16 days NIR reflectance"
                        DataType=H5T_NATIVE_SHORT
                        DimList=("YDim","XDim")
                        MaxdimList=("YDim","XDim")
                        CompressionType=HE5_HDFE_COMP_DEFLATE
                        DeflateLevel=5
                END_OBJECT=DataField_6
```

```
            OBJECT=DataField_7
                DataFieldName="500 m 16 days blue reflectance"
                DataType=H5T_NATIVE_SHORT
                DimList=("YDim","XDim")
                MaxdimList=("YDim","XDim")
                CompressionType=HE5_HDFE_COMP_DEFLATE
                DeflateLevel=5
            END_OBJECT=DataField_7
            OBJECT=DataField_8
                DataFieldName="500 m 16 days green reflectance"
                DataType=H5T_NATIVE_SHORT
                DimList=("YDim","XDim")
                MaxdimList=("YDim","XDim")
                CompressionType=HE5_HDFE_COMP_DEFLATE
                DeflateLevel=5
            END_OBJECT=DataField_8
            OBJECT=DataField_9
                DataFieldName="500 m 16 days SWIR1 reflectance"
                DataType=H5T_NATIVE_SHORT
                DimList=("YDim","XDim")
                MaxdimList=("YDim","XDim")
                CompressionType=HE5_HDFE_COMP_DEFLATE
                DeflateLevel=5
            END_OBJECT=DataField_9
            OBJECT=DataField_10
                DataFieldName="500 m 16 days SWIR2 reflectance"
                DataType=H5T_NATIVE_SHORT
                DimList=("YDim","XDim")
                MaxdimList=("YDim","XDim")
                CompressionType=HE5_HDFE_COMP_DEFLATE
                DeflateLevel=5
            END_OBJECT=DataField_10
            OBJECT=DataField_11
                DataFieldName="500 m 16 days SWIR3 reflectance"
                DataType=H5T_NATIVE_SHORT
                DimList=("YDim","XDim")
                MaxdimList=("YDim","XDim")
                CompressionType=HE5_HDFE_COMP_DEFLATE
                DeflateLevel=5
            END_OBJECT=DataField_11
            OBJECT=DataField_12
                DataFieldName="500 m 16 days view zenith angle"
                DataType=H5T_NATIVE_SHORT
                DimList=("YDim","XDim")
                MaxdimList=("YDim","XDim")
                CompressionType=HE5_HDFE_COMP_DEFLATE
                DeflateLevel=5
            END_OBJECT=DataField_12
            OBJECT=DataField_13
                DataFieldName="500 m 16 days sun zenith angle"
                DataType=H5T_NATIVE_SHORT
                DimList=("YDim","XDim")
                MaxdimList=("YDim","XDim")
                CompressionType=HE5_HDFE_COMP_DEFLATE
                DeflateLevel=5
            END_OBJECT=DataField_13
            OBJECT=DataField_14
                DataFieldName="500 m 16 days relative azimuth angle"
                DataType=H5T_NATIVE_SHORT
                DimList=("YDim","XDim")
                MaxdimList=("YDim","XDim")
                CompressionType=HE5_HDFE_COMP_DEFLATE
                DeflateLevel=5
            END_OBJECT=DataField_14
            OBJECT=DataField_15
```

```
                    DataFieldName="500 m 16 days composite day of the year"
                    DataType=H5T_NATIVE_SHORT
                    DimList=("YDim","XDim")
                    MaxdimList=("YDim","XDim")
                    CompressionType=HE5_HDFE_COMP_DEFLATE
                    DeflateLevel=5
                END_OBJECT=DataField_15
                OBJECT=DataField_16
                    DataFieldName="500 m 16 days pixel reliability"
                    DataType=H5T_NATIVE_SCHAR
                    DimList=("YDim","XDim")
                    MaxdimList=("YDim","XDim")
                    CompressionType=HE5_HDFE_COMP_DEFLATE
                    DeflateLevel=5
                END_OBJECT=DataField_16
        END_GROUP=DataField
        GROUP=MergedFields
        END_GROUP=MergedFields
    END_GROUP=GRID_1
END_GROUP=GridStructure
GROUP=PointStructure
END_GROUP=PointStructure
GROUP=ZaStructure
END_GROUP=ZaStructure
END

GROUP = INVENTORYMETADATA
  GROUPTYPE = MASTERGROUP
        GROUP = ECSDATAGRANULE
        OBJECT = LOCALGRANULEID
            NUM_VAL = 1
            VALUE = "VNP13A1.A2015145.h09v05.002.2015335163419.he5"
        END_OBJECT = LOCALGRANULEID
        OBJECT = PRODUCTIONDATETIME
            NUM_VAL = 1
            VALUE = "2016-06-28T17:27:03.000Z"
        END_OBJECT = PRODUCTIONDATETIME
        OBJECT = DAYNIGHTFLAG
            NUM_VAL = 1
            VALUE = "DAY"
        END_OBJECT = DAYNIGHTFLAG
        OBJECT = REPROCESSINGACTUAL
            NUM_VAL = 1
            VALUE = "reprocessed"
        END_OBJECT = REPROCESSINGACTUAL
        OBJECT = LOCALVERSIONID
            NUM_VAL = 1
            VALUE = "2.2.4"
        END_OBJECT = LOCALVERSIONID
        OBJECT = REPROCESSINGPLANNED
            NUM_VAL = 1
            VALUE = "further update is anticipated"
        END_OBJECT = REPROCESSINGPLANNED
    END_GROUP = ECSDATAGRANULE
    GROUP = MEASUREDPARAMETER
      OBJECT = MEASUREDPARAMETERCONTAINER
            CLASS = "1"
      OBJECT = PARAMETERNAME
            CLASS = "1"
            NUM_VAL = 1
            VALUE = "500 m 16 days NDVI"
      END_OBJECT = PARAMETERNAME
            GROUP = QAFLAGS
                CLASS = "1"
      OBJECT = SCIENCEQUALITYFLAG
```

```
            CLASS = "1"
            NUM_VAL = 1
            VALUE = "Not Investigated"
        END_OBJECT = SCIENCEQUALITYFLAG
        OBJECT = AUTOMATICQUALITYFLAGEXPLANATION
            CLASS = "1"
            NUM_VAL = 1
            VALUE = "No automatic quality assessment is performed in the PGE"
        END_OBJECT = AUTOMATICQUALITYFLAGEXPLANATION
        OBJECT = AUTOMATICQUALITYFLAG
            CLASS = "1"
            NUM_VAL = 1
            VALUE = "Passed"
        END_OBJECT = AUTOMATICQUALITYFLAG
        OBJECT = SCIENCEQUALITYFLAGEXPLANATION
            CLASS = "1"
            NUM_VAL = 1
            VALUE = "see http://landweb.nascom.nasa.gov/"
        END_OBJECT = SCIENCEQUALITYFLAGEXPLANATION
         END_GROUP = QAFLAGS
          GROUP = QASTATS
              CLASS = "1"
        OBJECT = QAPERCENTMISSINDATA
            CLASS = "1"
            NUM_VAL = 1
            VALUE = 0
        END_OBJECT = QAPERCENTMISSINDATA
        OBJECT = QAPERCENTOUTOFBOUNDSDATA
            CLASS = "1"
            NUM_VAL = 1
            VALUE = 0
        END_OBJECT = QAPERCENTOUTOFBOUNDSDATA
        OBJECT = QAPERCENTCLOUDCOVER
            CLASS = "1"
            NUM_VAL = 1
            VALUE = 0
        END_OBJECT = QAPERCENTCLOUDCOVER
        OBJECT = QAPERCENTINTERPOLATEDDATA
            CLASS = "1"
            NUM_VAL = 1
            VALUE = 100
        END_OBJECT = QAPERCENTINTERPOLATEDDATA
          END_GROUP = QASTATS
       END_OBJECT = MEASUREDPARAMETERCONTAINER
       END_OBJECT = MEASUREDPARAMETERCONTAINER
     END_OBJECT = MEASUREDPARAMETER
     GROUP = COLLECTIONDESCRIPTIONCLASS
        OBJECT = VERSIONID
            NUM_VAL = 1
            VALUE = "2.0"
        END_OBJECT = VERSIONID
        OBJECT = SHORTNAME
            NUM_VAL = 1
            VALUE = "VNP13A1"
        END_OBJECT = SHORTNAME
     END_GROUP = COLLECTIONDESCRIPTIONCLASS
     GROUP = INPUTGRANULE
        OBJECT = INPUTPOINTER
            NUM_VAL = 80
            VALUE = ("VNP09G1KI.A2013009.h08v05.001.2016332102924.hdf",
 "VNP09G1KI.A2013010.h08v05.001.2016332143303.hdf",
 "VNP09G1KI.A2013011.h08v05.001.2016333044746.hdf", …
 "VNPPT1KDI.A2013009.h08v05.001.2016332101753.hdf",
 "VNPPT1KDI.A2013010.h08v05.001.2016332142549.hdf",
 "VNPPT1KDI.A2013011.h08v05.001.2016333044352.hdf", …
```

```
"VNPMGGAD1I.A2013009.h08v05.001.2016332101753.hdf",
"VNPMGGAD1I.A2013010.h08v05.001.2016332142549.hdf",
"VNPMGGAD1I.A2013016.h08v05.001.2016333060401.hdf")
         END_OBJECT = INPUTPOINTER
     END_GROUP = INPUTGRANULE
   GROUP = SPATIALDOMAINCONTAINER
     GROUP = HORIZONTALSPATIALDOMAINCONTAINER
        GROUP = GPOLYGON
           OBJECT = GPOLYGONCONTAINER
                CLASS = "1"
              GROUP = GRING
                 CLASS = "1"
         OBJECT = EXCLUSIONRINGFLAG
           CLASS = "1"
           NUM_VAL = 1
           VALUE = "N"
         END_OBJECT = EXCLUSIONRINGFLAG
              END_GROUP = GRING
               GROUP = GRINGPOINT
               CLASS = "1"
         OBJECT = GRINGPOINTLATITUDE
           NUM_VAL = 4
           CLASS = "1"
           VALUE = (29.836100,40.000000,40.074200,29.900999)
         END_OBJECT = GRINGPOINTLATITUDE
         OBJECT = GRINGPOINTLONGITUDE
           NUM_VAL = 4
           CLASS = "1"
           VALUE = (-103.835899,-117.486702,-104.256699,-92.131897)
         END_OBJECT = GRINGPOINTLONGITUDE
         OBJECT = GRINGPOINTSEQUENCENO
           NUM_VAL = 4
           CLASS = "1"
           VALUE = (1, 2, 3, 4)
         END_OBJECT = GRINGPOINTSEQUENCENO
              END_GROUP = GRINGPOINT
          END_GROUP = GPOLYGONCONTAINER
        END_GROUP = GPOLYGON
     END_GROUP = HORIZONTALSPATIALDOMAINCONTAINER
   END_GROUP = SPATIALDOMAINCONTAINER
    GROUP = RANGEDATETIME
        OBJECT = RANGEENDINGDATE
           NUM_VAL = 1
           VALUE = "2015-06-09"
        END_OBJECT = RANGEENDINGDATE
        OBJECT = RANGEENDINGTIME
           NUM_VAL = 1
           VALUE = "23:59:59"
        END_OBJECT = RANGEENDINGTIME
        OBJECT = RANGEBEGINNINGDATE
           NUM_VAL = 1
           VALUE = "2015-05-25"
        END_OBJECT = RANGEBEGINNINGDATE
        OBJECT = RANGEBEGINNINGTIME
           NUM_VAL = 1
           VALUE = "00:00:00"
        END_OBJECT = RANGEBEGINNINGTIME
    END_GROUP = RANGEDATETIME
     GROUP = PGEVERSIONCLASS
        OBJECT = PGEVERSION
           NUM_VAL = 1
           VALUE = "2.0"
        END_OBJECT = PGEVERSION
     END_GROUP = PGEVERSIONCLASS
     GROUP = ASSOCIATEDPLATFORMINSTRUMENTSENSOR
```

```
     OBJECT = ASSOCIATEDPLATFORMINSTRUMENTSENSORCONTAINER
          CLASS = "1"
     OBJECT = ASSOCIATEDSENSORSHORTNAME
        CLASS = "1"
        NUM_VAL = 1
        VALUE = "VIIRS"
     END_OBJECT = ASSOCIATEDSENSORSHORTNAME
     OBJECT = ASSOCIATEDPLATFORMSHORTNAME
        CLASS = "1"
        NUM_VAL = 1
        VALUE = "NPP"
     END_OBJECT = ASSOCIATEDPLATFORMSHORTNAME
     OBJECT = ASSOCIATEDINSTRUMENTSHORTNAME
        CLASS = "1"
        NUM_VAL = 1
        VALUE = "VIIRS"
     END_OBJECT = ASSOCIATEDINSTRUMENTSHORTNAME
        END_OBJECT = ASSOCIATEDPLATFORMINSTRUMENTSENSORCONTAINER
   END_GROUP = ASSOCIATEDPLATFORMINSTRUMENTSENSOR
   GROUP = ADDITIONALATTRIBUTES
        OBJECT = ADDITIONALATTRIBUTESCONTAINER
          CLASS = "1"
     OBJECT = ADDITIONALATTRIBUTENAME
        CLASS = "1"
        NUM_VAL = 1
        VALUE = "QAPERCENTGOODQUALITY"
     END_OBJECT = ADDITIONALATTRIBUTENAME
     GROUP = INFORMATIONCONTENT
       CLASS = "1"
          OBJECT = PARAMETERVALUE
             NUM_VAL = 1
             CLASS = "1"
             VALUE = "77"
          END_OBJECT = PARAMETERVALUE
     END_GROUP = INFORMATIONCONTENT
        END_OBJECT = ADDITIONALATTRIBUTESCONTAINER
        OBJECT = ADDITIONALATTRIBUTESCONTAINER
          CLASS = "2"
     OBJECT = ADDITIONALATTRIBUTENAME
        CLASS = "2"
        NUM_VAL = 1
        VALUE = "QAPERCENTOTHERQUALITY"
     END_OBJECT = ADDITIONALATTRIBUTENAME
     GROUP = INFORMATIONCONTENT
       CLASS = "2"
          OBJECT = PARAMETERVALUE
             NUM_VAL = 1
             CLASS = "2"
             VALUE = "23"
          END_OBJECT = PARAMETERVALUE
     END_GROUP = INFORMATIONCONTENT
        END_OBJECT = ADDITIONALATTRIBUTESCONTAINER
        OBJECT = ADDITIONALATTRIBUTESCONTAINER
          CLASS = "3"
     OBJECT = ADDITIONALATTRIBUTENAME
        CLASS = "3"
        NUM_VAL = 1
        VALUE = "QAPERCENTNOTPRODUCEDCLOUD"
     END_OBJECT = ADDITIONALATTRIBUTENAME
     GROUP = INFORMATIONCONTENT
       CLASS = "3"
          OBJECT = PARAMETERVALUE
             NUM_VAL = 1
             CLASS = "3"
             VALUE = "0"
```

```
                END_OBJECT = PARAMETERVALUE
        END_GROUP = INFORMATIONCONTENT
          END_OBJECT = ADDITIONALATTRIBUTESCONTAINER
          OBJECT = ADDITIONALATTRIBUTESCONTAINER
                CLASS = "4"
OBJECT = ADDITIONALATTRIBUTENAME
          CLASS = "4"
          NUM_VAL = 1
          VALUE = "QAPERCENTNOTPRODUCEDOTHER"
END_OBJECT = ADDITIONALATTRIBUTENAME
GROUP = INFORMATIONCONTENT
          CLASS = "4"
                OBJECT = PARAMETERVALUE
                      NUM_VAL = 1
                      CLASS = "4"
                      VALUE = "0"
                END_OBJECT = PARAMETERVALUE
        END_GROUP = INFORMATIONCONTENT
          END_OBJECT = ADDITIONALATTRIBUTESCONTAINER
          OBJECT = ADDITIONALATTRIBUTESCONTAINER
                CLASS = "5"
OBJECT = ADDITIONALATTRIBUTENAME
          CLASS = "5"
          NUM_VAL = 1
          VALUE = "NDVI500M16DAYQCLASSPERENTAGE"
END_OBJECT = ADDITIONALATTRIBUTENAME
GROUP = INFORMATIONCONTENT
          CLASS = "5"
                OBJECT = PARAMETERVALUE
                      NUM_VAL = 1
                      CLASS = "5"
                      VALUE = "0"
                END_OBJECT = PARAMETERVALUE
        END_GROUP = INFORMATIONCONTENT
          END_OBJECT = ADDITIONALATTRIBUTESCONTAINER
          OBJECT = ADDITIONALATTRIBUTESCONTAINER
                CLASS = "6"
OBJECT = ADDITIONALATTRIBUTENAME
          CLASS = "6"
          NUM_VAL = 1
          VALUE = "EVI500M16DAYQCLASSPERCENTAGE"
END_OBJECT = ADDITIONALATTRIBUTENAME
GROUP = INFORMATIONCONTENT
          CLASS = "6"
                OBJECT = PARAMETERVALUE
                      NUM_VAL = 1
                      CLASS = "6"
                      VALUE = "0"
                END_OBJECT = PARAMETERVALUE
        END_GROUP = INFORMATIONCONTENT
          END_OBJECT = ADDITIONALATTRIBUTESCONTAINER
          OBJECT = ADDITIONALATTRIBUTESCONTAINER
                CLASS = "7"
OBJECT = ADDITIONALATTRIBUTENAME
          CLASS = "7"
          NUM_VAL = 1
          VALUE = "HORIZONTALTILENUMBER"
END_OBJECT = ADDITIONALATTRIBUTENAME
GROUP = INFORMATIONCONTENT
          CLASS = "7"

                OBJECT = PARAMETERVALUE
                      NUM_VAL = 1
                      CLASS = "7"
                      VALUE = "9"
```

```
                 END_OBJECT = PARAMETERVALUE
          END_GROUP = INFORMATIONCONTENT
            END_OBJECT = ADDITIONALATTRIBUTESCONTAINER
            OBJECT = ADDITIONALATTRIBUTESCONTAINER
                 CLASS = "8"
OBJECT = ADDITIONALATTRIBUTENAME
           CLASS = "8"
           NUM_VAL = 1
           VALUE = "VERTICALTILENUMBER"
END_OBJECT = ADDITIONALATTRIBUTENAME
GROUP = INFORMATIONCONTENT
   CLASS = "8"
                 OBJECT = PARAMETERVALUE
                      NUM_VAL = 1
                      CLASS = "8"
                      VALUE = "5"
                 END_OBJECT = PARAMETERVALUE
END_GROUP = INFORMATIONCONTENT
   END_OBJECT = ADDITIONALATTRIBUTESCONTAINER
   OBJECT = ADDITIONALATTRIBUTESCONTAINER
        CLASS = "9"
OBJECT = ADDITIONALATTRIBUTENAME
   CLASS = "9"
   NUM_VAL = 1
   VALUE = "TileID"
END_OBJECT = ADDITIONALATTRIBUTENAME
GROUP = INFORMATIONCONTENT
   CLASS = "9"
                 OBJECT = PARAMETERVALUE
                      NUM_VAL = 1
                      CLASS = "9"
                      VALUE = "51009005"
                 END_OBJECT = PARAMETERVALUE
END_GROUP = INFORMATIONCONTENT
   END_OBJECT = ADDITIONALATTRIBUTESCONTAINER
   OBJECT = ADDITIONALATTRIBUTESCONTAINER
        CLASS = "10"
OBJECT = ADDITIONALATTRIBUTENAME
   CLASS = "10"
   NUM_VAL = 1
   VALUE = "INPUTPRODUCTRESOLUTION"
END_OBJECT = ADDITIONALATTRIBUTENAME
GROUP = INFORMATIONCONTENT
   CLASS = "10"
                 OBJECT = PARAMETERVALUE
                      NUM_VAL = 1
                      CLASS = "10"
                      VALUE = "Product input resolution 500m"
                 END_OBJECT = PARAMETERVALUE
END_GROUP = INFORMATIONCONTENT
   END_OBJECT = ADDITIONALATTRIBUTESCONTAINER
   OBJECT = ADDITIONALATTRIBUTESCONTAINER
        CLASS = "11"
OBJECT = ADDITIONALATTRIBUTENAME
   CLASS = "11"
   NUM_VAL = 1
   VALUE = "identifier_product_doi"
END_OBJECT = ADDITIONALATTRIBUTENAME
GROUP = INFORMATIONCONTENT
   CLASS = "11"
                 OBJECT = PARAMETERVALUE
                      NUM_VAL = 1
                      CLASS = "11"
                      VALUE = "dox.ix.ix.123"
                 END_OBJECT = PARAMETERVALUE
```

```
       END_GROUP = INFORMATIONCONTENT
          END_OBJECT = ADDITIONALATTRIBUTESCONTAINER
          OBJECT = ADDITIONALATTRIBUTESCONTAINER
              CLASS = "12"
        OBJECT = ADDITIONALATTRIBUTENAME
           CLASS = "12"
           NUM_VAL = 1
           VALUE = "identifier_product_doi_authority"
        END_OBJECT = ADDITIONALATTRIBUTENAME
        GROUP = INFORMATIONCONTENT
           CLASS = "12"
               OBJECT = PARAMETERVALUE
                   NUM_VAL = 1
                   CLASS = "12"
                   VALUE = "LPDAAC"
               END_OBJECT = PARAMETERVALUE
        END_GROUP = INFORMATIONCONTENT
          END_OBJECT = ADDITIONALATTRIBUTESCONTAINER
    END_GROUP = ADDITIONALATTRIBUTES
END_GROUP = INVENTORYMETADATA
END

GROUP = ARCHIVEDMETADATA
  GROUPTYPE = MASTERGROUP
       OBJECT = ALGORITHMPACKAGEACCEPTANCEDATE
          NUM_VAL = 1
          VALUE = "not_set"
       END_OBJECT = ALGORITHMPACKAGEACCEPTANCEDATE
       OBJECT = ALGORITHMPACKAGEMATURITYCODE
          NUM_VAL = 1
          VALUE = "Normal"
       END_OBJECT = ALGORITHMPACKAGEMATURITYCODE
       OBJECT = ALGORITHMPACKAGENAME
          NUM_VAL = 1
          VALUE = "NPP_PR13A1"
       END_OBJECT = ALGORITHMPACKAGENAME
       OBJECT = ALGORITHMPACKAGEVERSION
          NUM_VAL = 1
          VALUE = "2"
       END_OBJECT = ALGORITHMPACKAGEVERSION
       OBJECT = INSTRUMENTNAME
          NUM_VAL = 1
          VALUE = "Visible Infrared Imaging Radiometer Suite"
       END_OBJECT = INSTRUMENTNAME
       OBJECT = LONGNAME
          NUM_VAL = 1
          VALUE = "VIIRS/NPP Vegetation Index 16-Day L3 SIN Grid 1km"
       END_OBJECT = LONGNAME
       OBJECT = PROCESSINGCENTER
          NUM_VAL = 1
          VALUE = "MODAPS"
       END_OBJECT = PROCESSINGCENTER
          GROUP = BOUNDINGRECTANGLE
       OBJECT = NORTHBOUNDINGCOORDINATE
          NUM_VAL = 1
          VALUE = 40.000000
       END_OBJECT = NORTHBOUNDINGCOORDINATE
       OBJECT = SOUTHBOUNDINGCOORDINATE
          NUM_VAL = 1
          VALUE = 30.000000
       END_OBJECT = SOUTHBOUNDINGCOORDINATE
       OBJECT = EASTBOUNDINGCOORDINATE
          NUM_VAL = 1
          VALUE = -92.366425
       END_OBJECT = EASTBOUNDINGCOORDINATE
```

```
        OBJECT = WESTBOUNDINGCOORDINATE
            NUM_VAL = 1
            VALUE = -117.486656
        END_OBJECT = WESTBOUNDINGCOORDINATE
          END_GROUP = BOUNDINGRECTANGLE
        OBJECT = SEAPROCESSED
            NUM_VAL = 1
            VALUE = "Yes"
        END_OBJECT = SEAPROCESSED
        OBJECT = PROCESSINGENVIRONMENT
            NUM_VAL = 1
            VALUE = "Linux nppdev-c64 2.6.18-308.20.1.el5 #1 SMP Tue Nov 13
10:15:12 EST 2012 x86_64 x86_64 x86_64 GNU/Linux"
        END_OBJECT = PROCESSINGENVIRONMENT
        OBJECT = DESCRREVISION
            NUM_VAL = 1
            VALUE = "2.0"
        END_OBJECT = DESCRREVISION
        OBJECT = CHARACTERISTICBINANGULARSIZE
            NUM_VAL = 1
            VALUE = 15.0
        END_OBJECT = CHARACTERISTICBINANGULARSIZE
        OBJECT = CHARACTERISTICBINSIZE
            NUM_VAL = 1
            VALUE = 463.312716527778
        END_OBJECT = CHARACTERISTICBINSIZE
        OBJECT = DATACOLUMNS
         NUM_VAL = 1
         VALUE = 2400
        END_OBJECT = DATACOLUMNS
        OBJECT = DATAROWS
         NUM_VAL = 1
         VALUE = 2400
        END_OBJECT = DATAROWS
        OBJECT = GLOBALGRIDCOLUMNS
         NUM_VAL = 1
         VALUE = 86400
        END_OBJECT = GLOBALGRIDCOLUMNS
        OBJECT = GLOBALGRIDROWS
         NUM_VAL = 1
         VALUE = 43200
        END_OBJECT = GLOBALGRIDROWS
        OBJECT = NUMBEROFDAYS
         NUM_VAL = 1
         VALUE = 16
        END_OBJECT = NUMBEROFDAYS
        OBJECT = DAYSOFYEAR
            NUM_VAL = 16
            VALUE = (145, 146, 147, 148, 149, 150, 151, 152, 153, 154, 155, 156,
157, 158, 159, 160)
        END_OBJECT = DAYSOFYEAR
        OBJECT = GEOANYABNORMAL
            NUM_VAL = 1
            VALUE = "False"
        END_OBJECT = GEOANYABNORMAL
        OBJECT = GEOESTMAXRMSERROR
            NUM_VAL = 1
            VALUE = "not_set"
        END_OBJECT = GEOESTMAXRMSERROR
        OBJECT = QAPERCENTPOORQ500M16DAYNDVI
            NUM_VAL = 16
            VALUE = (0, 55, 25, 17, 1, 2, 0, 0, 0, 0, 0, 0, 0, 0, 0, 0)
        END_OBJECT = QAPERCENTPOORQ500M16DAYNDVI
        OBJECT = QAPERCENTPOORQ500M16DAYEVI
            NUM_VAL = 16
```

```
          VALUE = (0, 55, 25, 17, 1, 2, 0, 0, 0, 0, 0, 0, 0, 0, 0, 0)
        END_OBJECT = QAPERCENTPOORQ500M16DAYEVI
        OBJECT = PERCENTLAND
         NUM_VAL = 1
         VALUE = 98
        END_OBJECT = PERCENTLAND
        OBJECT = DAYSPROCESSED
           NUM_VAL = 16
           VALUE = ("2015145", "2015146", "2015147", "2015148", "2015149",
"2015150", "2015151", "2015152", "2015153", "2015154", "2015155", "2015156",
"2015157", "2015158", "2015159", "2015160")
        END_OBJECT = DAYSPROCESSED
        OBJECT = PRODUCTIONTYPE
           NUM_VAL = 1
           VALUE = "Regular Production [1-16,17-32,33-48,...353-2/3]"
        END_OBJECT = PRODUCTIONTYPE
END_GROUP = ARCHIVEDMETADATA
END
```

Appendix – II - Global Metadata Attributes

```
GROUP=SwathStructure
END_GROUP=SwathStructure
GROUP=GridStructure
        GROUP=GRID_1
                GridName="NPP_Grid_16Day_VI_CMG"
                XDim=7200
                YDim=3600
                UpperLeftPointMtrs=(-180000000.000000,90000000.000000)
                LowerRightMtrs=(180000000.000000,-90000000.000000)
                Projection=HE5_GCTP_GEO
                GROUP=Dimension
                END_GROUP=Dimension
                GROUP=DataField
                    OBJECT=DataField_1
                            DataFieldName="CMG 0.05 Deg 16 days NDVI"
                            DataType=H5T_NATIVE_SHORT
                            DimList=("YDim","XDim")
                            MaxdimList=("YDim","XDim")
                            CompressionType=HE5_HDFE_COMP_DEFLATE
                            DeflateLevel=5
                    END_OBJECT=DataField_1
                    OBJECT=DataField_2
                            DataFieldName="CMG 0.05 Deg 16 days EVI"
                            DataType=H5T_NATIVE_SHORT
                            DimList=("YDim","XDim")
                            MaxdimList=("YDim","XDim")
                            CompressionType=HE5_HDFE_COMP_DEFLATE
                            DeflateLevel=5
                    END_OBJECT=DataField_2
                    OBJECT=DataField_3
                            DataFieldName="CMG 0.05 Deg 16 days EVI2"
                            DataType=H5T_NATIVE_SHORT
                            DimList=("YDim","XDim")
                            MaxdimList=("YDim","XDim")
                            CompressionType=HE5_HDFE_COMP_DEFLATE
                            DeflateLevel=5
                    END_OBJECT=DataField_3
                    OBJECT=DataField_4
                            DataFieldName="CMG 0.05 Deg 16 days VI Quality"
                            DataType=H5T_NATIVE_USHORT
                            DimList=("YDim","XDim")
                            MaxdimList=("YDim","XDim")
                            CompressionType=HE5_HDFE_COMP_DEFLATE
                            DeflateLevel=5
                    END_OBJECT=DataField_4
                    OBJECT=DataField_5
                            DataFieldName="CMG 0.05 Deg 16 days red reflectance"
                            DataType=H5T_NATIVE_SHORT
                            DimList=("YDim","XDim")
                            MaxdimList=("YDim","XDim")
                            CompressionType=HE5_HDFE_COMP_DEFLATE
                            DeflateLevel=5
                    END_OBJECT=DataField_5
                    OBJECT=DataField_6
                            DataFieldName="CMG 0.05 Deg 16 days NIR reflectance"
                            DataType=H5T_NATIVE_SHORT
                            DimList=("YDim","XDim")
                            MaxdimList=("YDim","XDim")
                            CompressionType=HE5_HDFE_COMP_DEFLATE
                            DeflateLevel=5
                    END_OBJECT=DataField_6
                    OBJECT=DataField_7
```

```
                    DataFieldName="CMG 0.05 Deg 16 days blue reflectance"
                    DataType=H5T_NATIVE_SHORT
                    DimList=("YDim","XDim")
                    MaxdimList=("YDim","XDim")
                    CompressionType=HE5_HDFE_COMP_DEFLATE
                    DeflateLevel=5
            END_OBJECT=DataField_7
            OBJECT=DataField_8
                    DataFieldName="CMG 0.05 Deg 16 days green reflectance"
                    DataType=H5T_NATIVE_SHORT
                    DimList=("YDim","XDim")
                    MaxdimList=("YDim","XDim")
                    CompressionType=HE5_HDFE_COMP_DEFLATE
                    DeflateLevel=5
            END_OBJECT=DataField_8
            OBJECT=DataField_9
                    DataFieldName="CMG 0.05 Deg 16 days SWIR1 reflectance"
                    DataType=H5T_NATIVE_SHORT
                    DimList=("YDim","XDim")
                    MaxdimList=("YDim","XDim")
                    CompressionType=HE5_HDFE_COMP_DEFLATE
                    DeflateLevel=5
            END_OBJECT=DataField_9
            OBJECT=DataField_10
                    DataFieldName="CMG 0.05 Deg 16 days SWIR2 reflectance"
                    DataType=H5T_NATIVE_SHORT
                    DimList=("YDim","XDim")
                    MaxdimList=("YDim","XDim")
                    CompressionType=HE5_HDFE_COMP_DEFLATE
                    DeflateLevel=5
            END_OBJECT=DataField_10
            OBJECT=DataField_11
                    DataFieldName="CMG 0.05 Deg 16 days SWIR3 reflectance"
                    DataType=H5T_NATIVE_SHORT
                    DimList=("YDim","XDim")
                    MaxdimList=("YDim","XDim")
                    CompressionType=HE5_HDFE_COMP_DEFLATE
                    DeflateLevel=5
            END_OBJECT=DataField_11
            OBJECT=DataField_12
                    DataFieldName="CMG 0.05 Deg 16 days Avg sun zen angle"
                    DataType=H5T_NATIVE_SHORT
                    DimList=("YDim","XDim")
                    MaxdimList=("YDim","XDim")
                    CompressionType=HE5_HDFE_COMP_DEFLATE
                    DeflateLevel=5
            END_OBJECT=DataField_12
            OBJECT=DataField_13
                    DataFieldName="CMG 0.05 Deg 16 days NDVI std dev"
                    DataType=H5T_NATIVE_SHORT
                    DimList=("YDim","XDim")
                    MaxdimList=("YDim","XDim")
                    CompressionType=HE5_HDFE_COMP_DEFLATE
                    DeflateLevel=5
            END_OBJECT=DataField_13
            OBJECT=DataField_14
                    DataFieldName="CMG 0.05 Deg 16 days EVI std dev"
                    DataType=H5T_NATIVE_SHORT
                    DimList=("YDim","XDim")
                    MaxdimList=("YDim","XDim")
                    CompressionType=HE5_HDFE_COMP_DEFLATE
                    DeflateLevel=5
            END_OBJECT=DataField_14
            OBJECT=DataField_15
                    DataFieldName="CMG 0.05 Deg 16 days EVI2 std dev"
```

```
                                DataType=H5T_NATIVE_SHORT
                                DimList=("YDim","XDim")
                                MaxdimList=("YDim","XDim")
                                CompressionType=HE5_HDFE_COMP_DEFLATE
                                DeflateLevel=5
                        END_OBJECT=DataField_15
                        OBJECT=DataField_16
                                DataFieldName="CMG 0.05 Deg 16 days #1km pix used"
                                DataType=H5T_NATIVE_UCHAR
                                DimList=("YDim","XDim")
                                MaxdimList=("YDim","XDim")
                                CompressionType=HE5_HDFE_COMP_DEFLATE
                                DeflateLevel=5
                        END_OBJECT=DataField_16
                        OBJECT=DataField_17
                                DataFieldName="CMG 0.05 Deg 16 days #1km pix +-30deg
VZ"
                                DataType=H5T_NATIVE_UCHAR
                                DimList=("YDim","XDim")
                                MaxdimList=("YDim","XDim")
                                CompressionType=HE5_HDFE_COMP_DEFLATE
                                DeflateLevel=5
                        END_OBJECT=DataField_17
                        OBJECT=DataField_18
                                DataFieldName="CMG 0.05 Deg 16 days pixel reliability"
                                DataType=H5T_NATIVE_SCHAR
                                DimList=("YDim","XDim")
                                MaxdimList=("YDim","XDim")
                                CompressionType=HE5_HDFE_COMP_DEFLATE
                                DeflateLevel=5
                        END_OBJECT=DataField_18
                END_GROUP=DataField
                GROUP=MergedFields
                END_GROUP=MergedFields
        END_GROUP=GRID_1
END_GROUP=GridStructure
GROUP=PointStructure
END_GROUP=PointStructure
GROUP=ZaStructure
END_GROUP=ZaStructure
END
GROUP = INVENTORYMETADATA
  GROUPTYPE = MASTERGROUP
    GROUP  = ECSDATAGRANULE
        OBJECT = LOCALGRANULEID
            NUM_VAL = 1
            VALUE = "VNP13C1.A2015145.002.2016111183024.h5"
        END_OBJECT = LOCALGRANULEID

        OBJECT = PRODUCTIONDATETIME
            NUM_VAL = 1
            VALUE = "2016-04-20T11:28:16.000Z"
        END_OBJECT = PRODUCTIONDATETIME
        OBJECT = DAYNIGHTFLAG
            NUM_VAL = 1
            VALUE = ""
        END_OBJECT = DAYNIGHTFLAG
        OBJECT = REPROCESSINGACTUAL
            NUM_VAL = 1
            VALUE = "reprocessed"
        END_OBJECT = REPROCESSINGACTUAL
        OBJECT = LOCALVERSIONID
            NUM_VAL = 1
            VALUE = "2.0.0"
        END_OBJECT = LOCALVERSIONID
```

```
      OBJECT = REPROCESSINGPLANNED
          NUM_VAL = 1
          VALUE = "further update is anticipated"
      END_OBJECT = REPROCESSINGPLANNED
   END_GROUP = ECSDATAGRANULE
   GROUP = MEASUREDPARAMETER
      OBJECT = MEASUREDPARAMETERCONTAINER
      CLASS = 1GROUP  = QAFLAGS
CLASS="1"
      OBJECT = SCIENCEQUALITYFLAG
          NUM_VAL = 1
          VALUE = "Not Investigated"
      END_OBJECT = SCIENCEQUALITYFLAG
      OBJECT = AUTOMATICQUALITYFLAGEXPLANATION
          NUM_VAL = 1
          VALUE = "No automatic quality assessment is performed in the PGE"
      END_OBJECT = AUTOMATICQUALITYFLAGEXPLANATION
      OBJECT = AUTOMATICQUALITYFLAG
          NUM_VAL = 1
          VALUE = "Passed"
      END_OBJECT = AUTOMATICQUALITYFLAG
      OBJECT = SCIENCEQUALITYFLAGEXPLANATION
          NUM_VAL = 1
          VALUE = "see http://landweb.nascom.nasa.gov/"
      END_OBJECT = SCIENCEQUALITYFLAGEXPLANATION
   END_GROUP = QAFLAGS
      GROUP = QASTATS
CLASS="1"
      END_GROUP = QASTATS
      OBJECT = PARAMETERNAME
          NUM_VAL = 1
          VALUE = "CMG 16 day NDVI"
      END_OBJECT = PARAMETERNAME
 END_OBJECT = MEASUREDPARAMETERCONTAINER
   GROUP = MEASUREDPARAMETER
      OBJECT = MEASUREDPARAMETERCONTAINER
      CLASS = 2GROUP  = QAFLAGS
CLASS="2"
      OBJECT = SCIENCEQUALITYFLAG
          NUM_VAL = 1
          VALUE = "Not Investigated"
      END_OBJECT = SCIENCEQUALITYFLAG
      OBJECT = AUTOMATICQUALITYFLAGEXPLANATION
          NUM_VAL = 1
          VALUE = "No automatic quality assessment is performed in the PGE"
      END_OBJECT = AUTOMATICQUALITYFLAGEXPLANATION

      OBJECT = AUTOMATICQUALITYFLAG
          NUM_VAL = 1
          VALUE = "Passed"
      END_OBJECT = AUTOMATICQUALITYFLAG
      OBJECT = SCIENCEQUALITYFLAGEXPLANATION
          NUM_VAL = 1
          VALUE = "see http://landweb.nascom.nasa.gov/"
      END_OBJECT = SCIENCEQUALITYFLAGEXPLANATION
   END_GROUP = QAFLAGS
      END_GROUP = QASTATS
      OBJECT = PARAMETERNAME
          NUM_VAL = 1
          VALUE = "CMG 16 day EVI"
      END_OBJECT = PARAMETERNAME
 END_OBJECT = MEASUREDPARAMETERCONTAINER
   GROUP = COLLECTIONDESCRIPTIONCLASS
      OBJECT = VERSIONID
          NUM_VAL = 1
```

```
                VALUE = "2"
            END_OBJECT = VERSIONID
            OBJECT = SHORTNAME
                NUM_VAL = 1
                VALUE = "VNP13C1"
            END_OBJECT = SHORTNAME
        END_GROUP = COLLECTIONDESCRIPTIONCLASS
        GROUP = INPUTGRANULE
            OBJECT = INPUTGRANULE
                NUM_VAL = 3
                VALUE = ("VNP13A2.A2015145.h09v05.002.2015335163419.h5",
 "VNP13A2.A2015145.h20v11.002.2015335163419.h5",
 "VNP13A2.A2015145.h30v11.002.2015335163419.h5")
            END_OBJECT = INPUTGRANULE
        END_GROUP = INPUTGRANULE
GROUP = SPATIALDOMAINCONTAINER
 GROUP = HORIZONTALSPATIALDOMAINCONTAINER
  GROUP = BOUNDINGRECTANGLE
            OBJECT = EASTBOUNDINGCOORDINATE
                NUM_VAL = 1
                VALUE = 180.0
            END_OBJECT = EASTBOUNDINGCOORDINATE
            OBJECT = WESTBOUNDINGCOORDINATE
                NUM_VAL = 1
                VALUE = -180.0
            END_OBJECT = WESTBOUNDINGCOORDINATE

            OBJECT = SOUTHBOUNDINGCOORDINATE
                NUM_VAL = 1
                VALUE = -90.0
            END_OBJECT = SOUTHBOUNDINGCOORDINATE
            OBJECT = NORTHBOUNDINGCOORDINATE
                NUM_VAL = 1
                VALUE = 90.0
            END_OBJECT = NORTHBOUNDINGCOORDINATE
  END_GROUP = BOUNDINGRECTANGLE
 END_GROUP = HORIZONTALSPATIALDOMAINCONTAINER
 GROUP = GRANULELOCALITY
            OBJECT = LOCALITYVALUE
                NUM_VAL = 1
                VALUE = Global
            END_OBJECT = LOCALITYVALUE
 END_GROUP = GRANULELOCALITY
END_GROUP = SPATIALDOMAINCONTAINER
        GROUP = RANGEDATETIME
            OBJECT = RANGEENDINGDATE
                NUM_VAL = 1
                VALUE = "2015-06-10"
            END_OBJECT = RANGEENDINGDATE
            OBJECT = RANGEENDINGTIME
                NUM_VAL = 1
                VALUE = "23:59:59"
            END_OBJECT = RANGEENDINGTIME
            OBJECT = RANGEBEGINNINGDATE
                NUM_VAL = 1
                VALUE = "2015-05-25"
            END_OBJECT = RANGEBEGINNINGDATE
            OBJECT = RANGEBEGINNINGTIME
                NUM_VAL = 1
                VALUE = "00:00:00"
            END_OBJECT = RANGEBEGINNINGTIME
        END_GROUP = RANGEDATETIME
        GROUP = PGEVERSIONCLASS
            OBJECT = PGEVERSION
                NUM_VAL = 1
```

```
                 VALUE = "2.0"
             END_OBJECT = PGEVERSION
        END_GROUP = PGEVERSIONCLASS
 END_GROUP = INVENTORYMETADATA
 GROUP = ARCHIVEDMETADATA
   GROUPTYPE = MASTERGROUP
         OBJECT = ALGORITHMPACKAGEACCEPTANCEDATE
            NUM_VAL = 1
            VALUE = "2004-10-01"
         END_OBJECT = ALGORITHMPACKAGEACCEPTANCEDATE
         OBJECT = ALGORITHMPACKAGENAME
            NUM_VAL = 1
            VALUE = ""
         END_OBJECT = ALGORITHMPACKAGENAME
         OBJECT = ALGORITHMPACKAGEVERSION
            NUM_VAL = 1
            VALUE = "5"
         END_OBJECT = ALGORITHMPACKAGEVERSION
         OBJECT = INSTRUMENTNAME
            NUM_VAL = 1
            VALUE = "Visible Infrared Imaging Radiometer Suite"
         END_OBJECT = INSTRUMENTNAME
         OBJECT = LONGNAME
            NUM_VAL = 1
            VALUE = "VIIRS Vegetation Indices 16-Day Global 0.05Deg CMG"
         END_OBJECT = LONGNAME
         OBJECT = SENSORSHORTNAME
            NUM_VAL = 1
            VALUE = "VIIRS"
         END_OBJECT = SENSORSHORTNAME
         OBJECT = PROCESSINGCENTER
            NUM_VAL = 1
            VALUE = "Not_set"
         END_OBJECT = PROCESSINGCENTER
         OBJECT = SEAPROCESSED
            NUM_VAL = 1
            VALUE = "No"
         END_OBJECT = SEAPROCESSED
         OBJECT = DESCRREVISION
            NUM_VAL = 1
            VALUE = "2.0"
         END_OBJECT = DESCRREVISION
         OBJECT = DATACOLUMNS
            NUM_VAL = 1
            VALUE = 7200
         END_OBJECT = DATACOLUMNS
         OBJECT = DATAROWS
            NUM_VAL = 1
            VALUE = 3600
         END_OBJECT = DATAROWS
         OBJECT = GLOBALGRIDCOLUMNS
            NUM_VAL = 1
            VALUE = 7200
         END_OBJECT = GLOBALGRIDCOLUMNS
         OBJECT = GLOBALGRIDROWS
            NUM_VAL = 1
            VALUE = 3600
         END_OBJECT = GLOBALGRIDROWS
         OBJECT = NUMBEROFDAYS
          NUM_VAL = 1
          VALUE = 16
         END_OBJECT = NUMBEROFDAYS
         OBJECT = DAYSOFYEAR
            NUM_VAL = 16
            VALUE = ((145, 146, 147, 148, 149, 150, 151, 152, 153, 154, 155, 156,
```

```
157, 158, 159, 160))
        END_OBJECT = DAYSOFYEAR
        OBJECT = DAYSPROCESSED
            NUM_VAL = 16
            VALUE = ("2015145", "2015146", "2015147", "2015148", "2015149",
"2015150", "2015151", "2015152", "2015153", "2015154", "2015155", "2015156",
"2015157", "2015158", "2015159", "2015160")
        END_OBJECT = DAYSPROCESSED
        OBJECT = GEOANYABNORMAL
            NUM_VAL = 1
            VALUE = "False"
        END_OBJECT = GEOANYABNORMAL
        OBJECT = GEOESTMAXRMSERROR
            NUM_VAL = 1
            VALUE = "50.0"
        END_OBJECT = GEOESTMAXRMSERROR
        OBJECT = QAPERCENTPOORQCMG16DAYNDVI
         NUM_VAL = 16
         VALUE = 21565436
        END_OBJECT = QAPERCENTPOORQCMG16DAYNDVI
        OBJECT = QAPERCENTPOORQCMG16DAYEVI
         NUM_VAL = 16
         VALUE = 21565500
        END_OBJECT = QAPERCENTPOORQCMG16DAYEVI
        OBJECT = QAPERCENTPOORQCMG16DAYEVI2
         NUM_VAL = 16
         VALUE = 21565436
        END_OBJECT = QAPERCENTPOORQCMG16DAYEVI2
        OBJECT = PERCENTLAND
         NUM_VAL = 1
         VALUE = 0
        END_OBJECT = PERCENTLAND
        OBJECT = SNOWICEFLAGGED
            NUM_VAL = 1
            VALUE = "YES"
        END_OBJECT = SNOWICEFLAGGED
        OBJECT = PRODUCTIONTYPE
            NUM_VAL = 1
            VALUE = "Regular Production [1-16,17-32,33-48,...353-2/3]"
        END_OBJECT = PRODUCTIONTYPE
    GROUP = DATAIDENTIFICATION
END_GROUP = ARCHIVEDMETADATA
END
```